1.0

1.1

1.25 1.4 1.6

2.8 2.5

2.2

2.0

1.8

LEVEL ⅠⅠ (12)

NOSC

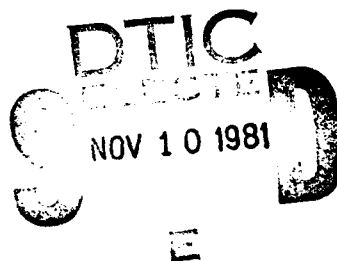AD A107097

Technical Report 695

ACCURACY OF HIGH FREQUENCY MAXIMUM USABLE FREQUENCIES (MUF) PREDICTION

DTIC

NOV 10 1981

E

D. B. Sailors
W. K. Moision
R. P. Brown

15 September 1981

Final Report

Prepared for
Naval Electromagnetic Spectrum Center

**NAVAL OCEAN SYSTEMS CENTER
SAN DIEGO, CALIFORNIA 92152**

81 11 09 130

NAVAL OCEAN SYSTEMS CENTER, SAN DIEGO, CA 92152

AN ACTIVITY OF THE NAVAL MATERIAL COMMAND

SL GUILLE, CAPT, USN
Commander

HL BLOOD
Technical Director

ADMINISTRATIVE INFORMATION

Released by
J. H. Richter, Head
EM Propagation Division

Under Authority of
J. D. Hightower, Head
Environmental Sciences Department

REPORT DOCUMENTATION PAGE		READ INSTRUCTIONS BEFORE COMPLETING FORM
1. REPORT NUMBER NOSC Technical Report 695 (TR 695)	2. GOVT ACCESSION NO. AD-A107097	3. RECIPIENT'S CATALOG NUMBER
4. TITLE (and Subtitle) ACCURACY OF HIGH FREQUENCY MAXIMUM USABLE FREQUENCIES (MUF) PREDICTION.		5. TYPE OF REPORT & PERIOD COVERED Sep 1979–Jan 1981
		6. PERFORMING ORG. REPORT NUMBER
7. AUTHOR(s) D. B. Sailors W. K. Moision R. P. Brown		8. CONTRACT OR GRANT NUMBER(s)
9. PERFORMING ORGANIZATION NAME AND ADDRESS Naval Ocean Systems Center San Diego, CA 92152		10. PROGRAM ELEMENT, PROJECT, TASK AREA & WORK UNIT NUMBERS 62759N, F59551 ZF59551002
11. CONTROLLING OFFICE NAME AND ADDRESS Naval Electromagnetic Spectrum Center Naval Communication Unit Washington, DC 20390		12. REPORT DATE 15 September 1981
		13. NUMBER OF PAGES 120
14. MONITORING AGENCY NAME & ADDRESS(if different from Controlling Office)		15. SECURITY CLASS. (of this report) Unclassified
		15a. DECLASSIFICATION DOWNGRADING SCHEDULE

16. DISTRIBUTION STATEMENT (of this Report)

Approved for public release; distribution unlimited

17. DISTRIBUTION STATEMENT (of the abstract entered in Block 20, if different from Report)

18. SUPPLEMENTARY NOTES

19. KEY WORDS (Continue on reverse side if necessary and identify by block number)

Maximum observed frequencies (MOF)	Ionospheric predictions
Maximum usable frequencies (MUF)	High frequency propagation
Root mean square (rms)	Maximum transmission frequencies
Ionospheric characteristics	Sky wave propagation
Sounding oblique incidence	Curves, statistics, data

20. ABSTRACT (Continue on reverse side if necessary and identify by block number)

The residuals between observed oblique sounder medium maximum observed frequencies (MOF) and predicted maximum usable frequencies (MUF) were used to assess the accuracy of high frequency MUF prediction. 4668 MOFs measured on 25 paths were compared against the predicted values from ITSA-1, HFMUFES 4 and MINIMUF-3.5. The data was screened into subsets to see the effect of particular paths, path length and orientation, season, month, latitude, sunspot number, diurnal trends, geographic region and sounder type. MINIMUF-3.5 was most accurate, having a bias of 0.08 MHz (0.6 percent) and a root mean square (rms) error of 3.71 MHz (3.6 percent). It was least accurate during the sunrise and sunset

20. ABSTRACT (continued)

transition hours and for path lengths 5000 to 7000 km. Linear regression analysis identified the probable source of this error to begin the M factor calculation. Except for land paths the performance of HFMUFES 4 was disappointing. It was least accurate for paths over the ocean and with lengths between 4000 and 5000 km. Linear regression analysis identified the source of this error to be a bias in the foF2 numerical coefficient map over ocean areas. The "k sec" factor accentuated this bias as the range increased. The version of ITSA-1 with ionospheric characteristics mapped in universal time appeared to be slightly more accurate than the one with its characteristics mapped in local time. All of the programs had difficulty predicting MUFs accurately at high latitude.

Accession For

NTIS CRA81	X
DTIC TAB	
Unannounced	
Justification	

By

Distribution/

Availability Codes

| Dist | Avail and/or Special |

A

SUMMARY

OBJECTIVE

Assess the accuracy of predicted MUFs by prediction programs, commonly used in Navy applications, using a previously assembled data base of observed oblique sounder median MOFs from 25 paths.

RESULTS

1. The programs compared were the ITSA-1, HFMUFES 4, MINIMUF-3.5, and the version of ITSA-1 used to produce Naval Telecommunications Publication (NTP) 6 Supplement 1.

2. Predicted MUFs for these 25 paths and the observed MOFs themselves were screened into nine subsets of data to see the effect of particular paths, path length, path orientation, season, month, latitude, solar sunspot number, diurnal trends, geographic region and sounder type.

3. An indication of the accuracy of the numerical predictions of MUF was obtained from the study of the residuals between the observed data and predicted values.

4. MINIMUF 3.5 appeared most accurate overall, with its bias of 0.08 MHz (0.6 percent) and an rms error of 3.71 MHz (3.6 percent).

5. MINIMUF 3.5 had difficulty predicting accurately during the sunrise and sunset transition hours and for path lengths 5000 to 7000 km.

6. The version of ITSA-1 with ionospheric characteristics mapped in universal time was slightly more accurate than the version of ITSA-1 used to produce NTP 6 Supp. 1.

7. Except for land paths, the performance of HFMUFES 4 was disappointing; it was biased 1.49 MHz high (7.2 percent high) and rms error of 4.24 MHz (8.3 percent).

8. HFMUFES 4 had difficulty predicting MUFs accurately for paths over ocean areas and for paths with lengths between 4000 and 5000 km.

i

9. All of the programs had difficulty predicting MUFs accurately at high latitude.

10. The use of linear regress analysis demonstrated that the source of error in HFMUFES 4 predicted MUFs (and to some extent ITSA-1 predicted MUFs) was due to a bias in the critical frequency calculation. This bias occurred over ocean areas where no real vertical ionosonde data were available to generate the numerical map of f_oF2. The "k sec ϕ" factor accentuated the error in predicted MUF as range increased.

11. For MINIMUF-3.5 linear regression, analysis showed that its errors in predicted MUF at sunrise and for path lengths 5000 to 7000 km were non-linear and could be attributed to the "k sec ϕ" factor (M factor) in its calculation of MUF.

RECOMMENDATIONS

1. Use MINIMUF-3.5 where the only desired parameters are MUF and FOT.

2. Use the universal time ionospheric data tape in NTP 6 Supp. 1 predictions.

3. Develop an improved M factor equation for use in MINIMUF-3.5.

4. Augment the MOF data base to better represent the Atlantic Ocean, northern latitudes and transequatorial paths.

5. Use this augmented data base to more accurately assess the errors in predicted MUF.

6. Assess the effect of the minimum take-off angle on accuracy of predicted MUF.

7. Use multiple-linear regression to remove the bias in predicted MUF due to f_oF2 bias.

8. In future numerical mapping of f_oF2, use topside sounder data to aid in the representation of over ocean areas.

ACRONYMS

CCIR	Consultative Committeee International Radio
CRPL	Central Radio Propagation Laboratory
DASCR3	Data Screening 3
ESSA	Environmental Science Services Administration
FOT	Frequency of Optimum Transmission
H	High latitude (propagation)
HF	High Frequency
HFDR	High Frequency Digital Recorder
HPF	Highest Possible Frequency
ITS	Institute for Telecommunication Sciences
ITSA	Institute for Telecommunication Sciences and Aeronomy
LO	Low Latitude (propagation)
LUF	Lowest Usable Frequency
MAE	Mean Absolute Error
M	Mid-Latitude (propagation)
MINIMUF	Simplified HF MUF prediction algorithm
MOF	Maximum Observed Frequency
MUF	Maximum Usable Frequency
NBS	National Bureau of Standards
NELIAC	Computer language related to ALOG
NTP	National Telecommunications Publication
NTSS	Navy Tactical Sounder System
PROPHET	Propagation Forecasting Terminal
RADC	Rome Air Development Center
RMS	Root Mean Square
SRI	Stanford Research Institute
TA	Transauroral (propagation)
TE	Transequatorial (propagation)
USACEEIA	US Army Communication-Electronics Engineering Installation Agency

CONTENTS

ILLUSTRATIONS

TABLES

INTRODUCTION

The effective operation of long distance high frequency (HF) systems has increased in proportion to the ability to predict variations in the ionosphere, since such an ability has permitted the selection of optimum frequencies, antennas and other circuit parameters. Most variations in HF system performance are directly related to changes in the ionosphere, which in turn are affected in a complex manner by solar activity, seasonal and diurnal variations as well as latitude and longitude.

Manual methods were developed for analyzing these effects on HF circuits of short, intermediate and long distances.[1] Because the manual methods were laborious and time consuming, various organizations developed computer programs to analyze HF circuit performance. A commonly predicted parameter in these programs is the maximum usable frequency (MUF). The MUF is the highest frequency that can be propagated by ionospheric refraction between given points at a given time.

There has been very little attempt to systematically verify the accuracy of HF prediction programs. At the Naval Electronics Laboratory Center (NELC), predecessor to the Naval Ocean Systems Center (NOSC), three HF prediction programs were compared against oblique sounder data.[2] MINIMUF-3 was also compared against the same data base.[3] The results showed all four programs to be comparable. In the latter study the data base of oblique sounder maximum observed frequency (MOF) was also enlarged. This data base consists of measurements of median monthly MOF on 25 paths and includes over 4700 hourly observed MOFs. Geographically, the data base covers the Pacific Ocean, Europe and the continental United States as well.

In this report the accuracy will be discussed of predicted median MUFs by four prediction programs commonly used in Navy applications. The first of these, the ITSA-1 with local time ionospheric data tape, is used by the Navy Electromagnetic Spectrum Center to produce its recommended frequency bands published in Naval Telecommunications Publication 6 Supplement 1 (NTP6 Supp. 1). This is a Navy publication designed to provide the operating personnel, establishing ship, shore and aircraft communication circuits, with a sample reference for ionospheric propagation predictions in the form of recommended operating frequencies.[4] The second of these, the ITSA-1 with ionospheric data

mapped in universal time, is used to produce a frequency guide and a frequency time transmission schedule for a particular operating communication system.[5] The third program, HFMUFES 4, is used at NOSC in system design analysis. The final program to be compared is the MINIMUF-3.5, which has been used by NOSC in a first-generation forecasting terminal called PROPHET (a pseudoacronym for a propagation forecasting terminal).[6] Its code is small enough to be used on a minicomputer.

The scope of the report is limited to the accuracy of the predicted MUF for point-to-point paths. The accuracy of the predicted MUF in its application (i.e., sector predictions rather than point-to-point; seasonal rather than months, etc.) will be considered in a subsequent report. The comparison is limited to the existing data base of oblique sounder MOF data. In a future project, data for the Atlantic Ocean, northern latitude and transequatorial paths will be added to provide a better balanced data base.

HISTORY OF HIGH FREQUENCY PREDICTION

The increased dependence in the past 25 years upon high frequency telecommunication circuits has resulted in the need for computer-produced radio predictions. This is especially true because of the speed with which modern electronic computers can handle the large volumes of data and can perform the lengthy computations. Many different models of ionospheric radio propagation in all its facets have been developed, ranging from extremely simple approximations to very complex ray-tracing techniques.

In the United States, the first automated HF path prediction computer program was developed in 1957 for the US Army Signal Corps, Radio Propagation Agency, now part of the US Army Communications-Electronics Engineering Installation Agency (USACEEIA).[7] A later version was published in 1962 by Stanford Research Institute (SRI).[8] A NELIAC language version of this program was adapted to work on NELC's CDC 1604B computer in 1965 and was used until 1969 when NELC changed to the IBM 360/65, which didn't support the NELIAC computer language.[9] This program used ionospheric data taken from NBS Technical Notes 2 and 2-2; the latest version of this program also used noise data from CCIR report 322.[10-12]

The first program to use a numerical representation of the monthly f_0F2 and M-3000 factor by tables of numerical coefficients similar to those in a Fourier series was produced by Lucas and Haydon in 1961.[13] Subsequent to this they produced a program that also calculated the field strength, the transmission loss, the available signal-to-noise ratio and the circuit reliability.[14] At NEL this program was modified to include CCIR Report 322 noise.[12] The Collins Radio Company program produced in 1963 is similar to that of the CRPL and yields comparable data, but its calculation of LUF and auroral absorption was different.[15-16] In 1964, AVCO Corporation developed a computer program to determine the possible ways by which HF communication to and within polar regions may be maintained throughout ionospherically disturbed conditions.[17] Their program was intended only to be used at high sunspot number.

The first fully automated program, in which the oblique transmission equations for parabolic layers were used, was developed in August 1966 by Lucas and Haydon at Environmental Sciences Service Administration's (ESSA) Institute for Telecommunication Sciences and Aeronomy (ITSA).[18] This program

is commonly called ITSA-1 or HFMUFS. It provides better statistical description of the expected performance of radio systems depending upon ionospheric propagation of radio waves. The concepts of service probability and reliability are introduced in the HFMUFS program. The earlier versions of this program calculated f_0F2 and the $M(3000)F2$ as a function of local time by the method of Jones and Gallet.[19] Later versions of the program calculated f_0F2 and $M(3000)F2$ as a function of universal time using the method of Jones et al.[20] The former method had two major problems: (1) tendency of numerical maps to smooth out physical properties of the ionosphere, particularly at low latitudes, and (2) ambiguous values at geographic poles and resulting distortions in immediate surroundings. In the latter method, the second problem was overcome by means of a universal time analysis; a significant improvement was made in solving the first problem by incorporating the effect of the magnetic field variations. The version of the ITSA-1 program, obtained in May 1968 at NELC and now in use at NOSC, uses the new Jones method.

DNC-14, the Navy's recommended frequency bands and frequency guide for operating personnel establishing ship, shore and aircraft communication circuits, was adapted on the IBM 7090 from the ESSA-ITSA-1 program in August 1966. The data tape containing the numerical coefficients of f_0F2 and $M(3000)F2$ uses the earlier local time method of Jones and Gallet.[19] This data tape, dated August 1966, was never replaced by a tape containing the new coefficients because CNO (OP-094F) was considering the possibility of adapting the DNC-14 output into the newer ITS-78 program and because DNC-14 itself was being converted to the Univac 1108 computer. When the DNC-14 was converted to the Univac 1108 on November 1972, the old August 1966 tape was retained. The results using this program are promulgated in NTP 6 Supp. 1.[4]

Bell Aerosystems Company in 1967 developed a program for Rome Air Development Center (RADC) to provide loss calculations for RADC's interference prediction computer program.[21] Raytracing equations were used to obtain an output directly applicable to interference analysis. Techniques employed in this model, unlike most models, identified possible stable and unstable modes, including mixed modes. The ionospheric data used were the same as in the latest ESSA-ITSA version. Modes, radiation angles and losses were given for the different probability levels of ionospheric support.

In 1969 Barghausen et al, at the Institute for Telecommunication Sciences (ITS), developed a program, commonly called ITS-78 (Red Deck) or HFMUFES, which employed more extensive techniques; though similar to that in the ITSA-1 program, it incorporated significant changes.[22] The major changes are:

(a) All numerical coefficients representing the ionospheric characteristics are calculated as functions of universal time

(b) E-layer propagation characteristics are calculated from numerical coefficients representing the E-layer critical frequencies

(c) Numerical coefficients representing the minimum virtual height of the F-region have been included for calculating the semi-thickness of the F-layer

(d) Revised values of man-made noise and its frequency dependence have been included

(e) A method for combining two or more noise sources of nearly equal amplitudes has been added

(f) A new formula is used for estimating absorption, based upon extensive measurements, and including a winter anomaly effect

(g) System performance predictions can be made for sporadic-E propagation

(h) The chi-square probability distribution is used to evaluate all distributions

(i) Revised excess system losses have been included

In December 1970 ITS issued a revised version of the ITS-78, commonly called either the Blue Deck or HFMUFES 2. This program followed closely the models and methods described in ITS-78, except as outlined briefly below:

(a) Numerical coefficients representing the F2 layer critical frequency as a function of latitude, longitude and time were revised to include the solar cycle and seasonal variations of f_0F2[23]

(b) Numerical coefficients representing atmospheric noise as a function of universal time were included[24]

(c) The numerical maps of the representing minimum virtual height were revised

(d) Some revision was made to the world maps representing f_0E[25]

(e) Provision was made to use up to three different transmitting and receiving antennas over the HF band.

In December 1974 ITS issued a revised version of its ITS-78 line of computer programs, commonly called either the yellow deck or HFMUFES 3. Mainly, this version contained corrections to the code to remove known errors in the programming. Further, this version was the first of the HFMUFES series to allow input of antenna pattern data via magnetic tape.

Finally, in September of 1976 ITS issued HFMUFES 4, the current version of the HFMUFES series of programs.[26] The main difference between this program and earlier versions is that sporadic-E is no longer considered in the calculation of the MUF and reliability. In the earlier versions, sporadic-E was allowed as an option.

In 1978 NOSC developed a simplified HF MUF prediction algorithm called MINIMUF-3.[3] It was designed to complement existing large-scale HF propagation codes when computation resources were limited and large-scale codes were not feasible to execute. It was based on the idea that f_0F2 can be modeled to a first approximation as the logged response to a driving function proportional to $(\cos x)^n$ where x is the instantaneous solar zenith angle and when the daytime lag is quite seasonally dependent. It was shown to be sufficiently accurate to provide a MUF prediction suitable for use on small mobile propagation forecast (PROPHET) terminals. The most current model, called MINIMUF-3.5, allows MINIMUF-3 to be used out to the antipodal point.[27] MINIMUF-3 was constrained to be used in the 800-8000 km range. MINIMUF-3.5 has been compared against short range (192 km and 433 km) oblique sounder data.[28] Predictions for the 433 km path are reasonably close to observed mean MOFs. There is some over-prediction during the daytime, but very close correlation at night. However, the data for the 192 km path displayed a drastic MOF depression, caused by E-region cutoff. In this case, MINIMUF-3.5 was inadequate.

COMPARISON PROCEDURE

To develop a sufficient knowledge about the capabilities of the four pro-
grams being compared, they were compared against swept frequency HF oblique
sounder data. A MOF data base previously assembled for the MINIMUF develop-
ment task was used. The results will indicate how the models perform when
correlated with "real-world" propagation and will provide a relative indica-
tion of the differences between a first-order approximation and more sophisti-
cated prediction codes.

OBLIQUE SOUNDER DATA BASE PREPARATION

The oblique sounder data base that was assembled was derived from a vari-
ety of sources and spans the period between 1960 and 1976. This represents
over one complete solar sunspot cycle of propagation data. Attempts were made
to make the data base as diverse as possible including a variety of different
path lengths, orientations and geographical locations. While measurements
from several different types of oblique sounder systems were included, the
majority of data came from the Navy Tactical Sounder (NTSS).

Navy Tactical Sounder System (NTSS)

The Navy's oblique ionospheric sounder system consists of several shore-
based sounder transmitters and a number of sounder receivers. AN/FPT-11 (XN-
1) sounder transmitters were installed at selected Naval communication sta-
tions. The system receiver and an AN/UPR-2 receiver were installed at
selected Naval communications stations, research installations and aboard
ships.

Once each minute the FPT-11 transmitter sequentially transmitted a
double, biphase, Barker-coded pulse on each of 80 discrete frequencies between
2 and 32 MHz; the total scan consisted of 160 pulses lasting 16 seconds. The
frequency range is divided into four octave bands, with 20 channels linearly
spaced in each band. The 80 frequencies were spaced in 100 kHz increments in
the 2 to 4 MHz range (Band A), 200 kHz increments from 4 to 8 MHz (Band B),
400 kHz increments from 8 to 16 MHz (Band C) and 800 kHz increments from 16 to
32 MHz (Band D).

The UPR-2 receiver sequentially processed the pulse-train input by starting the gated receiver scan at the same time as the transmission. This was accomplished by synchronizing to a common timing source (i.e., WWV) and maintaining an accurate time base generator in the receiver. Since each sounder signal is composed of a series of 13 Barker-coded subpulses, signal processing is required in the receiver. The process gain over noise is 11 dB. A permanent record of the daily variations of the scanned spectrum between 2 and 32 MHz is produced on strip charts. To supplement this capability, NOSC developed a method of digitizing the video output signal and recording it on magnetic tape. The HF digital recorder (HFDR) developed for this purpose operates concurrently with the AN/UPR-2 receiver and in no way affects normal operation. Hence, with the HFDF equipped sounding receiving, all amplitude, time delay and frequency information are recorded once every minute, 24 hours a day.

Other Sounder Systems

Data collected prior to 1968 were measured on a variety of sounder systems. One system, used primarily by SRI, used the Model 900 series of sounders made by Granger Associates.[29] These scanned the range of frequencies from approximately 4 to 64 MHz in 4 one-octave bands of 40 linearly spaced channels each. The transmitted output is in pulses of 0.1 msec (short pulse) or 1.0 msec (long pulse) at 30-kw peak amplitude, repeated 2 or 4 times each channel. The long pulse is more appropriate for communication system sounding and also presents a higher average power which is often needed on long paths. The short pulse is used for mode resolution and is normally made as narrow as possible within the limitations set by the length of the sounded path. The entire scan was completed in 29 seconds and was repeated every 20 minutes. Another sounder system, a modified C-3 ionosonde transmitted 0.1 msec pulses; the transmitting frequency was swept linearly between 2 and 25 MHz.[30] In some instances data were acquired by means of a Granger transmitter and UPR-2 receiver.

Data Categorization

The source of the oblique sounder data is important because it influences the statistical significance of a given path-month. The overall sounder data were categorized into five sources:

a. NTSS-HFDF

b. NTSS-strip chart

c. Non-NTSS

d. Granger 900 series

e. Modified C-3

A path-month MOF curve from the NTSS-HFDF system is generally the product of approximately 40,000 digitally processed measurements (up to 1861 an hour over the month). The resolution of the NTSS-strip chart system limits this to about 2880 hand-scaled data points per path-month (120 per hour of the month). The Granger series data consisted of three scans per hour or 90 per hour of a month and 2160 per path-month. The modified C-3 data consisted of one 7.5 minute sweep every hour. This was equivalent to 720 per path-month (30 per hour per month). The non-NTSS system consists of 180 points per hour or 4320 data points per month.

The data can also be categorized according to the frequency range of the sounder transmitter. In the first three categories, the sounder scanned the range from 2 to 32 MHz. The Granger 900 series scanned the range from 4 to 64 MHz, and the modified C-3 scanned the range from 2 to 25 MHz.

DESCRIPTION OF OVERALL SOUNDER DATA BASE

The final oblique sounder data set consisted of 198 path-months of median hourly MOF values derived from 25 different HF transmission paths. The longest path was 7808 km and the shortest path was 192 km. The set contains a cross-section of transmission paths including mid-latitude, transauroral, transequatorial, all seasons and all solar sunspot numbers (SSN). Table 1 summarizes the basis against which the four programs were compared. The locations of the paths are shown in Figure 1 except for the two shortest paths (the scale is too small to illustrate them).

Path Number	Transmission Path	Latitude	Longitude	Path Length, km	Approximate Orientation from North	Number of Path Months	Percent of Sample	Year	OBN Range	Transmit Antenna	Receiver Antenna	Sounder Frequency Range, MHz	Data Type	Data Source
1.	Guam to Yokohama	13.47°N 35.48°N	144.79°E 139.47°E	2505	348.6°	13	6.6	1968-71 1974-76	71-107 12,34	Conical Monopole	HERMES 4R/8E13	2-32	NTSS(ST) NTSS(HFDR)	Ref 31 NOSC File
2.	Ft. Monmouth to Palo Alto	40.19°N 37.26°N	74.03°W 122.10°W	4131	281.4°	6	3.0	1961-63	26-50	VLPA G/A 726	VLPA G/A 726	4-64	Granger 900 Series	Ref 29
3.	Guam to Honolulu	13.47°N 21.51°N	144.79°E 158.00°W	6101	73.0°	24	12.1	1969-71 1974-76	72-106 13-33	Conical Monopole	Rhombic	2-32	NTSS(ST) NTSS(HFDR)	Ref 31 NOSC File
4.	Guam to Kodiak	13.47°N 57.67°N	144.79°E 152.46°W	7140	21.9°	6	3.0	1969-71	71-106	Conical Monopole		2-32	NTSS(ST)	Ref 31
5.	Honolulu to Kodiak	21.42°N 57.67°N	158.14°W 152.46°W	4057	5.1°	6	3.0	1969-71	71-106	Conical Monopole		2-32	NTSS(ST)	Ref 31
6.	Honolulu to Washington, DC	21.42°N 38.75°N	158.14°W 76.85°W	7808	55.0°	4	2.0	1964	10	Conical Monopole		4-64	Granger 900 Series	Ref 32
7.	Davis, CA to Honolulu	38.50°N 21.51°N	121.68°W 158.00°W	3944	241.2°	4	2.0	1964	10			4-64	Granger 900 Series	Ref 32
8.	Palo Alto to Falmouth	37.26°N 44.00°N	122.10°W 11.70°W	8344	53.4°	1	0.5	1964	10			4-64	Granger 900 Series	Ref 11
9.	Boulder to Pt. Barrow	40.00°N 71.10°N	105.10°W 156.79°W	4482	330.9°	3	1.5	1960	114-120	Horizontal V	Sloping V	2-25		Ref 30
10.	Honolulu to Yokohama	21.42°N 35.48°N	158.14°W 139.47°E	6194	299.2°	8	4.0	1968 1974-76	105-108 13-34	Conical Monopole		2-32	NTSS(ST) NTSS(HFDR)	Ref 31 NOSC File
11.	Philippines to Yokohama	15.35°N 35.48°N	120.37°E 139.47°E	2937	36.8°	2	1.0	1968	105-106	Conical Monopole		2-32	NTSS(ST)	Ref 31
12.	Philippines to N.E. Holt	15.35°N 22.32°S	120.37°E 114.15°E	4244	189.3°	16	8.1	1968-69	105-110	Conical Monopole		2-32	NTSS(ST)	Ref 31
13.	Guam to N.E. Holt	13.47°N 22.32°S	144.79°E 114.15°E	5197	220.4°	18	9.1	1968-71	71-110	Conical Monopole	Rhombic	2-32	NTSS(ST)	NOSC File
14.	Davis, CA to Kodiak	38.12°N 57.76°N	121.47°W 152.52°W	3112	324.1°	10	5.1	1969	104-108	VLPA		2-32	NTSS(ST)	Ref 31
15.	Honolulu to Corona	21.42°N 33.86°N	158.14°W 117.55°W	4200	61.9°	22	11.1	1968-70	104-111	Conical Monopole	HERMES 8E13 Loop	2-32	NTSS(ST)	NOSC File
16.	Andora to Thessaloniki	69.00°N 40.38°N	15.00°E 22.56°E	3214	168.0°	1	0.5	1964	18	Rhombic Vee	Vee	4-64	Granger 900 Series	Ref 33
17.	Davis, CA to La Posta	38.50°N 12.67°N	121.68°W 116.43°W	802	142.2°	6	3.0	1971	64-70	VLPA	HERMES 8E13 Loop	2-32	NTSS*(ST)	NOSC File

Table 1. HF propagation oblique sounder data links.

10

Path Number	Transmission Path	Latitude	Longitude	Path length, km	Approximate Orientation (from North)	Number of Path Months	Percent of Sample	Year	SSN Range	Transmit Antenna	Receive Antenna	Sounder Frequency Range, MHz	Data Type	Data Source
18.	Toulouse to Neihakri	41.00°N 30.09°N	2.00°E 23.90°E	1521	99.1°	4	2.0	1974-75	22-26		CDAA	2-32	NTSS**(HFDR)	NOSC File
19.	Honolulu to La Posta	21.42°N 32.67°N	158.14°W 116.43°W	4387	64.0°	14	7.1	1974-76	12-35	Conical Monopole	Hermes BE13 Loop	2-32	NTSS(HFDR)	NOSC File
20.	Coco Solo to Stockbridge	9.37°N 43.00°N	79.88°W 75.50°W	3764	5.8°	7	3.5	1966-67	56-79	VLPA	CDAA	4-64	Granger 3902	Ref 34
21.	Andoya to New Delhi	69.00°N 28.59°N	15.00°E 77.20°E	5958	105.2°	6	3.0	1964	10-20	Rhombic	VLPA G/A 726	4-64	Granger 900 Series	Ref 35
22.	Palo Alto to Thule	37.26°N 76.50°N	122.10°W 68.80°W	5069	15.2°	2	1.0	1964	10-18	VLPA G/A 726	VLPA G/A 726	4-64	Granger 900 Series	Ref 33
23.	Toulouse to Keflavik	43.00°N 63.98°N	2.00°E 22.59°E	2806	334.6°	13	6.6	1975-76	12-22	Conical Monopole	VLP-3	2-32	NTSS**(HFDR)	NOSC File
24.	Ft. Monmouth to Aberdeen	40.19°N 39.58°N	74.03°W 76.14°W	196	247.6	1	0.5	1970	16?	Granger 798	Vertical Delta	2-32	Granger 3905-5	Ref 36
25.	Ft. Monmouth to Camp Drum	40.19°N 44.00°N	74.03°W 75.69°W	44?	342.6	1	0.?	1971	71	Log-spiral	Vertical Delta	2-32	Granger 3905-5	Ref 37

Table 1. continued.

11
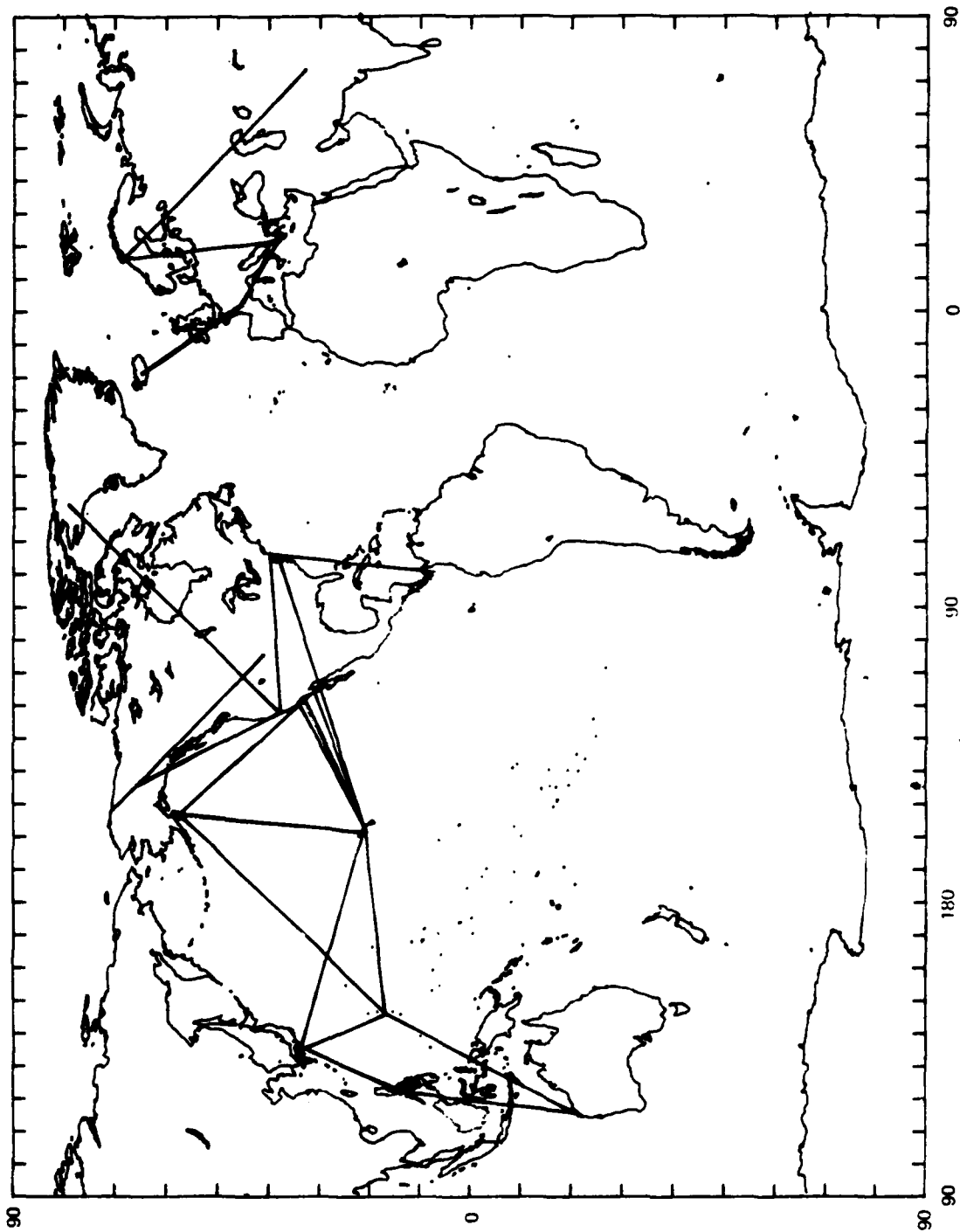
Figure 1.   HF oblique sounder paths in MOF data base.

DATA SCREENING

In the comparison of the program, it is highly desirable to subdivide the data base into subsets according to variables influencing the predicted and observed results (e.g., path length, season, month, geomagnetic latitude, sunspot number, local time at path midpoint, etc.). To accomplish this a computer program called DASCR3 (acronym for data screening 3) was used. Each of the prediction programs was run for each of the paths in Table 1. The results along with auxillary information about the propagation situation (e.g., path length, local time of day, sunspot number, etc.) were stored in a data file to be used later by DASCR3.

DASCR3

DASCR3 is a program designed to perform data screening and statistical comparison on two large matrices of observations. For each set of matrices, up to 10 sets of information are read in on propositions to be satisfied and limits on a selected variable. A portion of each matrix is read in and tested for each set of propositions in turn. For each subset satisfying a given set of conditions, the variable to be analyzed is stored temporarily on disc. The next portion of each matrix is then read in and screened and the good observations are added to those already on disc. When the entire matrix has been screened the screened data are then read into core and the difference (or residual) between the two matrices is taken. These arrays are then sorted to ensure maximum computer efficiency for the statistical evaluation. Finally, a statistical evaluation is then performed of the screened data and their residuals.

An example of the output from DASCR3 is given in Figure 2. In this sample the ITSA-1 program, using the universal time set of numerical coefficients, is compared to the observed data. The proposition to be satisfied is that the data to be evaluated be for month equal 1 (January). The variables being compared are the observed MOF and predicted MUF. In the printout the observed data are represented by column A and the predicted values are represented by column B. The residual (the observed data minus the predicted value) is given by column D. The relative residual is given by column D/A, and the absolute relative residual by column ABS(D)/A. The left hand side of

DATA SCREENING PROBLEM 1   ESSAI TSA1(UNIV) HF PROPAGATION

CONDITIONS TO BE SATISFIED
MONTH   EQ   1.000000

SUMMARY STATISTICS FOR VARIABLE 15

	OBSERVED MUF	PREDICTED MUF			
STATISTIC	A	B	D	D/A-1	ABS(D)/A
TOTAL					
POPULATION SIZE					
AVERAGE					
R.M.S. VALUE					
MEAN ABSOLUTE ERROR					
STANDARD DEVIATION					
3RD MOMENT ABOUT MEAN					
4TH MOMENT ABOUT MEAN					
5TH MOMENT ABOUT MEAN					
6TH MOMENT ABOUT MEAN					
LOWER DECILE					
LOWER QUARTILE					
MEDIAN					
UPPER QUARTILE					
UPPER DECILE					
5.00TH PERCENTILE					
95.00TH PERCENTILE					
INTERQUARTILE RANGE					
COEFFICIENT OF VARIATION					
MINIMUM					
MAXIMUM					
COEFFICIENT OF SKEWNESS					
COEFFICIENT OF EXCESS					
INTERVAL SIZE					
GIVEN LOWER BOUND					
GIVEN UPPER BOUND					
CORRELATION COEFFICIENT					

A MATRIX = OBSERVED

MEAN SQUARE ERROR   15.414810
LINEAR MEAN SQUARE ERROR   14.62997
SLOPE   .934087
INTERCEPT   .407082

Figure 2.   Example output from DASCR3.

14

the page shows the statistics calculated for each of these columns. In addition the correlation coefficient between the observed and predicted data are given. Included also are the slope, intercept and mean square error of linear regression. In this example 288 data points were selected by DASCR3 from 4668 data points. Note that the average absolute relative residual for this case is 25.9 percent.

Screening Data Base

Each computer program was run to produce a data base corresponding to the observed data base. Auxilliary information outputted to be screened included: universal time of propagation, month, year, sunspot number, path length in kilometers, geographic latitude and longitude of the path midpoint, the local time at the path midpoint, the path orientation with respect to north, the geomagnetic latitude at each of the control points, the predicted MUF, E-layer MUF, F-layer MUF, FOT, HPF and path identification number and sounder type.

Before the actual data screening was begun, data points in both observed and predicted bases corresponding to observed values at the extremes of the particular measuring sounder were removed from the data base. The final number of hourly values in the data base was 4668 points.

ANALYSIS OF RESIDUALS BETWEEN PREDICTIONS AND OBSERVED DATA

An indication of the accuracy of the numerical predictions of MUF can be obtained from a study of the residuals between observed data and predicted values. The terms residual, relative residual and absolute relative residual are used with the following standard meaning:

$$\text{residual} = (\text{observed datum}) - (\text{predicted value}) \tag{1}$$

$$\text{relative residual} = \frac{\text{residual}}{\text{observed datum}} \tag{2}$$

$$\text{absolute relative residual} = \frac{\text{absolute residual}}{\text{observed datum}}. \tag{3}$$

Certain statistical measures of these terms have proved useful in past ionospheric studies in comparing predicted and observed data.[23] These include:

(1) The average residual (av. res.)

(2) Root mean square residual (rms res.)

(3) The mean absolute error of the residual (mae res.)

(4) The average relative residual (av. rel. res.)

(5) The root mean square relative residual (rms rel. res.)

(6) The mean absolute error of the relative residual (mae rel. res.)

(7) The average absolute relative residual (ave. abs. rel. res.)

(8) Correlation coefficient between observed and predicted values

(9) The standard error of the estimate of linear regression.

Values of each of these parameters are produced by DASCR3 as can be seen by examining Figure 2.

The average residual and the average relative residual locate the center of the distributions of error and are sometimes referred to as the bias in the estimate. Figures 3 and 4 illustrate the average residual and average relative residual, respectively, as a function of month for the four programs being compared. In this example, MINIMUF-3.5 is shown to have the smallest bias; whereas, HFMUFES 4 tends to always predict high by as much as 3.5 MHz or 17.5 percent.

The mean absolute errors of th residual and relative residual are a measure range of the error and are the first moments about the average residual and average relative residual, respectively. They provide information about the range of variation. Figures 5 and 6 are examples of these two parameters, respectively, for MINIMUF-3.5. They are displayed as bars about the average residual (bias) as a function of month. The mae of the residual is rather uniform as a function of month. However, Figure 6 shows that the range of variation in the error during the equinox months March and September to be greater than the other months.

The average absolute relative residual is a measure of the average magnitude of the error. Figure 7 shows a plot of the average absolute relative residual as a function of month for the four programs being compared.
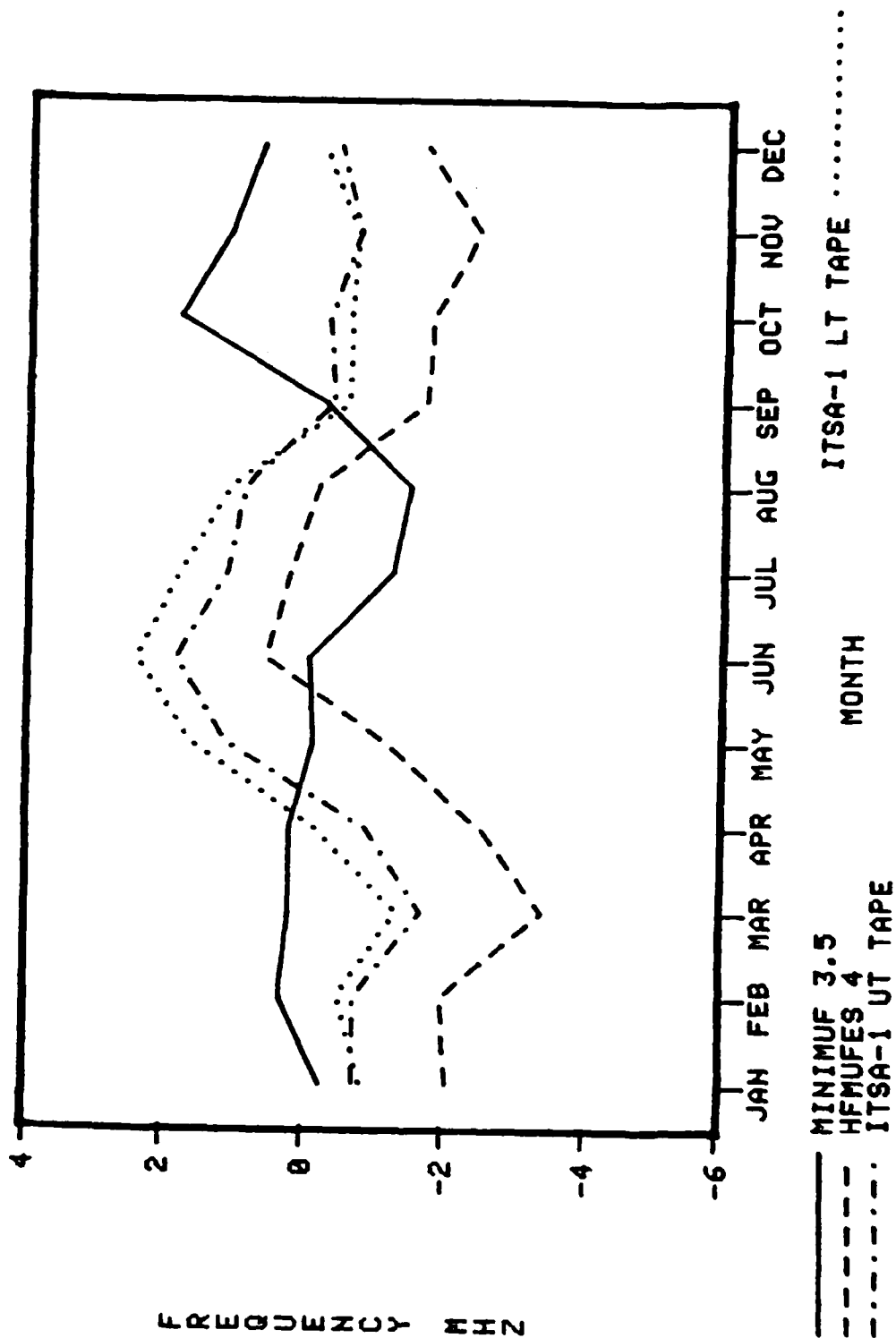
Figure 3.   Average residual (bias) as a function of month.

Figure 4. Average relative residual (relative bias) as a function of month

Figure 5. Average residual (bias) for MINIMUF-3.5 with the mean absolute error about the average residual.

19

Figure 6. Average relative residual (relative bias) for MINIMUF-3.5 with the mean absolute error about the average relative residual.

Figure 7. Magnitude of the error (average absolute relative residual) as a function of month.
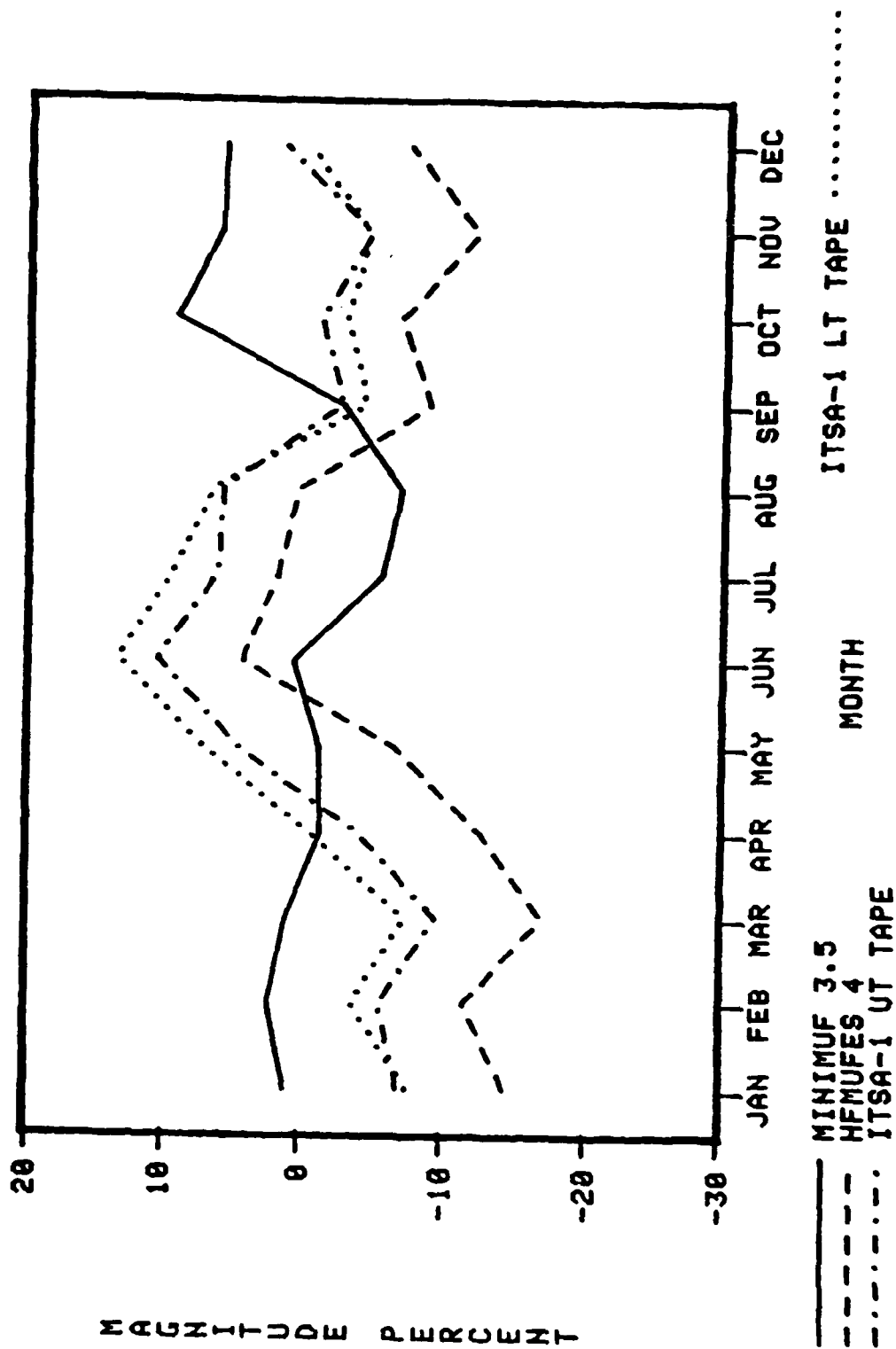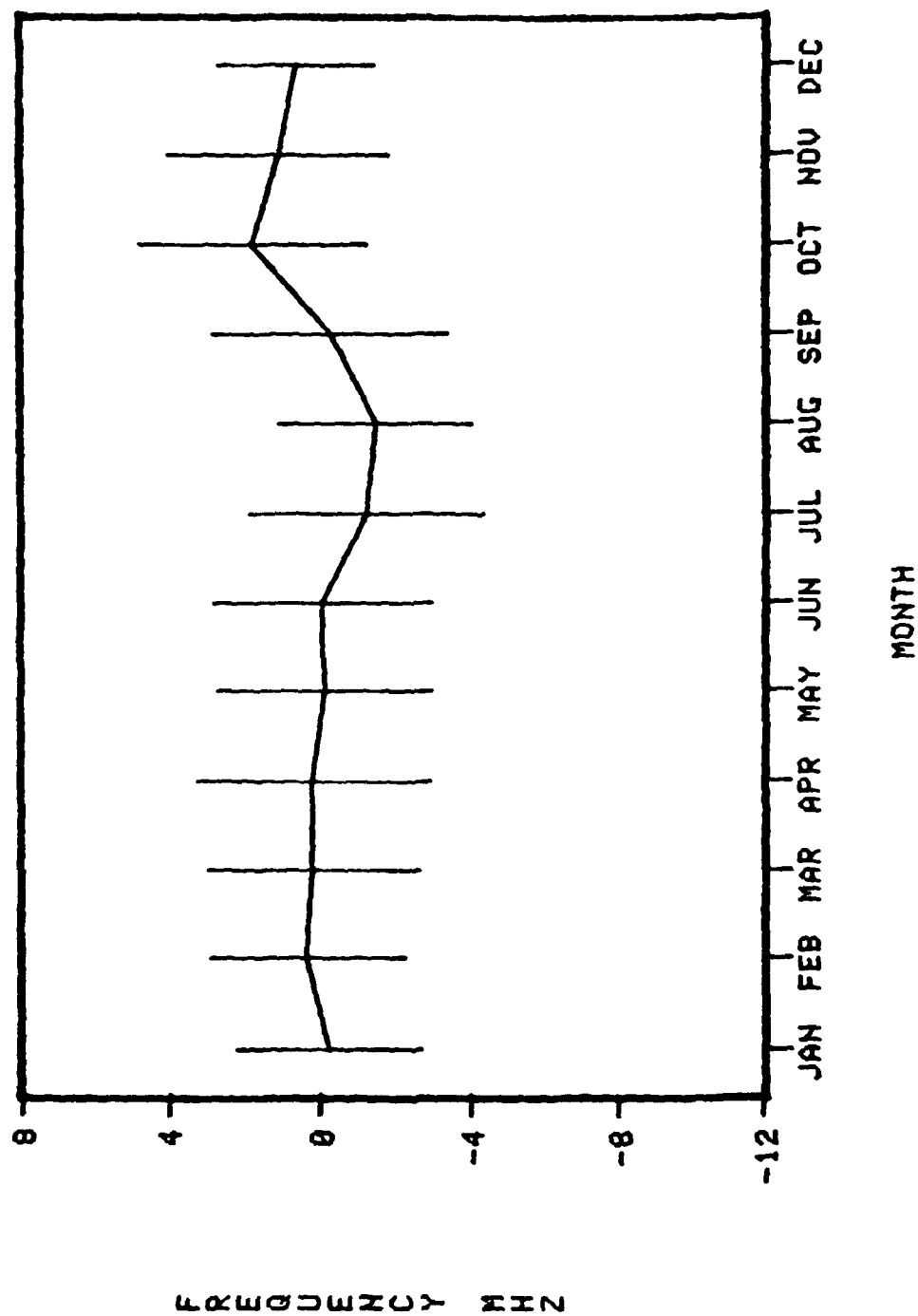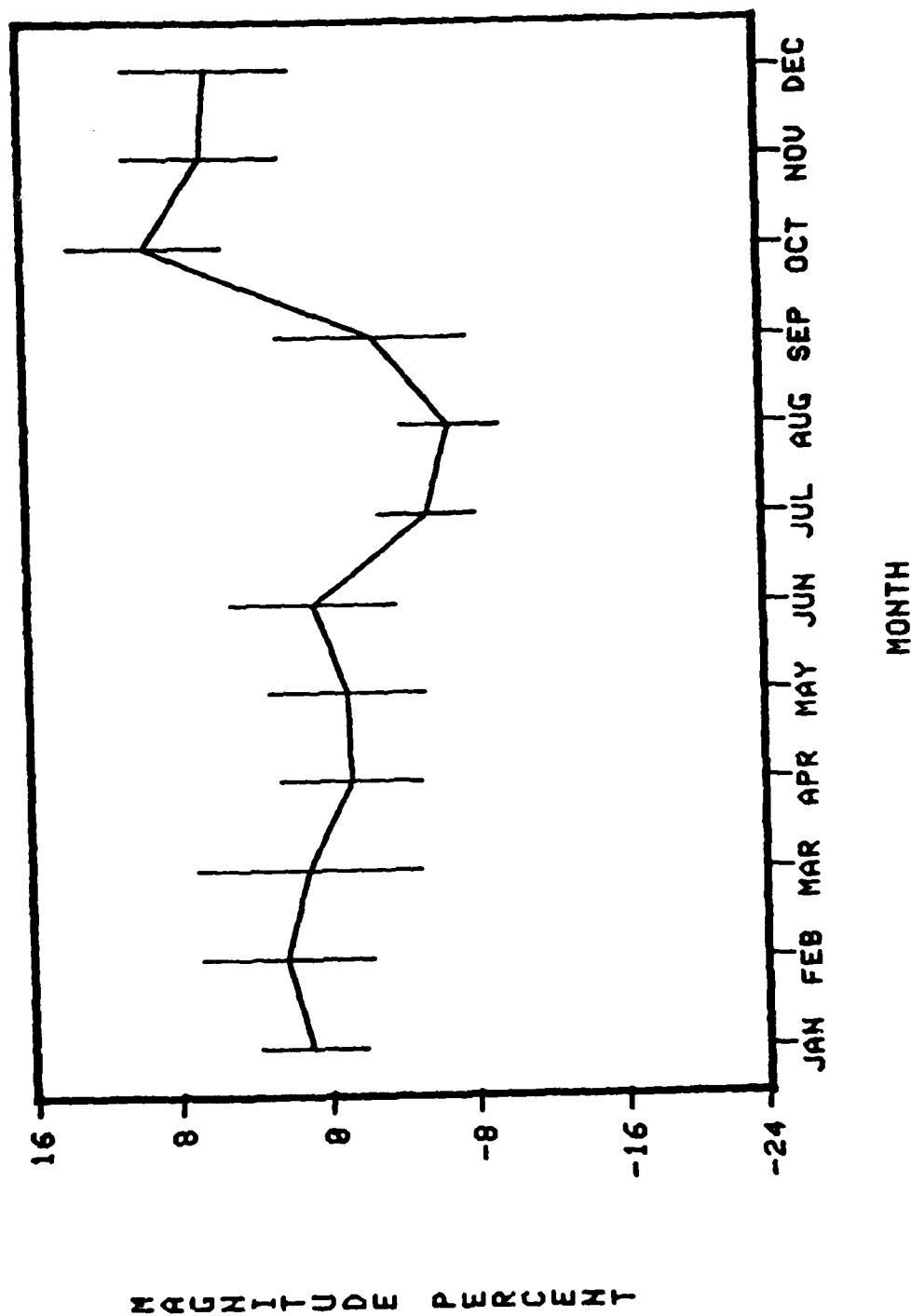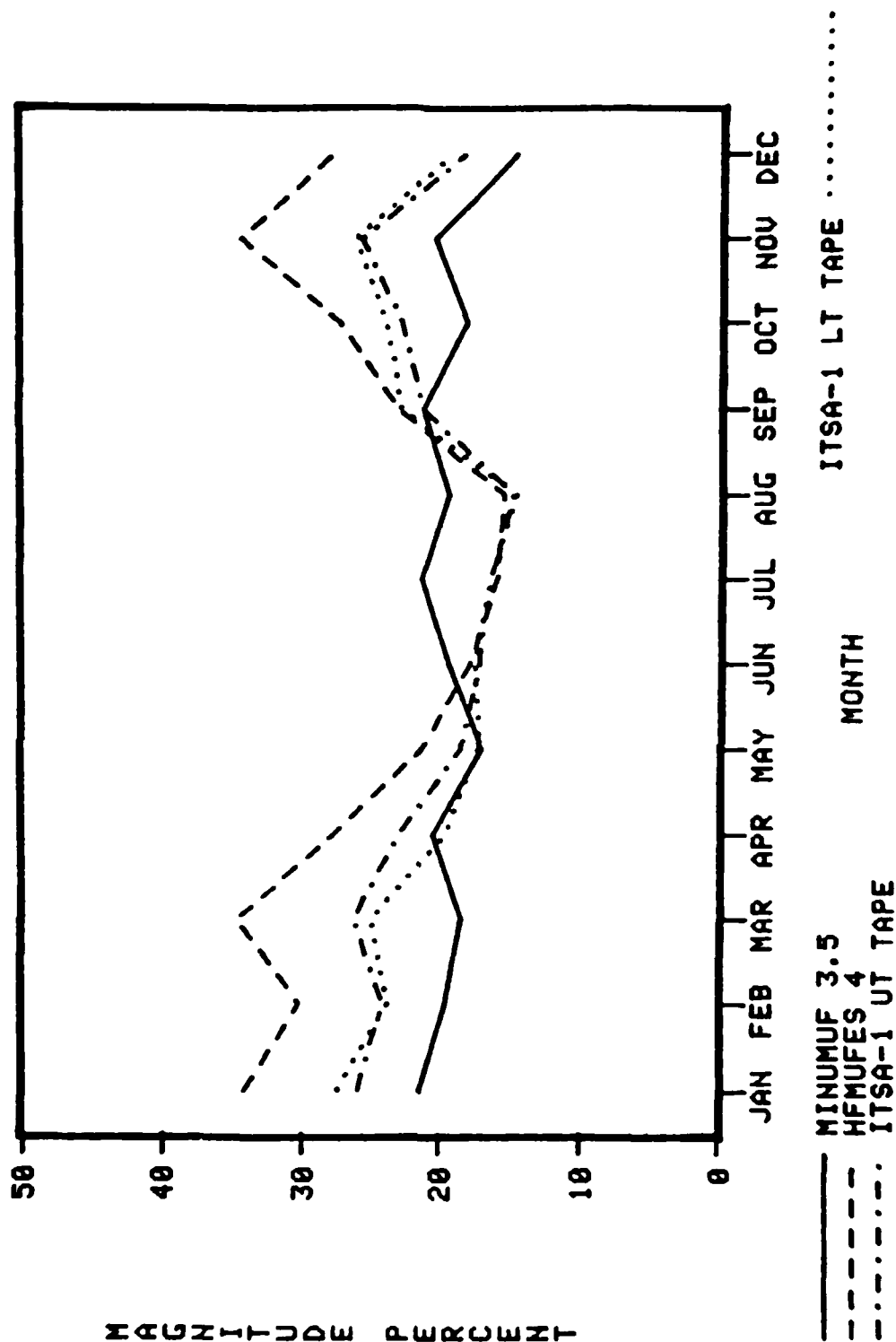
The root mean square residual and relative residuals are measures of the dispersion in the error. In fact, the rms residual and rms relative residual are the standard deviations of the error about the origin (zero bias) and are related to the standard deviation about the mean according to

$$\sigma^2 = \nu_2 - \nu_1^2 \qquad (4)$$

where ν_2 the mean square error (the square of the rms error) and ν_1 is the bias. When the bias is small or nearly zero, then the standard deviation and the rms error are nearly the same. Otherwise, the rms error is larger than the standard deviation. Figures 8 and 9 are examples of the rms residual and rms relative residual, respectively, for the four programs being compared as a function of month. MINIMUF-3.5 has the lowest rms error reaching its highest value of 4 MHz plus (12 percent) during October; whereas, HFMUFES 4 has its lowest values during the summer months and has the highest rms error during the winter months.

A measure of the degree of association or the closeness of fit between variables is given by the correlation coefficient. It indicates the strength of the tendency for high (or low) values of one variable to be associated with high (or low) values of the other variable. Figure 10 is an example of the correlation coefficients for the four programs being compared as a function of month. In this example HFMUFES 4 generally has the highest correlation coefficient with MINIMUF-3.5 also showing consistently high values.

A description of the nature of the relationship between variables is called regression analysis.[38] Regression analysis is concerned with the problem of describing or estimating the value of one variable, called the dependent variable, on the basis of one or more other variables, called independent variables. In other cases regression may be used merely to describe the relationship between known values of two or more variables.

Regression analysis that involves the determination of a linear relationship between two variables is referred to as simple linear regression. Here, the variable y is given as y = a + bx where x is the independent variable and y is the dependent variable. The coefficients a and b are determined in the regression analysis. A measure of the success of linear regression analysis is the standard error of the estimate given by
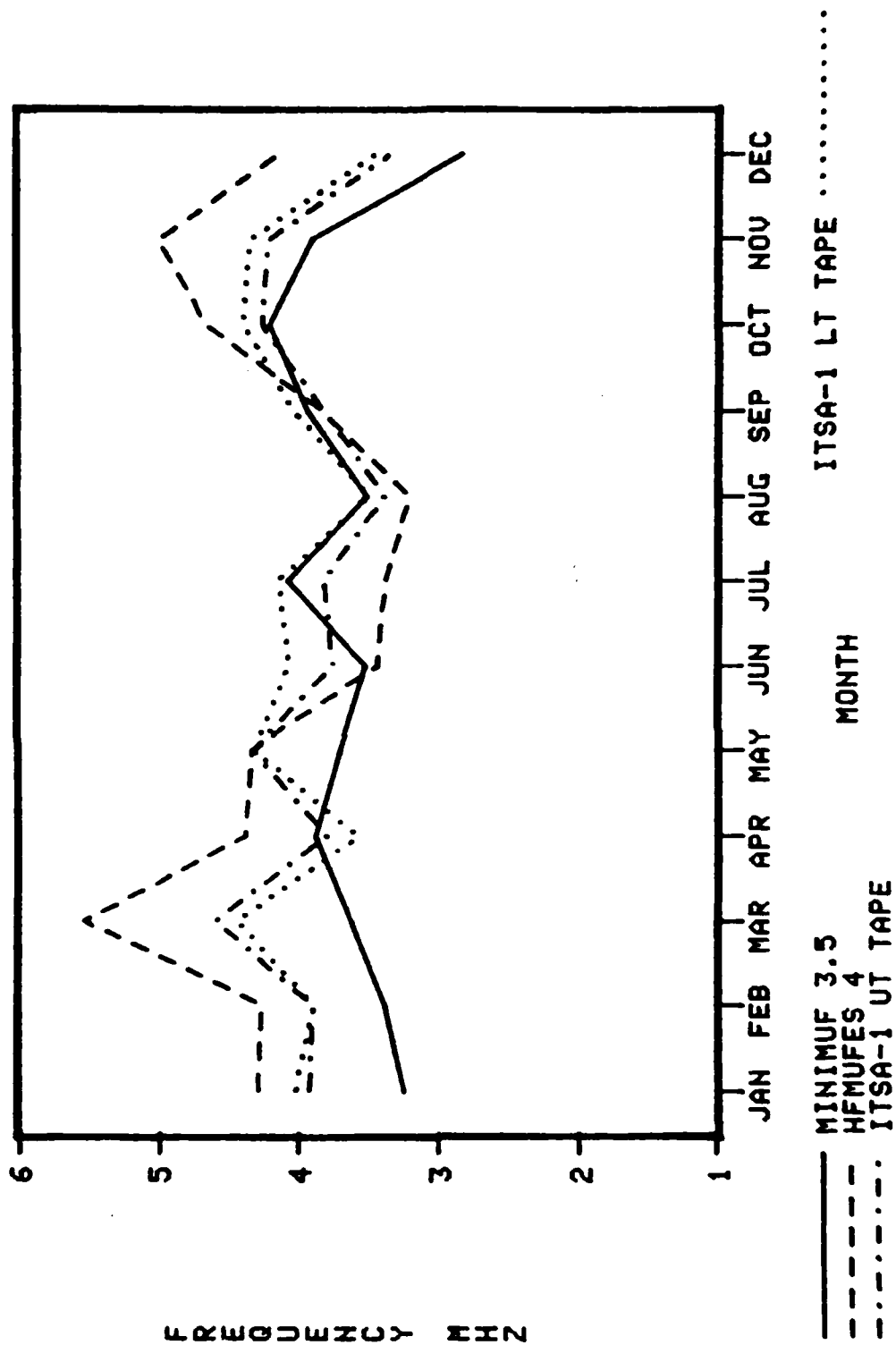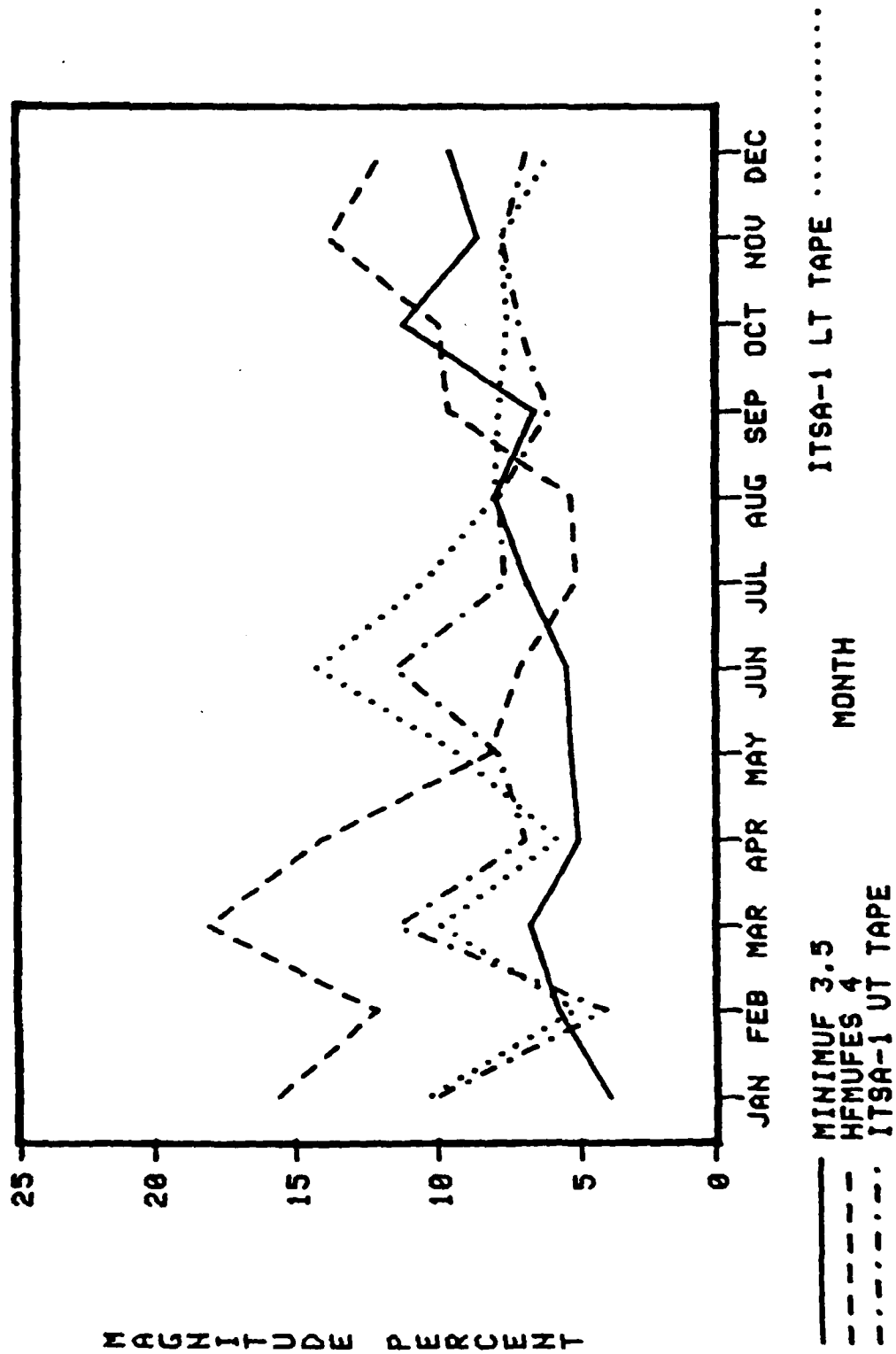
22

Figure 8. Rms error in MHz as a function of month.

Figure 9. Rms relative error in percent as a function of month.

24
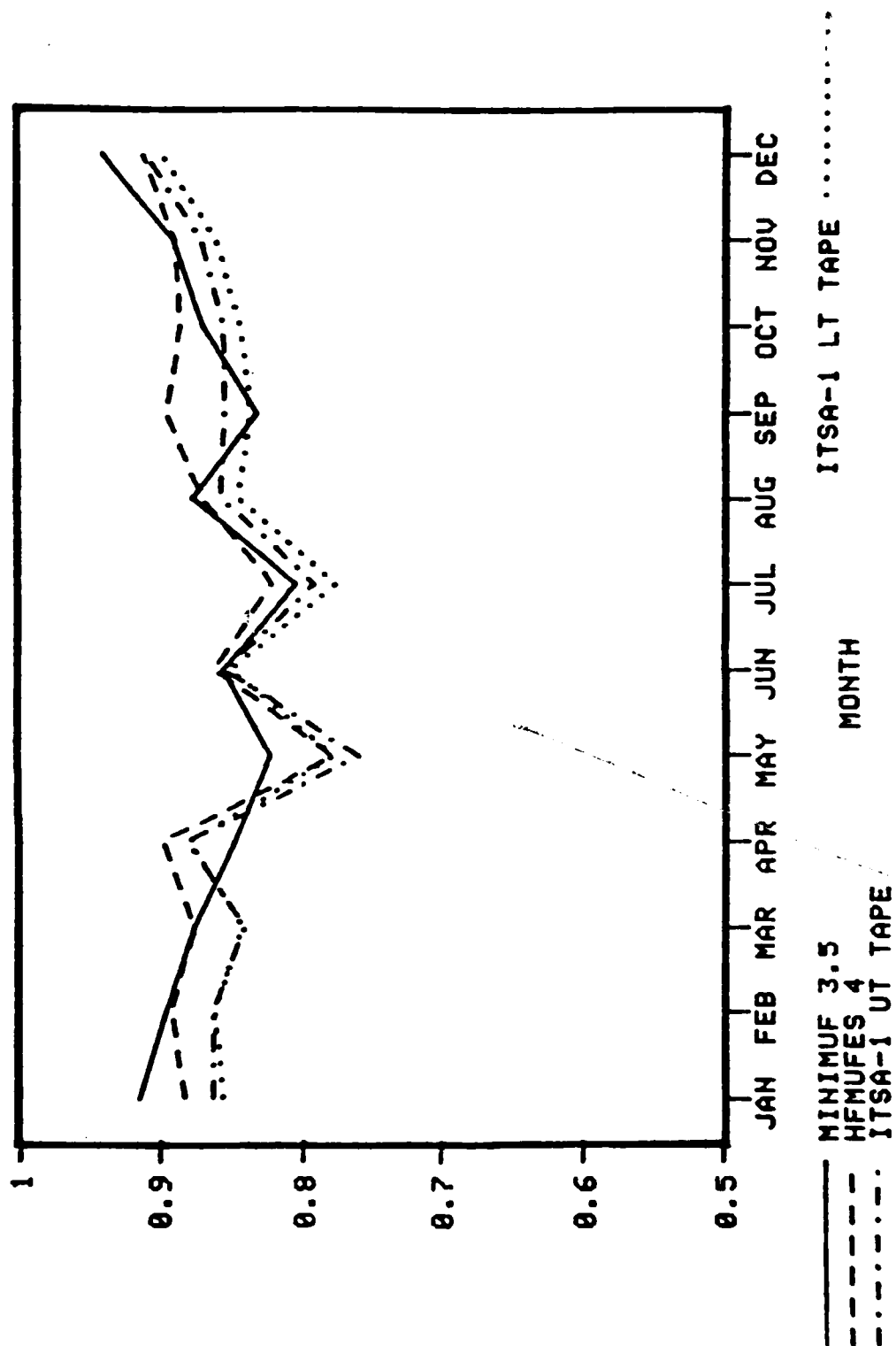
Figure 10. Correlation coefficients as a function of month.

$$S_{y \cdot x} = [\sigma_y^2 (1 - \gamma^2)]^{1/2} \qquad (5)$$

where σ_y is the standard deviation in the observed datum and γ is the correlation coefficient between the observed data and predicted values. If the relationship is truly linear, then the bias of the estimate should be removed (or made nearly zero). An estimate of the standard error of mean is given by

$$S_{\overline{y} \cdot x} = \frac{S_{y \cdot x}}{\sqrt{n}} \qquad (6)$$

A measure of the error in the regression coefficient is given by

$$S_b = \sqrt{\left[\frac{S_{\overline{y} \cdot x}}{\sigma_x} \right]^{1/2}} \qquad (7)$$

where σ_x the standard deviation in the predicted values. Figures 11 and 12 show the standard error of the estimate of linear regression and of standard error of mean in linear regression, respectively, as a function of month. When Figure 11 is compared to Figure 8, the largest change occurs for HFMUFES 4. Very little change is shown for ITSA-1 with local time tape. MINIMUF-3.5 shows some changes for some months but not all. Figure 12 shows that linear regression has removed much of the bias in the predicted MUFs.

COMPARISON RESULTS

This section will present the results MUF prediction comparisons. The objective is to provide the reader with a clear understanding of the capabilities and limitations of each prediction model.

ALL CASES

The oblique sounder data base consisted of 198 path-months of observed MOFs taken over 25 transmission paths. The shortest path was 196 km and the longest path was 7808 km. For each program being compared, Tables 2-5 list the paths and the bias, the rms error, the average magnitude of the error, and the correlation coefficient between the MOFs and MUFs for each path. Table 2 shows MINIMUF 3.5 to have zero percent bias for three paths and to predict

26

Figure 11. Standard rms error of estimate of linear regression as a function of month.

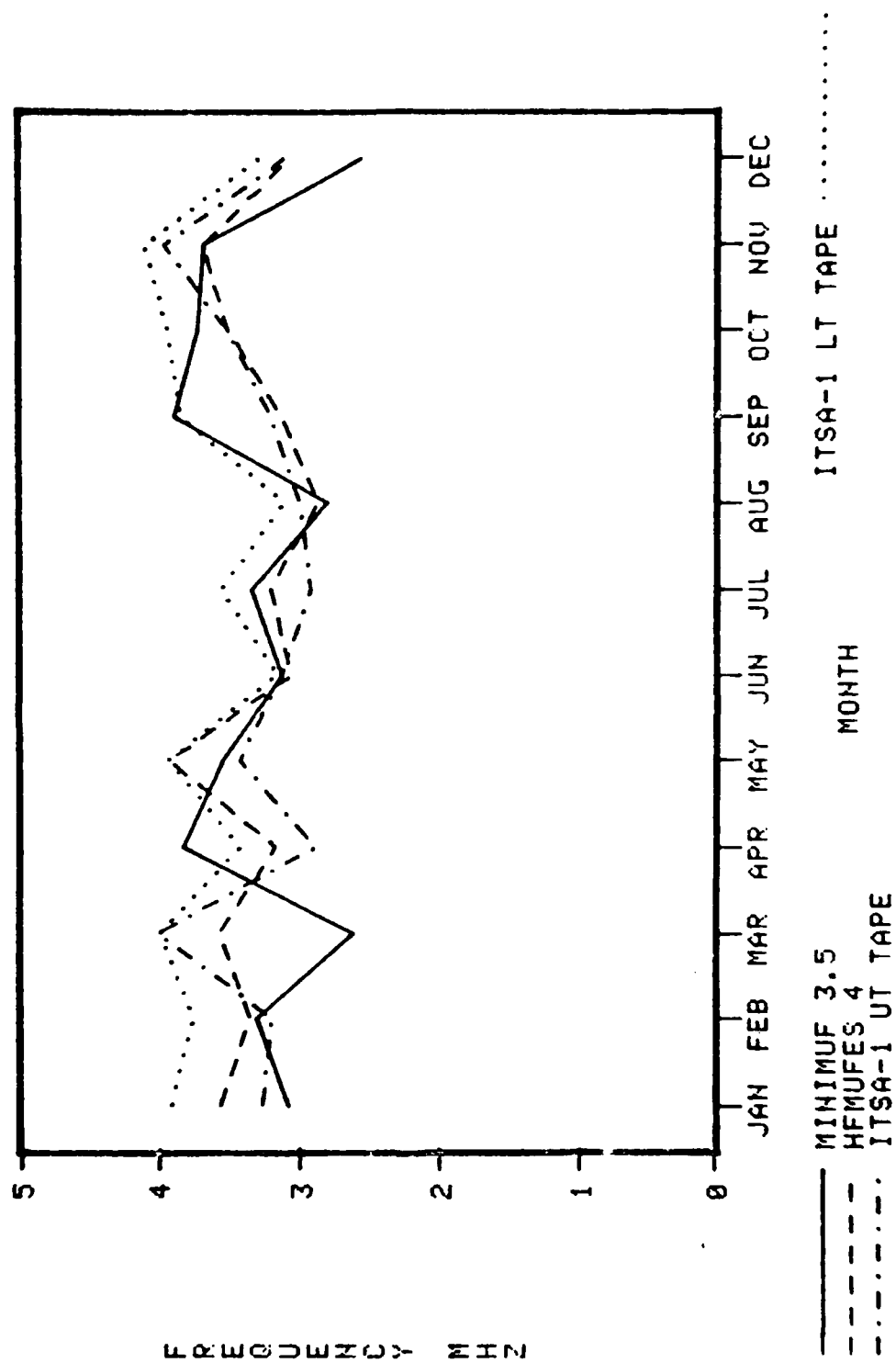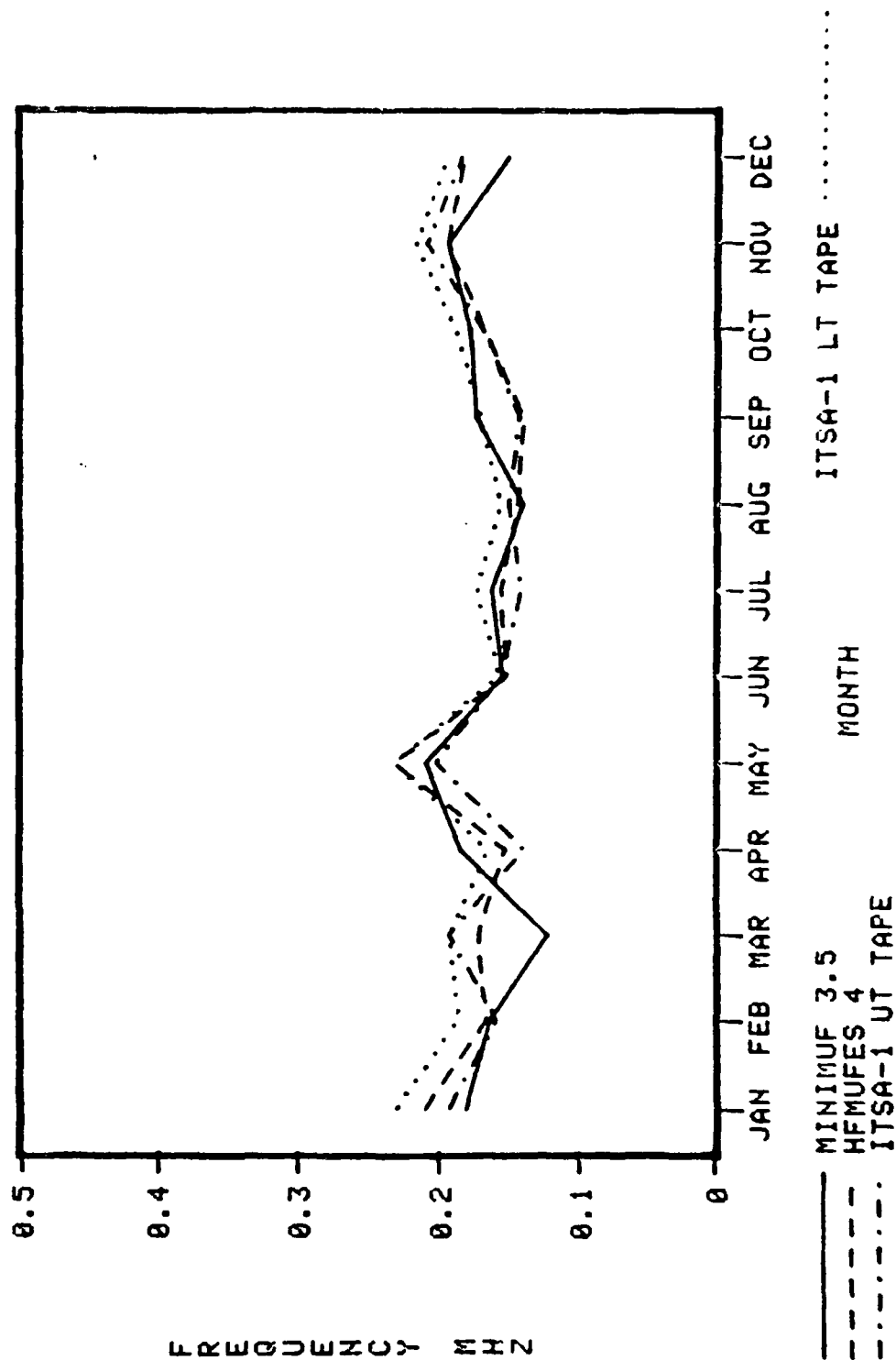Figure 12. Standard error of the mean of linear regression as a function of month.

No.	Transmission Path	Bias, MHz	%	rms, MHz	error, %	Magnitude, %	Correlation Coefficient
1	Guam to Yokohama, Japan	0.03	0.0	5.15	8.9	27.5	0.665
2	FT Monmouth, NJ to Palo Alto, CA	1.73	8.4	4.12	11.2	19.2	0.818
3	Guam to Honolulu, Hawaii	0.34	1.0	3.00	4.2	14.5	0.884
4	Guam to Kodiak, Alaska	-2.14	-10.5	3.87	14.5	22.2	0.872
5	Honolulu, Hawaii to Kodiak, Alaska	0.08	-0.0	2.40	5.8	12.2	0.928
6	Honolulu, Hawaii to Washington, DC	2.24	13.7	3.61	15.7	14.7	0.881
7	Davis, CA to Honolulu, Hawaii	-1.14	-5.3	3.29	9.5	19.0	0.861
8	Palo Alto, CA to Fairbanks, Alaska	0.83	3.2	2.17	9.7	9.3	0.747
9	Boulder, CO to Pt. Barrow, Alaska	-0.01	0.0	4.21	8.5	20.2	0.385
10	Honolulu, Hawaii to Yokohama, Japan	-2.31	-11.8	4.32	12.4	23.7	0.862
11	Tarlac, Philippines to Yokohama, Japan	-0.33	-0.0	3.55	13.1	13.3	0.877
12	Tarlac, Philippines to H.E. Holt, Australia	1.48	6.8	4.31	10.3	14.4	0.767
13	Guam to H. E. Holt, Australia	-1.55	-5.2	4.67	10.2	19.0	0.797
14	Davis, CA to Kodiak, Alaska	-2.07	-13.1	5.29	16.9	33.2	0.713
15	Honolulu, Hawaii to Corona, CA	1.25	1.9	3.33	11.2	15.1	0.947
16	Andoya, Norway to Thessoloniki, Greece	.94	4.5	2.36	8.7	15.4	0.933
17	Davis, CA to La Posta, CA	1.40	15.0	2.46	19.4	17.8	0.734
18	Toulouse, France to Neimakri, Greece	-2.99	-29.4	4.05	35.2	42.1	0.820
19	Honolulu, Hawaii to La Posta, CA	-0.79	-4.9	2.70	10.6	18.8	0.827
20	Coco Solo, Canal Zone to Stockbridge, NY	-0.50	-2.3	2.79	5.8	12.1	0.933
21	Andoya, Norway to New Delhi, India	2.17	14.8	3.00	15.7	14.9	0.891
22	Palo Alto, CA to Thule, Greenland	2.77	18.3	3.33	19.5	16.9	0.913
23	Toulouse, France to Keflavik, Iceland	1.42	11.0	2.46	13.3	11.8	0.896
24	FT Monmouth, NJ to Aberdeen, NY	-1.46	-18.3	1.89	21.7	23.8	0.806
25	FT Monmouth, NJ to Camp Drum, NY	-1.17	-14.8	1.61	15.3	20.9	0.875

Table 2. MINIMUF 3.5 comparison by sounder path.

29.4 percent too high for the Toulouse, France, to Nermakri, Greece path. This same path had the largest rms relative residual (35.2 percent) and the largest average magnitude of the error (42.1 percent). The paths with highest correlation coefficients (Honolulu, Hawaii, to Kodiak, Alaska; Honolulu, Hawaii, to Corona, California; Andoya, Norway, to Thessoloniki, Greece; and Coco Solo, Canal Zone, to Stockbridge, New York) all have low bias, rms error, and magnitude of error. Table 3 shows HFMUFES 4 to generally have larger bias than MINIMUF-3.5, but has more paths with correlation coefficient greater than 0.9 than does MINIMUF-3.5. Tables 4 and 5, for the two versions of ITSA-1, show them to have slightly higher bias than MINIMUF-3.5 but also to be slightly higher correlated with the observed data than MINIMUF 3.5.

Table 6 shows the overall comparison results. When compared, overall MINIMUF-3.5 and the two ITSA-1 versions can be separated by only a few tenths of a percent in bias and rms error and by just one percent in magnitude of the error. However, HFMUFES 4 clearly has the largest bias (7.2 percent high), rms error (8.3 percent), and magnitude of error (26.0 percent). Table 6 also shows that HFMUFES 4 has the highest value of correlation coefficient and that the largest reduction in rms using linear regression is achieved by HFMUFES 4 (rms error of 4.24 MHz reduced to a standard error of estimate of 3.50 MHz). This indicates that the relationship between predicted results by HFMUFES 4 and the observed MOFs is more nearly linear than the other programs and that its errors may be due in part to some simple reason.

DATA TYPE

A critical part of any investigation involving the use of observed measurements is the quality and time resolution of the measurements. This is particularly important when multiple samples are merged into mean values, as was the case with the oblique sounder data. As discussed in the section on data preparation, there were five types of sounder data used: (1) NTSS-HFDR, (2) NTSS-strip chart, (3) non-NTSS, (4) Granger 900 series and (5) modified C-3. The number of data points per hour per month determining the hourly medians were: (1) 160, (2) four, (3) six, (4) three, and (5) one for the five data categories, respectively. Table 7 gives sample percentage for each data category.

No.	Transmission Path	Bias, MHz	%	rms, MHz	error, %	Magni-tude, %	Corre-lation Coeffi-cient
1	Guam to Yokohama, Japan	-3.39	-18.5	6.75	19.4	41.6	0.697
2	FT Monmouth, NJ to Palo Alto, CA	-0.22	-4.1	2.82	11.0	16.7	0.901
3	Guam to Honolulu, Hawaii	-0.99	-3.1	3.31	7.6	18.5	0.924
4	Guam to Kodiak, Alaska	-3.14	-18.8	4.10	21.1	24.9	0.886
5	Honolulu, Hawaii to Kodiak, Alaska	-1.86	-12.7	4.02	17.5	23.1	0.834
6	Honolulu, Hawaii to Washington, DC	4.39	23.3	5.36	23.9	23.1	0.812
7	Davis, CA to Honolulu, Hawaii	-0.08	0.5	2.81	4.7	14.0	0.885
8	Palo Alto, CA to Fairbanks, Alaska	3.12	-15.9	3.65	16.6	15.5	0.777
9	Boulder, CO to Pt. Barrow, Alaska	0.28	-0.5	1.99	6.7	9.5	0.796
10	Honolulu, Hawaii to Yokohama, Japan	-2.00	-10.2	3.81	11.7	20.8	0.898
11	Tarlac, Philippines to Yokohama, Japan	-1.05	-3.8	2.46	6.1	8.7	0.844
12	Tarlac, Philippines to H.E. Holt, Australia	-3.34	-12.6	4.39	13.3	17.6	0.899
13	Guam to H. E. Holt, Australia	0.90	3.7	2.45	4.4	8.3	0.909
14	Davis, CA to Kodiak, Alaska	-1.25	-8.4	5.66	11.6	30.5	0.656
15	Honolulu, Hawaii to Corona, CA	5.67	32.7	2.44	14.2	52.2	0.929
16	Andoya, Norway to Thessoloniki, Greece	-1.52	-13.1	2.00	14.8	18.2	0.975
17	Davis, CA to La Posta, CA	1.66	17.0	2.62	20.4	19.0	0.739
18	Toulouse, France to Neimakri, Greece	-4.79	-49.3	6.04	50.7	65.2	0.639
19	Honolulu, Hawaii to La Posta, CA	-3.75	-26.0	4.96	26.7	37.5	0.816
20	Coco Solo, Canal Zone to Stockbridge, NY	-1.15	-4.4	2.71	6.5	12.9	0.961
21	Andoya, Norway to New Delhi, India	1.96	12.2	2.68	12.7	13.2	0.912
22	Palo Alto, CA to Thule, Greenland	2.46	11.9	3.67	20.5	21.7	0.864
23	Toulouse, France to Keflavik, Iceland	0.69	5.2	2.60	7.0	15.6	0.836
24	FT Monmouth, NJ to Aberdeen, NY	0.82	11.1	0.95	11.7	10.3	0.861
25	FT Monmouth, NJ to Camp Drum, NY	0.30	3.0	0.71	5.0	7.9	0.945

Table 3. HFMUFES 4 comparison by sounder path

No.	Transmission Path	Bias, MHz	%	rms, MHz	error, %	Magnitude, %	Correlation Coefficient
1	Guam to Yokohama, Japan	-3.16	-17.8	6.67	18.9	40.8	0.672
2	FT Monmouth, NJ to Palo Alto, CA	2.81	12.9	4.57	17.7	19.9	0.853
3	Guam to Honolulu, Hawaii	-1.12	-4.1	3.30	7.4	18.6	0.922
4	Guam to Kodiak, Alaska	-2.60	-15.9	3.48	18.3	21.1	0.902
5	Honolulu, Hawaii to Kodiak, Alaska	-0.09	-5.3	3.53	16.6	18.2	0.852
6	Honolulu, Hawaii to Washington, DC	4.52	23.3	5.37	23.8	22.6	0.832
7	Davis, CA to Honolulu, Hawaii	2.01	9.9	3.39	11.1	13.2	0.864
8	Palo Alto, CA to Fairbanks, Alaska	3.14	16.1	3.72	16.7	15.5	0.742
9	Boulder, CO to Pt. Barrow, Alaska	4.15	21.7	4.69	22.2	21.4	0.754
10	Honolulu, Hawaii to Yokohama, Japan	-1.77	-9.4	3.64	11.0	19.8	0.895
11	Tarlac, Philippines to Yokohama, Japan	-0.59	-1.9	2.03	5.4	7.1	0.888
12	Tarlac, Philippines to H.E. Holt, Australia	-0.10	1.8	4.36	11.0	16.8	0.819
13	Guam to H. E. Holt, Australia	1.41	5.8	2.69	6.3	8.8	0.907
14	Davis, CA to Kodiak, Alaska	-0.99	-7.4	5.39	11.1	28.4	0.665
15	Honolulu, Hawaii to Corona, CA	0.21	-4.9	4.43	18.4	23.3	0.844
16	Andoya, Norway to Thessoloniki, Greece	-1.53	-13.6	2.00	15.5	19.0	0.975
17	Davis, CA to La Posta, CA	1.94	19.3	2.77	21.7	19.3	0.710
18	Toulouse, France to Neimakri, Greece	-4.74	-49.1	5.91	50.4	64.1	0.649
19	Honolulu, Hawaii to La Posta, CA	-0.47	-2.9	2.34	6.3	15.3	0.862
20	Coco Solo, Canal Zone to Stockbridge, NY	0.17	-0.1	2.97	6.4	11.4	0.920
21	Andoya, Norway to New Delhi, India	1.66	10.1	2.52	10.9	12.7	0.905
22	Palo Alto, CA to Thule, Greenland	2.41	12.0	3.55	19.5	20.9	0.872
23	Toulouse, France to Keflavik, Iceland	0.51	4.0	2.68	6.1	16.7	0.824
24	FT Monmouth, NJ to Aberdeen, NY	1.06	14.4	1.19	14.8	13.6	0.816
25	FT Monmouth, NJ to Camp Drum, NY	0.56	6.3	0.90	7.7	10.4	0.935

Table 4. ITSA-1 (universal time tape) comparison by sounder path.

No.	Transmission Path	Bias, MHz	%	rms, MHz	error, %	Magnitude, %	Correlation Coefficient
1	Guam to Yokohama, Japan	-3.07	-17.5	6.57	18.9	40.4	0.668
2	FT Monmouth, NJ to Palo Alto, CA	2.58	10.6	4.66	18.2	21.6	0.827
3	Guam to Honolulu, Hawaii	-1.05	-4.2	3.34	6.7	18.8	0.906
4	Guam to Kodiak, Alaska	-1.92	-11.9	3.34	15.4	19.8	0.862
5	Honolulu, Hawaii to Kodiak, Alaska	0.50	-2.3	4.17	16.9	19.9	0.771
6	Honolulu, Hawaii to Washington, DC	4.38	22.7	5.17	23.0	22.2	0.852
7	Davis, CA to Honolulu, Hawaii	2.47	12.2	3.84	13.6	14.9	0.838
8	Palo Alto, CA to Fairbanks, Alaska	3.82	20.2	4.29	20.3	19.3	0.747
9	Boulder, CO to Pt. Barrow, Alaska	4.39	22.9	5.10	23.6	22.4	0.601
10	Honolulu, Hawaii to Yokohama, Japan	-1.32	-7.9	3.42	10.4	18.1	0.887
11	Tarlac, Philippines to Yokohama, Japan	-0.64	-2.0	2.04	6.5	6.9	0.932
12	Tarlac, Philippines to H.E. Holt, Australia	0.08	2.4	4.56	10.5	17.6	0.784
13	Guam to H. E. Holt, Australia	1.19	5.2	2.54	6.2	8.2	0.915
14	Davis, CA to Kodiak, Alaska	-0.96	-7.0	5.74	10.9	30.3	0.631
15	Honolulu, Hawaii to Corona, CA	0.68	-3.6	4.50	19.6	21.7	0.854
16	Andoya, Norway to Thessoloniki, Greece	-1.00	-9.6	1.45	11.6	13.7	0.982
17	Davis, CA to La Posta, CA	2.00	19.7	2.75	21.6	18.1	0.713
18	Toulouse, France to Neimakri, Greece	-4.30	-44.0	5.55	45.4	59.0	0.662
19	Honolulu, Hawaii to La Posta, CA	-0.41	-2.8	2.37	7.8	15.7	0.853
20	Coco Solo, Canal Zone to Stockbridge, NY	1.17	3.6	3.40	8.2	10.9	0.907
21	Andoya, Norway to New Delhi, India	2.04	13.1	2.77	13.8	13.4	0.908
22	Palo Alto, CA to Thule, Greenland	2.96	16.0	3.94	21.9	22.4	0.879
23	Toulouse, France to Keflavik, Iceland	0.72	5.6	2.95	7.7	18.0	0.792
24	FT Monmouth, NJ to Aberdeen, NY	1.07	14.2	1.17	14.3	13.6	0.820
25	FT Monmouth, NJ to Camp Drum, NY	0.89	11.1	1.23	11.7	14.1	0.893

Table 5. ITSA-1 (local time tape) comparison by sounder patn.

Program	Bias MHz	%	rms, MHz	error, %	Magni-tude %	Corre-lation Coeffi-cient	Standard Error of the Estimate, MHz
MINIMUF-3.5	0.08	0.6	3.71	3.6	20.3	0.866	3.56
HFMUFES 4	-1.49	-7.2	4.24	8.3	26.0	0.871	3.50
ITSA-1 (Universal Time Tape)	-0.06	-0.3	3.95	3.5	21.6	0.850	3.75
ITSA-1 (Local Time Tape)	0.16	0.7	4.04	3.5	21.5	0.840	3.86

Table 6. Overall comparison results.

Measurement Method	Sample Path Hours	Percent of Sample
NTSS-HFDR	1416	30.3
NTSS-strip chart	2388	51.2
Non-NTSS	48	1.0
Granger 900 series	744	15.9
Modified C-3	72	1.5

Table 7. Number of samples per sounder data type.

Figures 13 and 14 show the average residual (bias) and average relative residual, respectively, as a function of data type. MINIMUF-3.5 has a near zero bias much of the time except for the non-NTSS data. The biases in the two ITSA-1 programs follow each other very closely with the bias being smaller for ITSA-1 with universal time tape. HFMUFES 4 predicts high by more than 10 percent for 81.5 percent of the sample and low for the remaining portion of the data.

Figures 15 and 16 show the rms error and relative rms error, respectively. The rms error for MINIMUF-3.5 is less than 8 percent for all the data except the non-NTSS data, which represents only 1 percent of the sample. For the NTSS data, HFMUFES 4 has its highest rms error, being as high as 13 percent. For the NTSS data, the two ITSA-1 programs fall between MINIMUF-3.5 and HFMUFES 4. The ITSA-1 program is shown to have slightly lower rms error.

Figure 17 shows the magnitude of the error. This figure clearly illustrates the lower magnitude of the error of MINIMUF-3.5. For the type of data for which HFMUFES 4 has low bias and rms error, its magnitude of the error is also lowest.
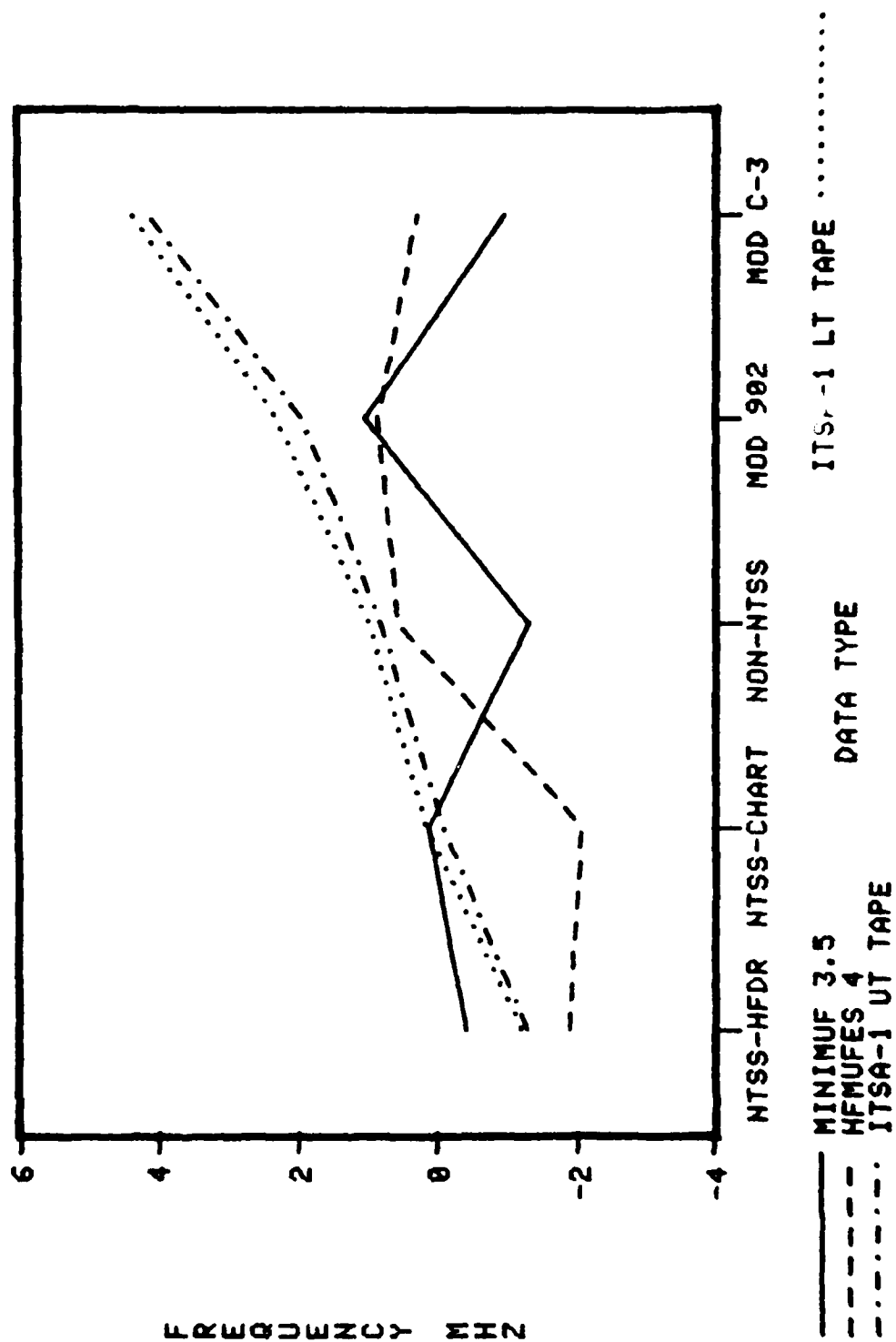
34

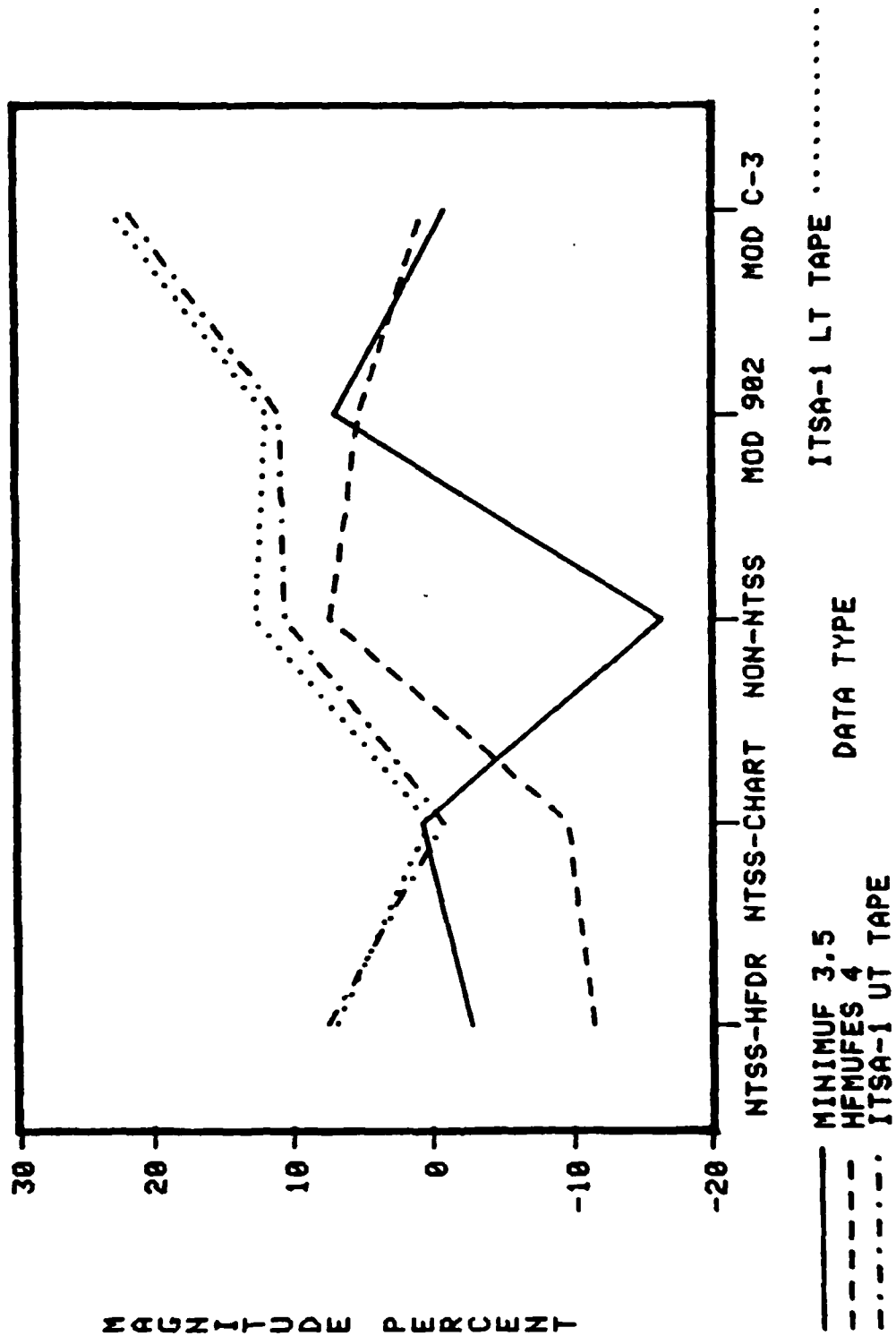Figure 13. Average residual (bias) as a function of data type.

35

Figure 14. Average relative residual (relative bias) as a function of data type.

FREQUENCY MHz

5

4

3

2

1

0

NTSS-HFDR NTSS NTSS-CHART NON-NTSS MOD 902 MOD C-3

DATA TYPE
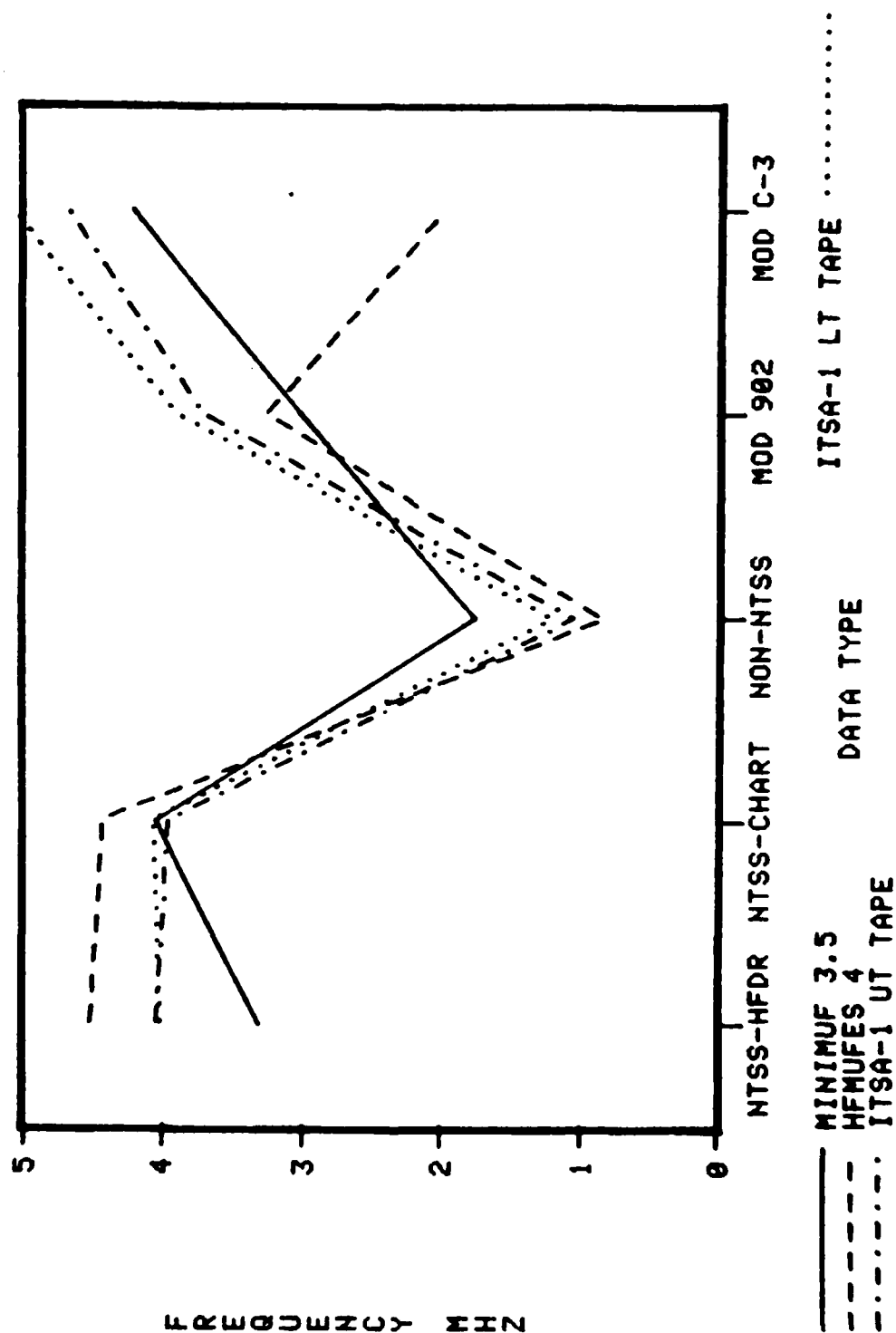
MINIMUF 3.5
HFMUFES 4
ITSA-1 UT TAPE

ITSA-1 LT TAPE

Figure 15. Rms error in MHz as a function of data type.

37
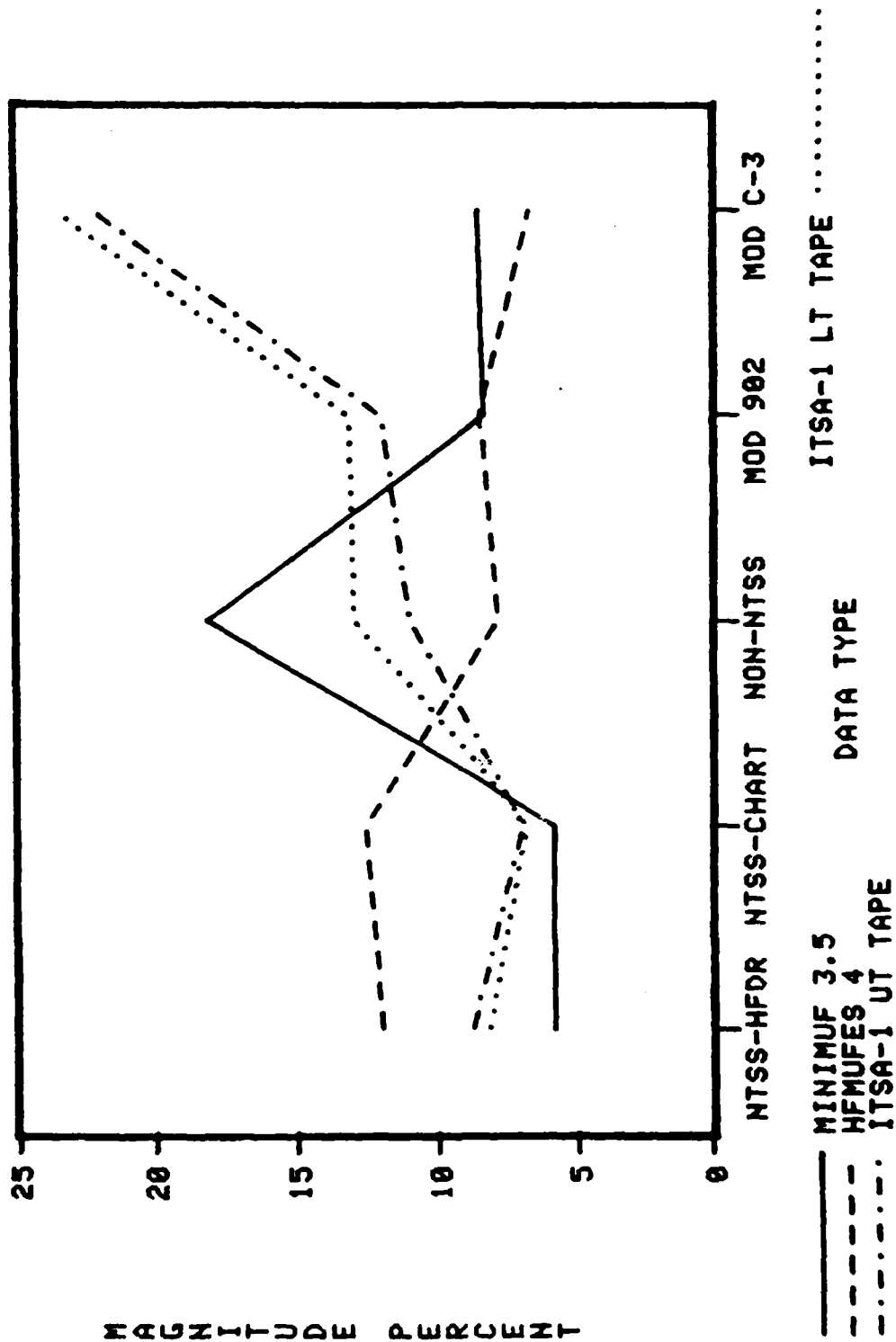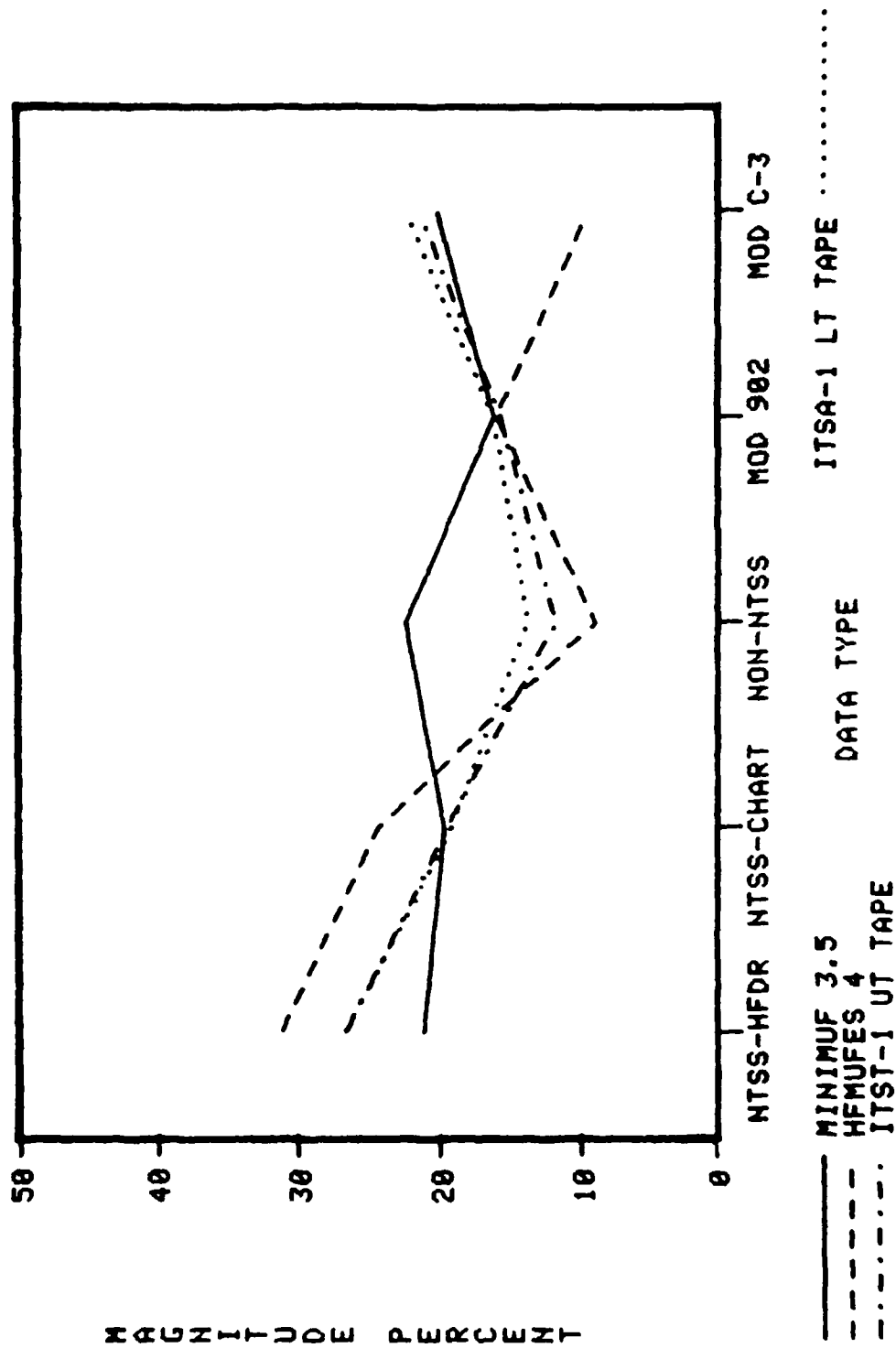
Figure 16. Relative rms error as a function of data type.

Figure 17. Magnitude of the error (average absolute relative residual) as a function of data type.

Figure 18 shows the correlation coefficient of the predicted MUF and observed MOF as a function of data type. It indicates the generally high correlation of all four programs with the data type except the modified C-3 data. In this case the one sample per hour might not be sufficient for obtaining a good monthly median at each hour.
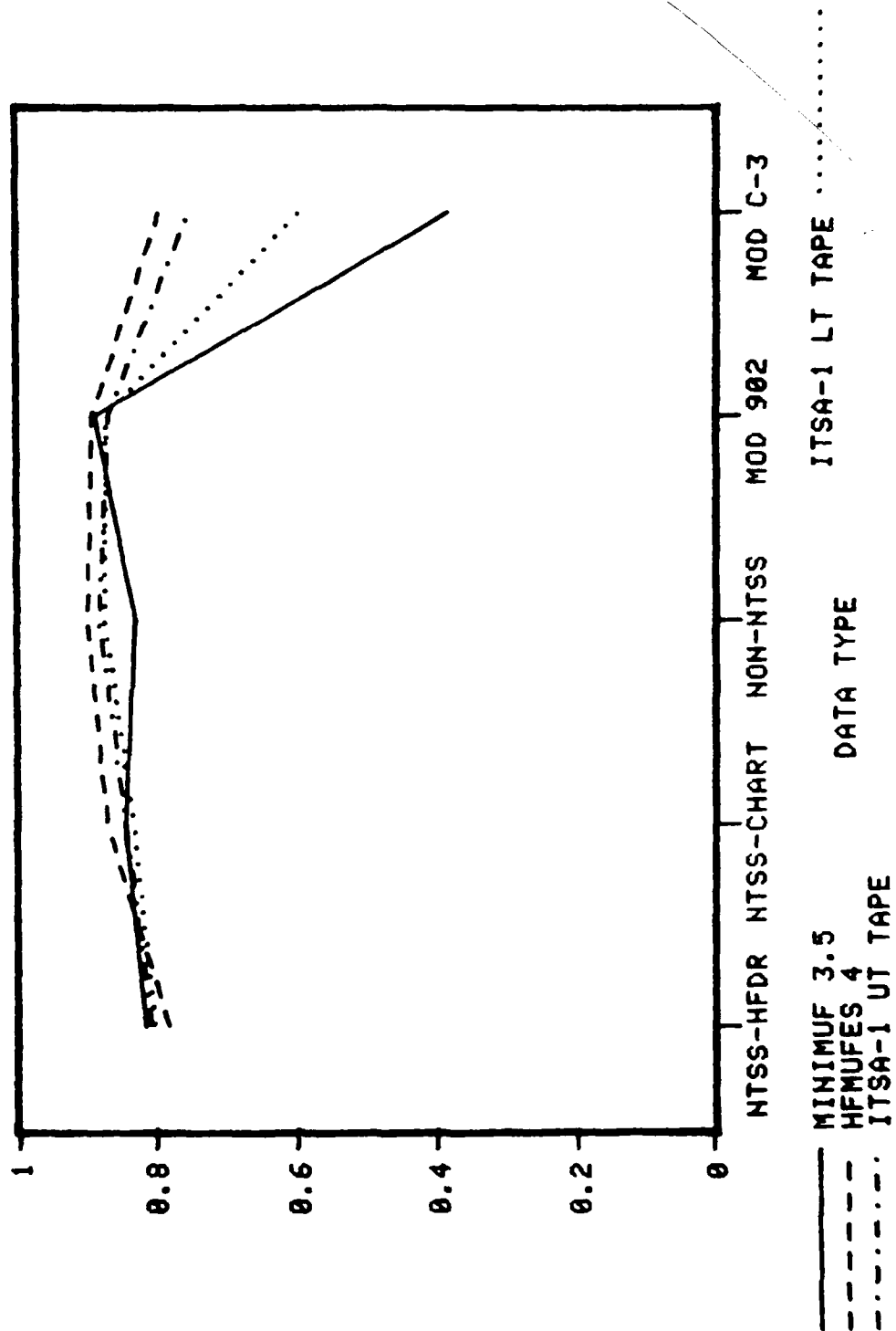
Figure 18. Correlation coefficients as a function of data type.

41

PATH LENGTH

Figures 19-24 show the distribution of MUF prediction error as a function of path length. Table 8 shows the percentage of the sample in each path length range. Figures 19 and 20 show the average residual and average relative residual, respectively. They show MINIMUF-3.5 to have the smallest bias in general for path lengths at or lower than 4000 km. Beyond 4000 km, MINIMUF-3.5 and the ITSA-1 programs have nearly the same bias. HFMUFES 4 has the highest bias and always tends to predict high. Figures 21 and 22 show the rms error and the relative rms error, respectively. There is a peak in rms error at 2000 km. However, this range is represented by only one path: the Toulouse, France, to Neimakri, Greece, path which comprises only two percent of the sample. With one exception Figure 22 shows all four programs to have less than 10 percent rms error beyond 2000 km. The exception occurs for HFMUFES 4 in the range 4000 to 5000 km. Figure 23 shows that the average magnitude of the error as a function of range is generally less than 20 percent except at the previously highlighted ranges: 1000-2000 km and 4000-5000 km. Figure 24 shows the correlation between the predicted MUF and observed MOF at ranges beyond 1000 km, MINIMUF-3.5 shows correlation coefficients greater than 0.8; whereas, the correlation coefficients for the other three programs increase with increasing range to a peak of approximately 0.95 at 7000 km where a sharp decline then begins.

Percentage of Sample	Length	Numbers of Hours
L < 1000	192	4.1
1000 < L < 2000	96	2.1
2000 < L < 3000	640	13.7
3000 < L < 4000	552	11.8
4000 < L < 5000	1608	34.4
5000 < L < 6000	586	12.6
6000 < L < 7000	754	16.2
7000 < L < 8000	240	5.1

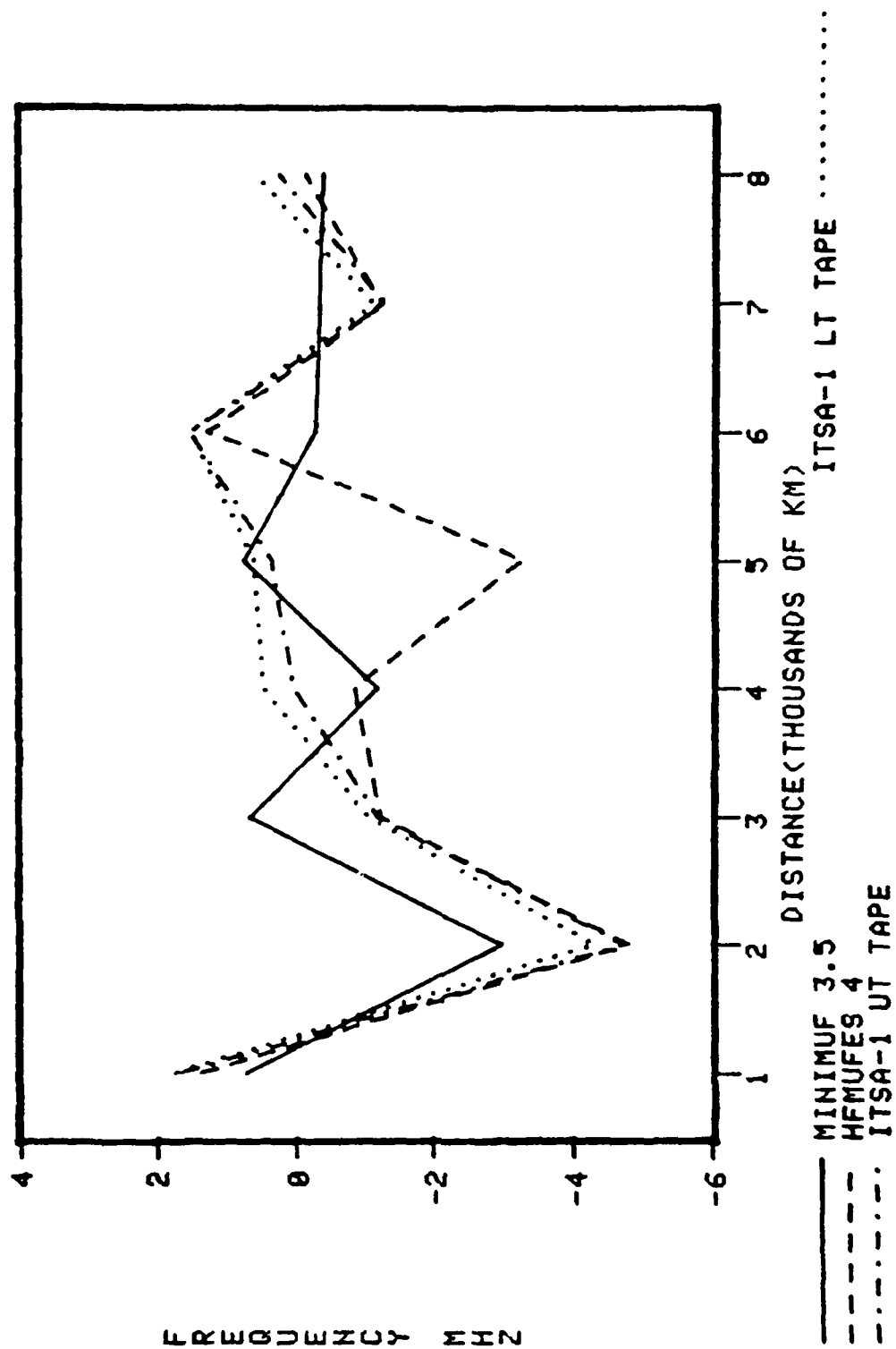Table 8. Percentage of sample in each path length range.

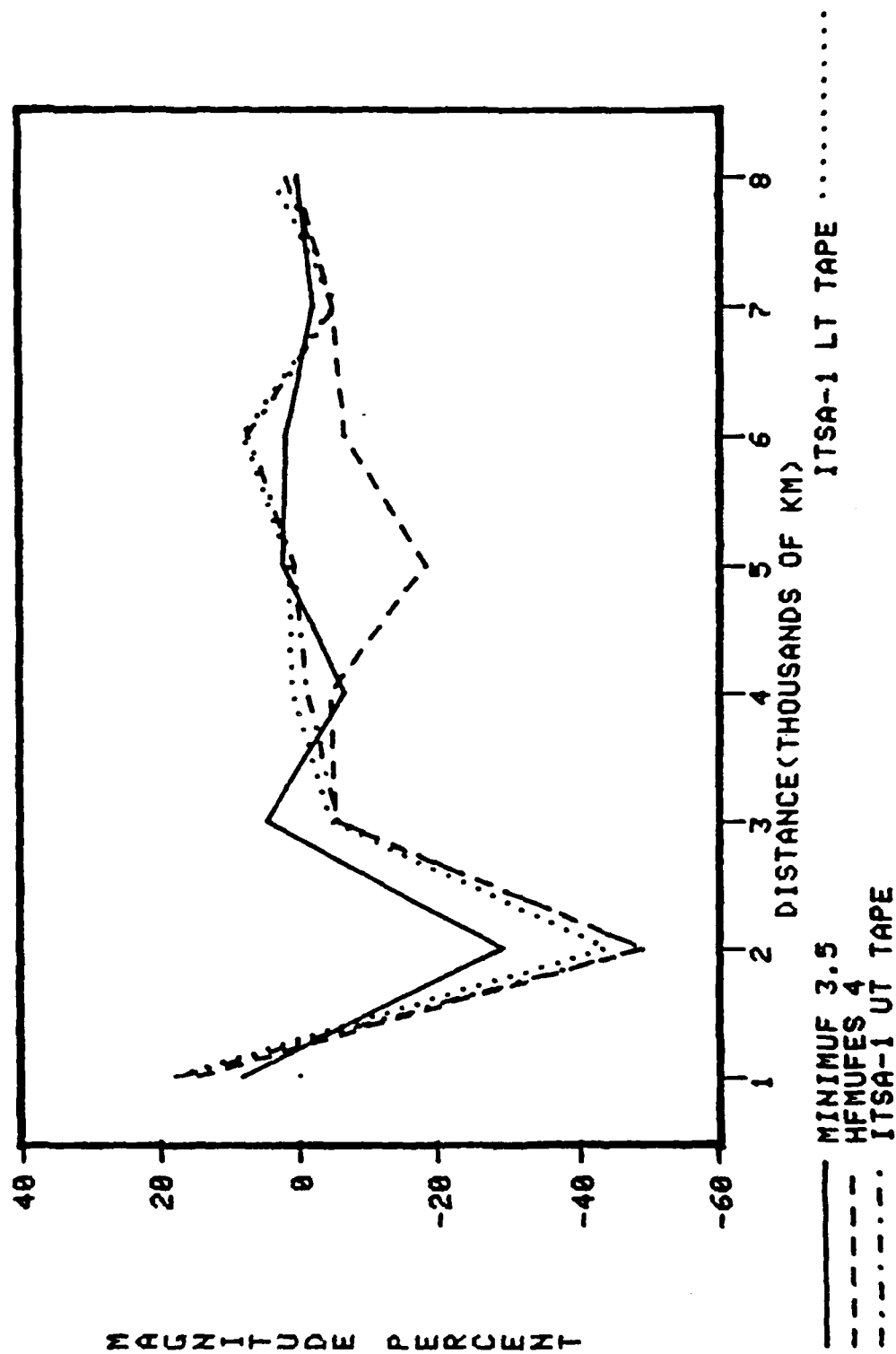Figure 19. Average residual (bias) as a function of path length.

43

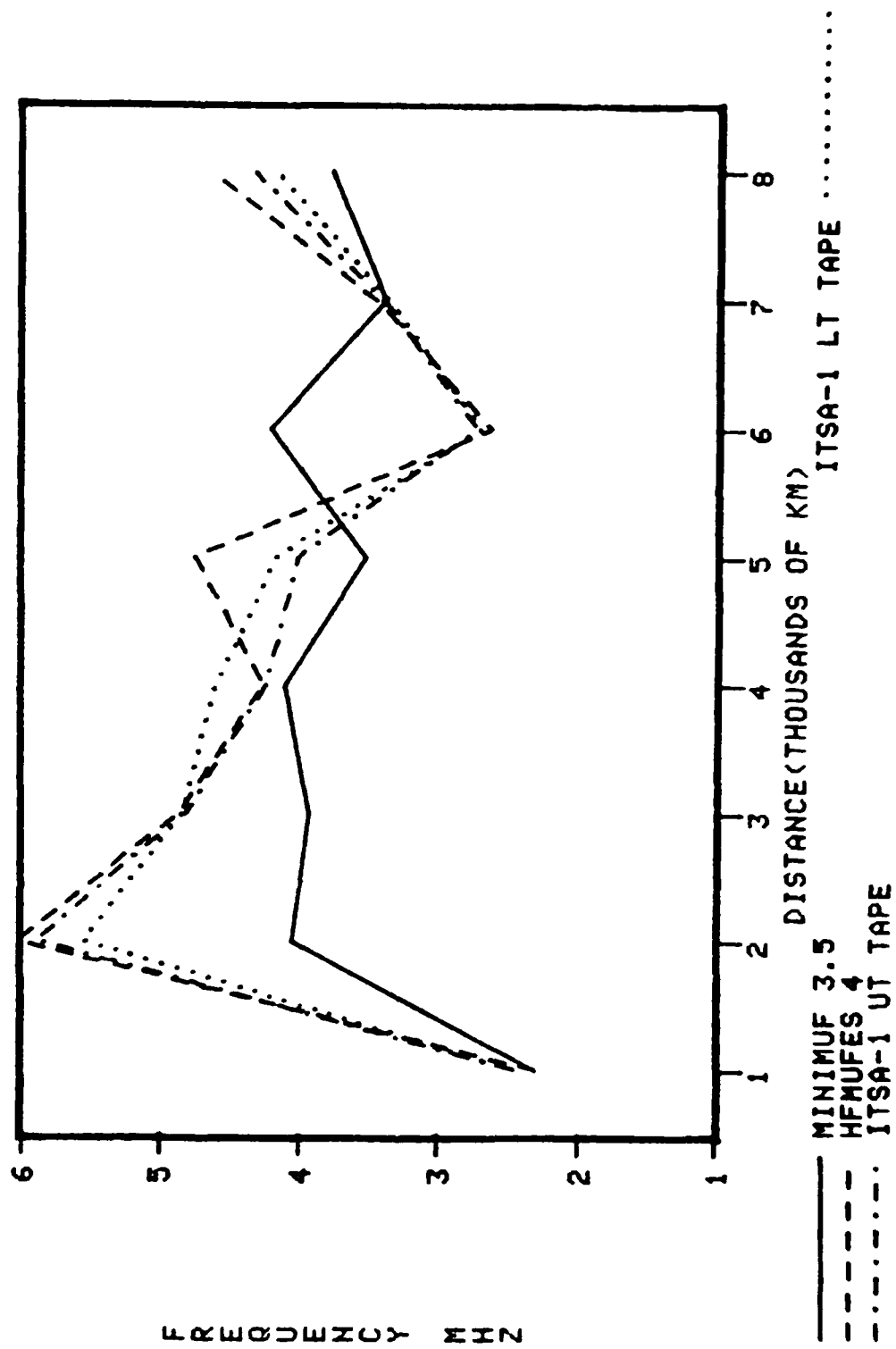Figure 20. Average relative residual (relative bias) as a function of path length

44

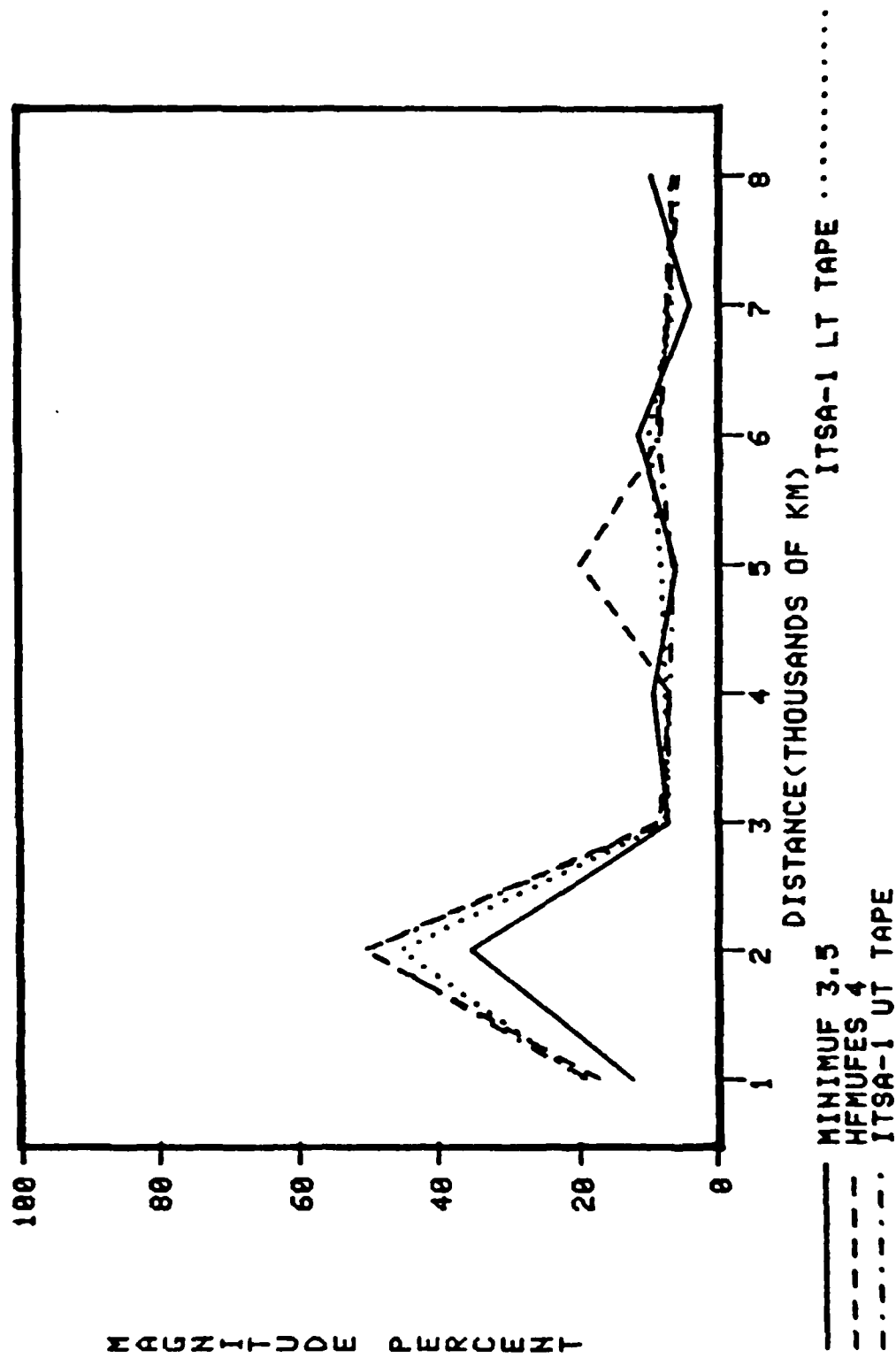Figure 21. rms error in MHz as a function of path length.

45

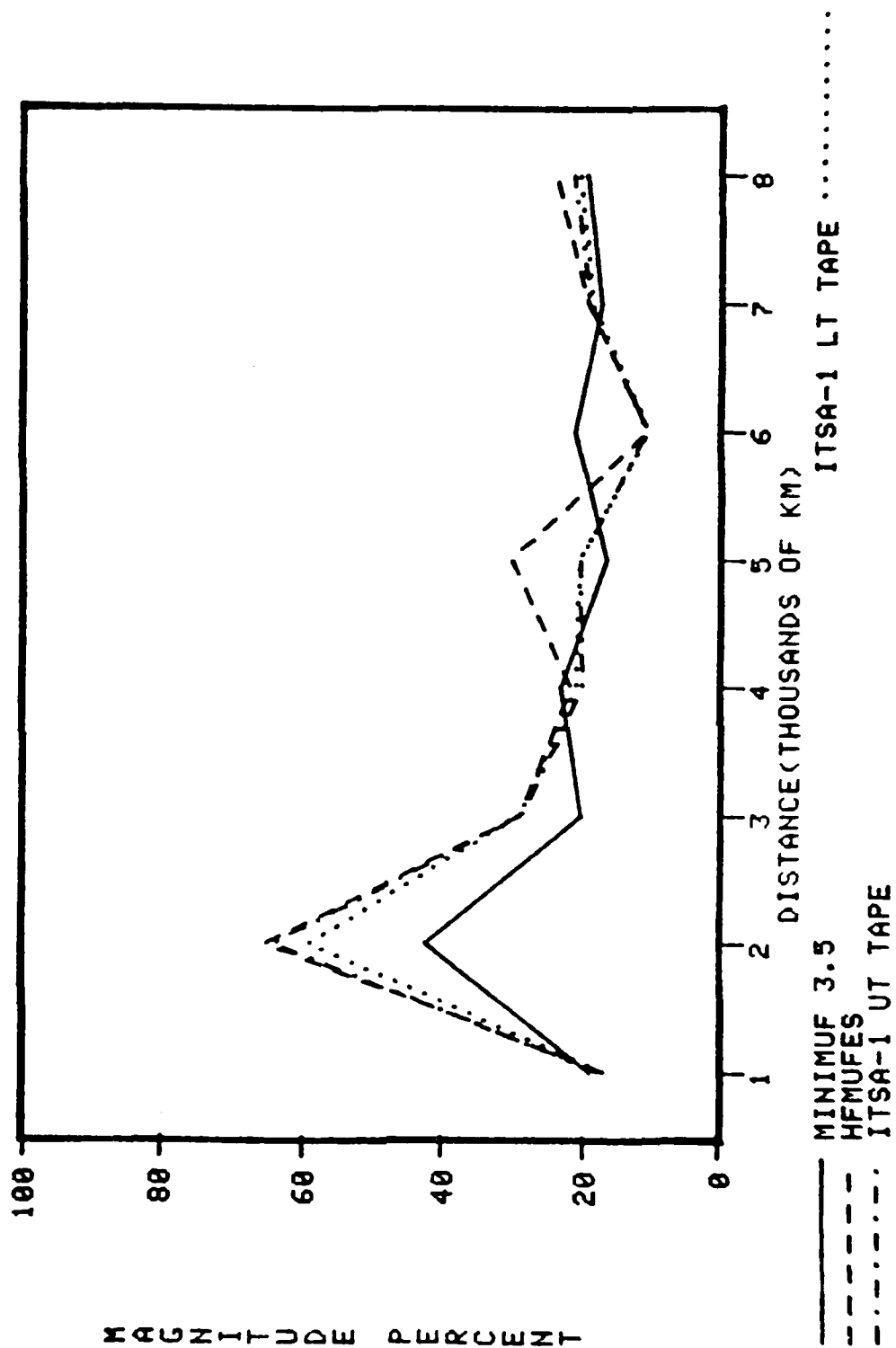Figure 22. Relative rms error as a function of path length.

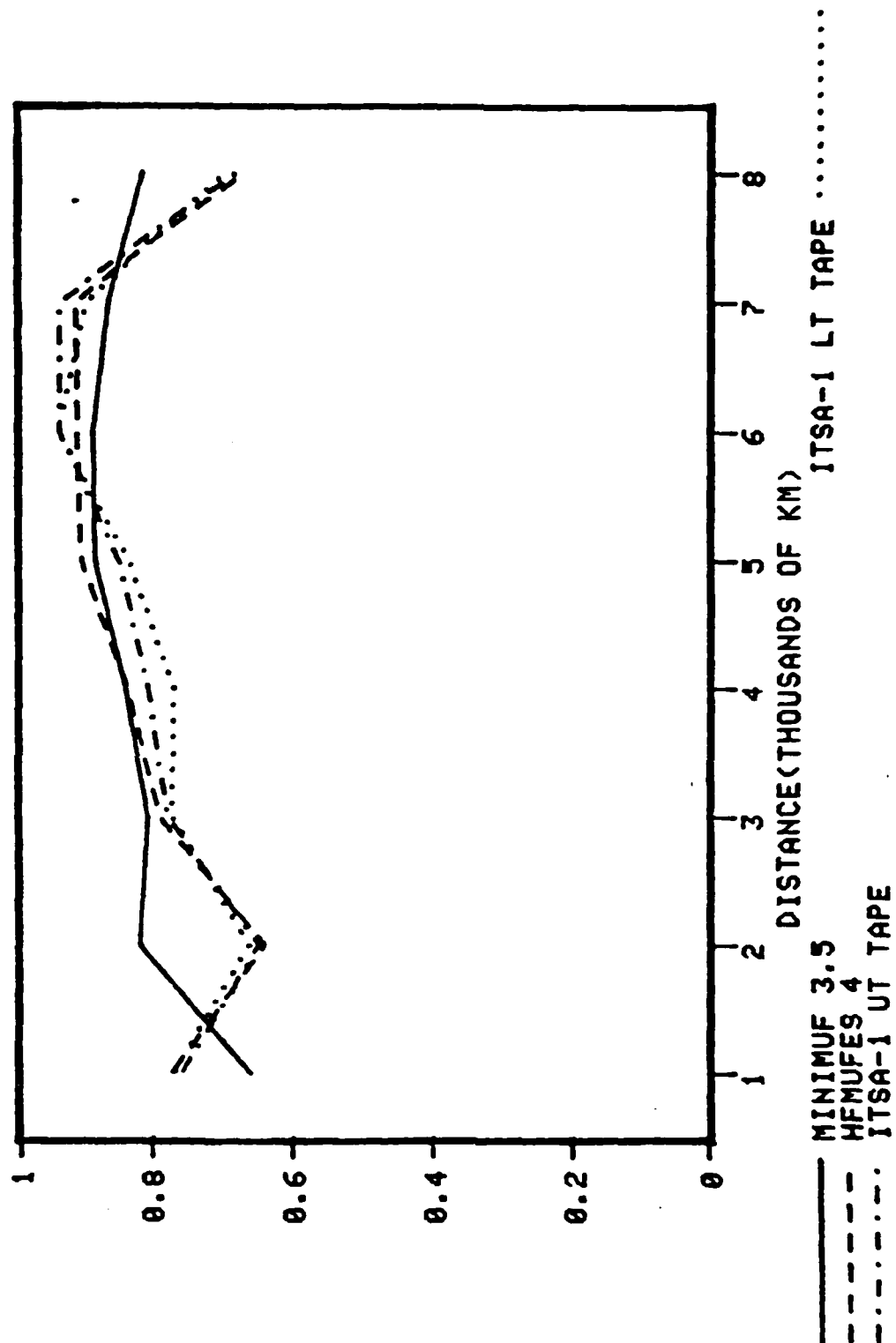Figure 23. Magnitude of the error (average absolute relative residual) as a function of distance.

47

Figure 24. Correlation coefficients as a function of distance.

PATH ORIENTATION

Figures 25-30 summarize the performance of the four programs as a function of path orientation. This categorization is important to assure that the sunrise/sunset reactions are correct for varying degrees of path illumination. The north-south (N-S) paths are those which lie nominally within ± 15° of a 0° or 180° bearing. The east-west (E-W) paths are those which fall nominally within ± 15° of a 90° or 270° bearing. The paths which did not meet either criterion were put in the "other" category. The percentage of the sample in each category is indicated in Table 9. Table 10 indicates which paths are in each category.

Path Orientation	Number of Hours	Percentage of Sample
North/South	1072	23.0
East/West	1042	22.3
Other	2554	54.7

Table 9. Percentage of sample in path orientation categories.

Figures 25 and 26 illustrate the bias in the four programs. All the programs have a higher bias for paths oriented in the north/south direction. This is not surprising, considering the dynamics of the abrupt F-region changes which occur when the entire path is illuminated suddenly, as on the N-S paths. However, in the case of MINIMUF-3.5 and the two ITSA-1 programs the amount of the bias is small enough to assume consistent results irrespective of path orientation.

Figures 27 and 28 illustrate the rms error and relative rms error, respectively. For MINIMUF-3.5 the rms error ranges between about 4 percent (3.3 MHz) and 6 percent (4 MHz); whereas, for HFMUFES 4 it ranges between 7.5 percent (3.5 MHz) and 12.5 percent (4.7 MHz).

Figure 29 shows the average magnitude of the error. For MINIMUF-3.5, the program with lowest error, it ranges between about 19 percent and 22 percent. For the worst program, HFMUFES 4, the error ranges from about 22.5 percent to 28 percent.

No.	Transmission Path	Orientation	Latitude of Control Points	Geographic Region
1	Guam to Yokohama, Japan	N-S	LO	B
2	FT Monmouth, NJ to Palo Alto, CA	E-W	M	A
3	Guam to Honolulu, Hawaii	E-W	LO	B
4	Guam to Kodiak, Alaska	Other	M	B
5	Honolulu, Hawaii to Kodiak, Alaska	N-S	M	B
6	Honolulu, Hawaii to Washington, DC	Other	M	C
7	Davis, CA to Honolulu, Hawaii	E-W	M	B
8	Palo Alto, CA to Fairbanks, Alaska	Other	H	C
9	Boulder, CO to Pt. Barrow, Alaska	Other	H	A
10	Honolulu, Hawaii to Yokohama, Japan	Other	M	B
11	Tarlac, Philippines to Yokohama, Japan	Other	LO	B
12	Tarlac, Philippines to H.E. Holt, Australia	N-S	TE	C
13	Guam to H. E. Holt, Australia	Other	TE	C
14	Davis, CA to Kodiak, Alaska	Other	M	B
15	Honolulu, Hawaii to Corona, CA	Other	M	B
16	Andoya, Norway to Thessoloniki, Greece	N-S	H	A
17	Davis, CA to La Posta, CA	Other	M	A
18	Toulouse, France to Neimakri, Greece	E-W	M	C
19	Honolulu, Hawaii to La Posta, CA	Other	M	B
20	Coco Solo, Canal Zone to Stockbridge, NY	N-S	M	B
21	Andoya, Norway to New Delhi, India	E-W	H	A
22	Palo Alto, CA to Thule, Greenland	N-S	TA	A
23	Toulouse, France to Keflavik, Iceland	Other	H	C
24	FT Monmouth, NJ to Aberdeen, NY	Other	M	A
25	FT Monmouth, NJ to Camp Drum, NY	N-S	M	A

TE = Transequatorial   E-W = East/west
LO = Low latitude   N-S = North/south
M = Mid-latitude   A = Continental
H = High latitude   B = Ocean
TA = Transauroral   C = Combined land/ocean

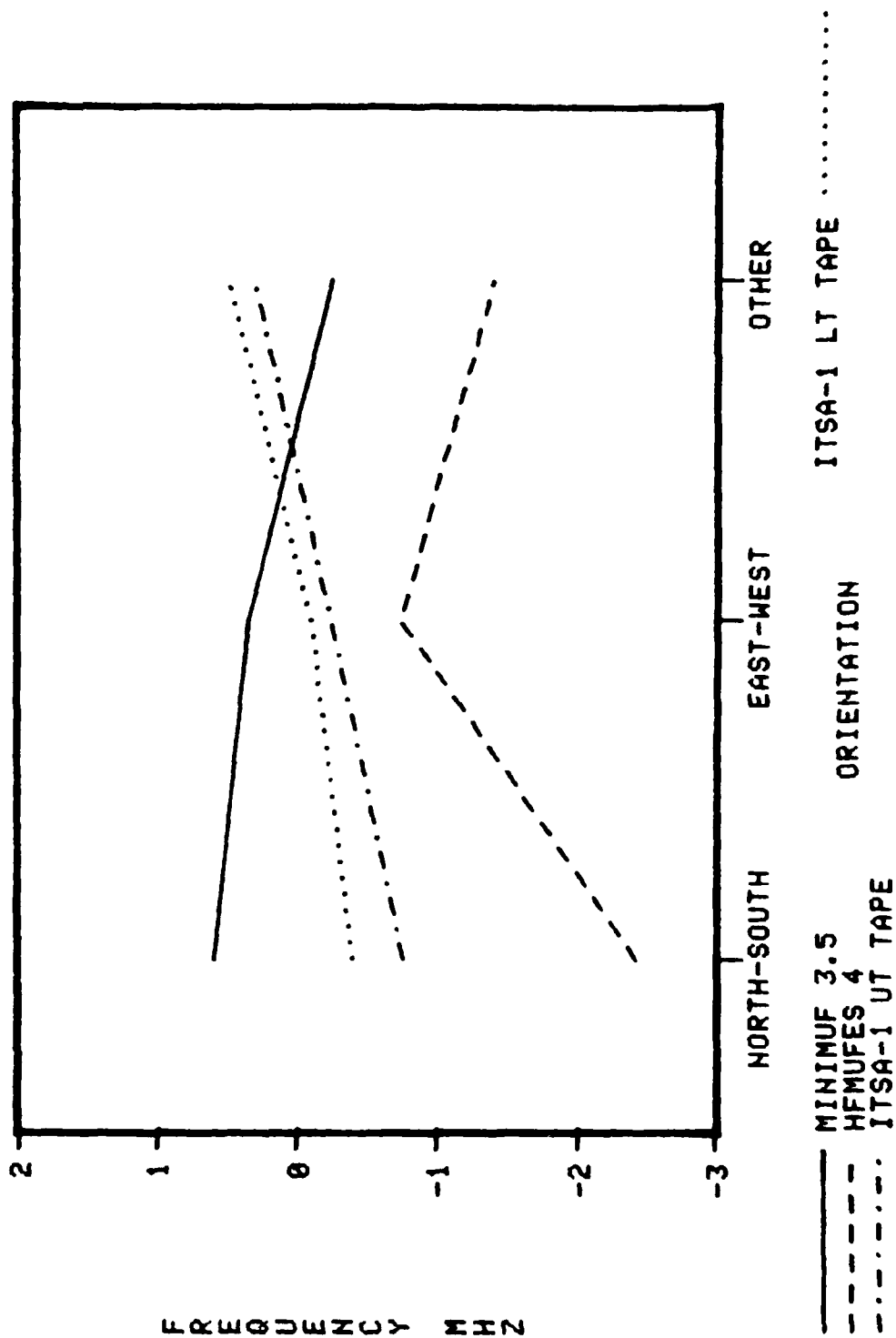Table 10. Additional path characteristics.

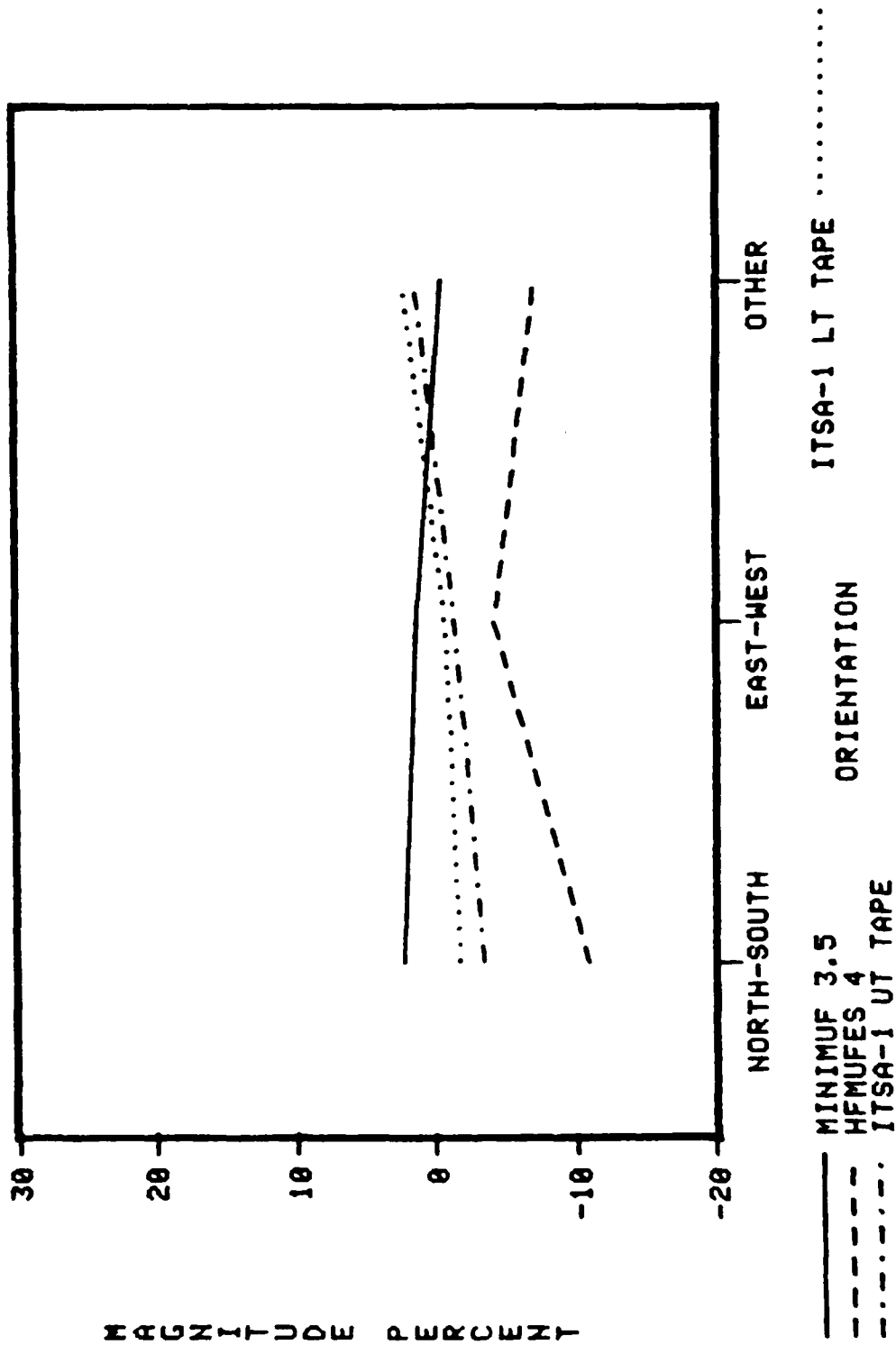Figure 25. Average residual (bias) as a function of orientation.

Figure 26. Average relative residual (relative bias) as a function of orientation
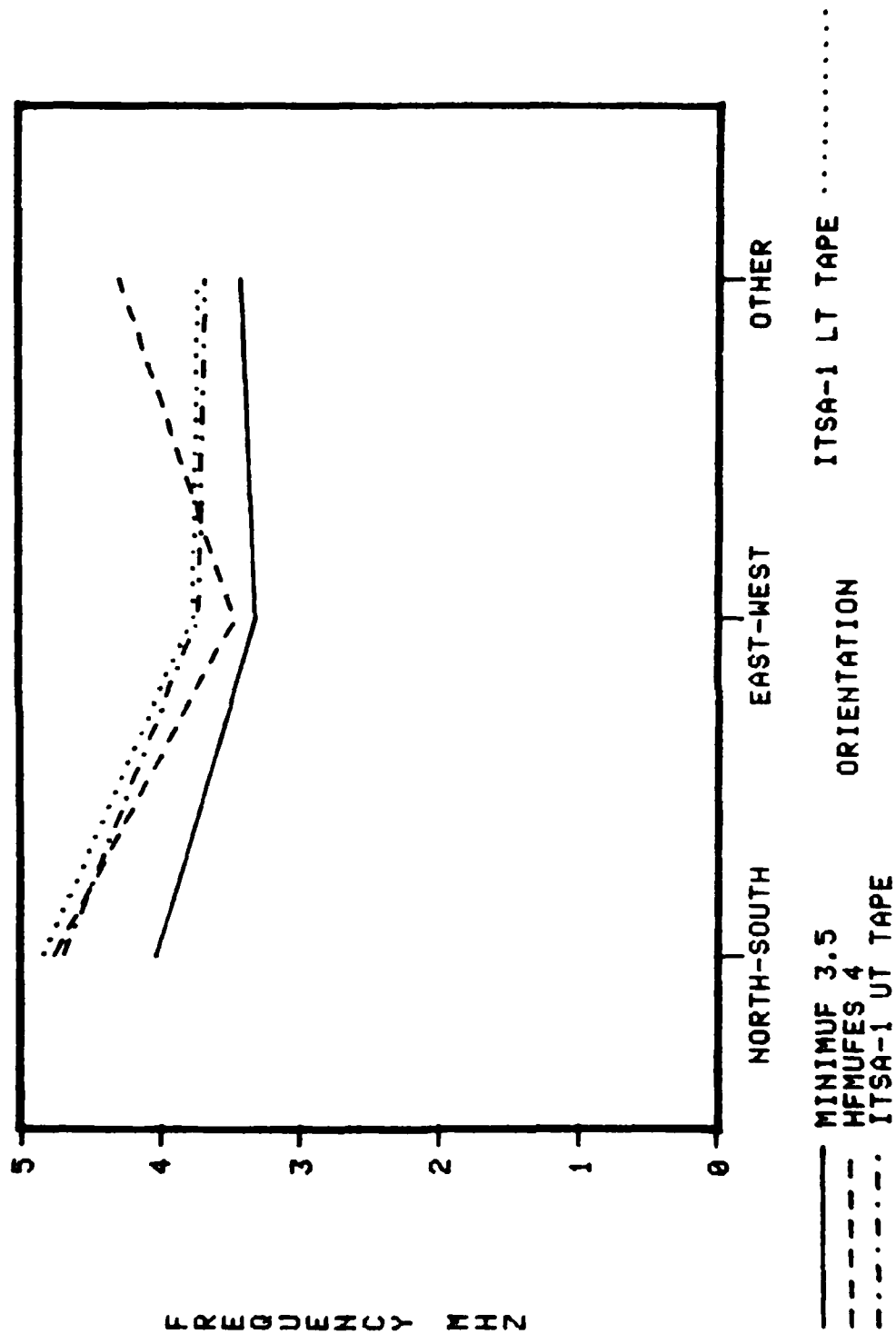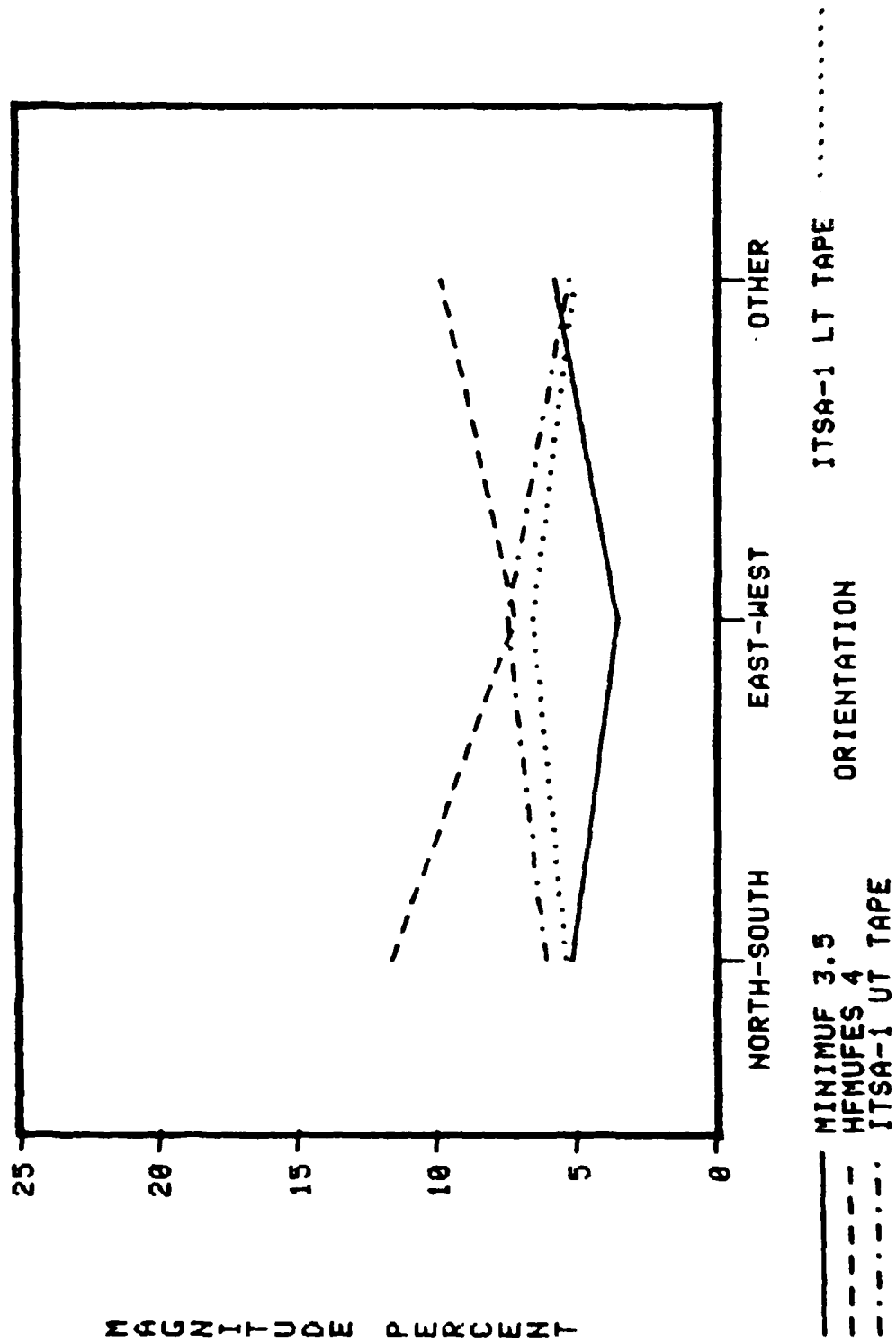
Figure 27. Rms error as a function of orientation.

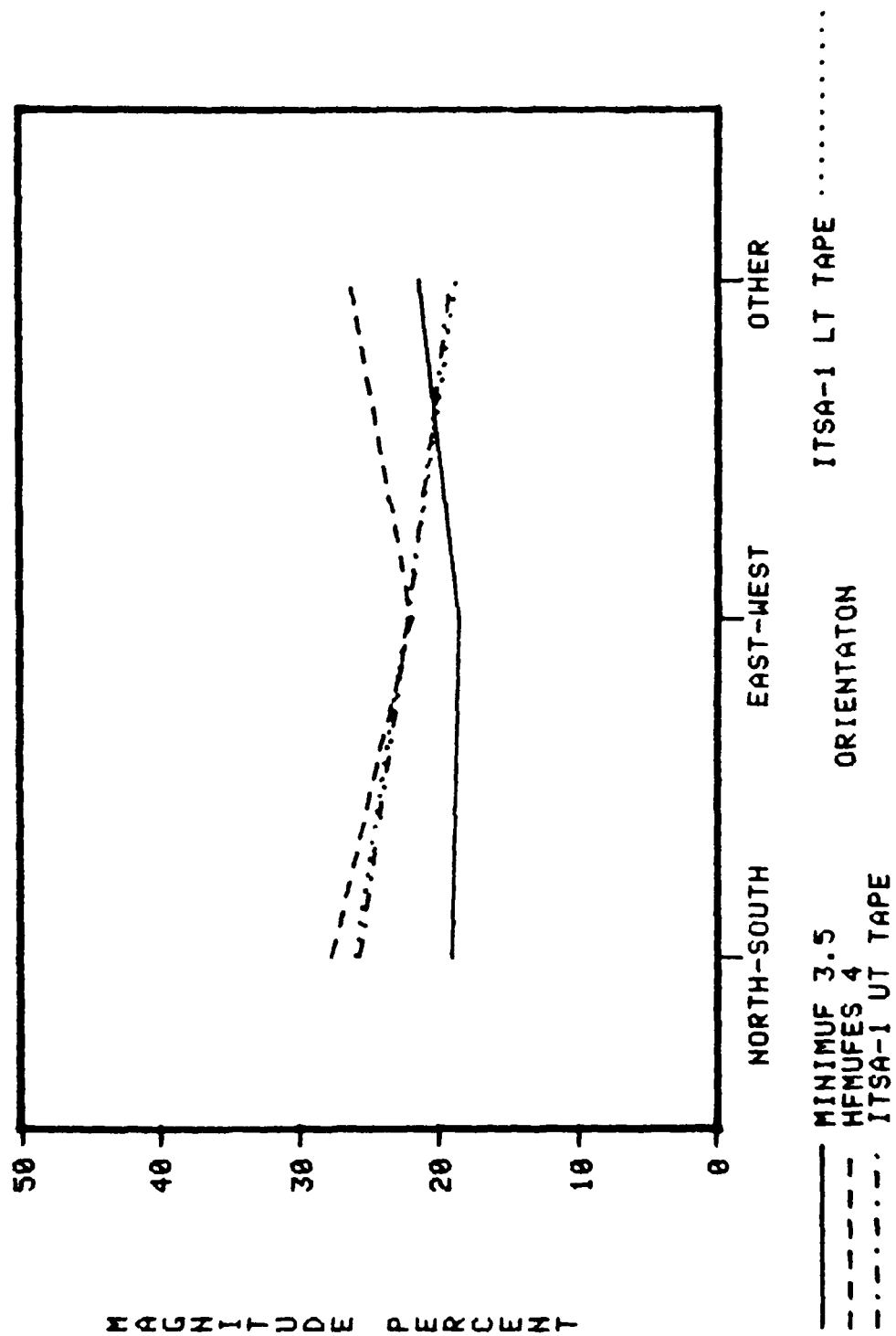Figure 28. Relative rms error as a function of orientation.

Figure 29. Magnitude of the error (average absolute relative residual) as a function of orientation.
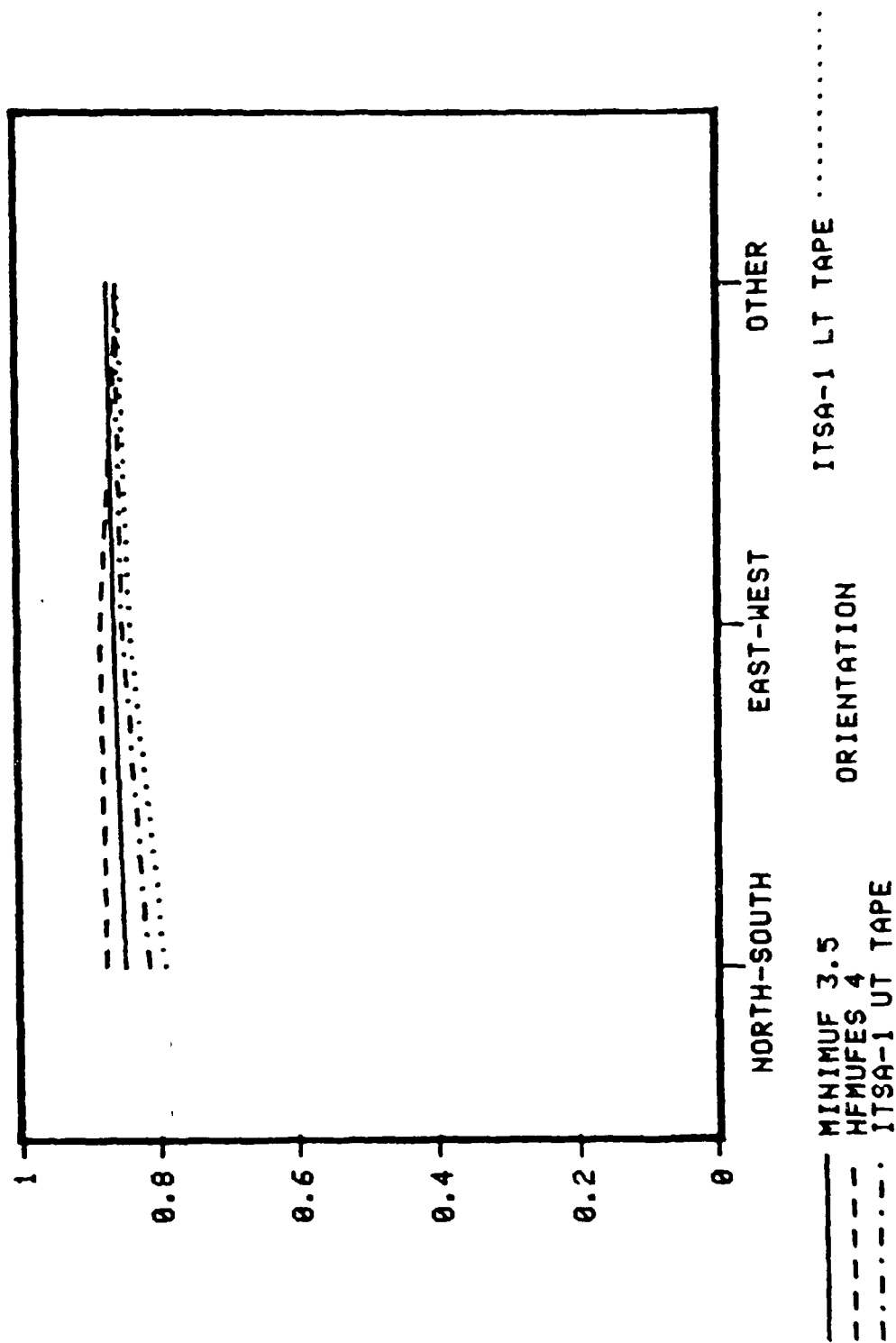
Figure 30. Correlation coefficients as a function of orientation.

In Figure 30, HFMUFES 4 is clearly shown to have the highest correlation with path orientation. All of the programs have correlation coefficients greater than 0.8.

SEASON/MONTH

Figures 31-36 summarize the performance of the four programs as a function of season and Figures 37-42 provide additional detail as a function of month. Here the seasons are defined as: (1) winter, November through February; (2) spring, March and April; (3) summer, May through August; and (4) autumn, September and October.

During the winter, MINIMUF predicts 0.5 MHz (3.5 percent) low as shown in Figures 31-32. The other programs predict high. The worst was HFMUFES 4, which predicted 2 MHz (11 percent) high. The months primarily affecting these results for MINIMUF-3.5 were November and December, for which it was low by as much as 6 percent.

During the summer months, HFMUFES 4 is shown to predict quite close; whereas MINIMUF-3.5 predicts high by as much as 0.8 MHz (2 percent). During these months the two ITSA-1 programs performed at their worst. ITSA-1 with universal time tape is low by 1.3 MHz (7 percent), and ITSA-1 with local time tape is low by 1.7 MHz (9 percent). The large scale programs have the most trouble predicting June accurately; whereas MINIMUF-3.5 has the most trouble predicting August accurately.

During the equinox months, MINIMUF-3.5 has most difficulty predicting October accurately, where it is low by 1.9 MHz (9 percent); whereas HFMUFES 4 had its chief difficulty predicting March, where it is high by 3.5 MHz (17 percent).

The rms error, as illustrated in Figures 33-34 and 39-40, shows somewhat the same pattern for each program. MINIMUF-3.5 has its largest rms error during fall (October) with a value of roughly 4.1 MHZ (7 percent). HFMUFES 4 has its highest value during spring (March) with a value of nearly 5 MHz (16.5 percent).

The magnitude of the error is shown in Figure 35 to be rather constant at about 20 percent for MINIMUF-3.5. Whereas for HFMUFES 4 it is above 30 per-
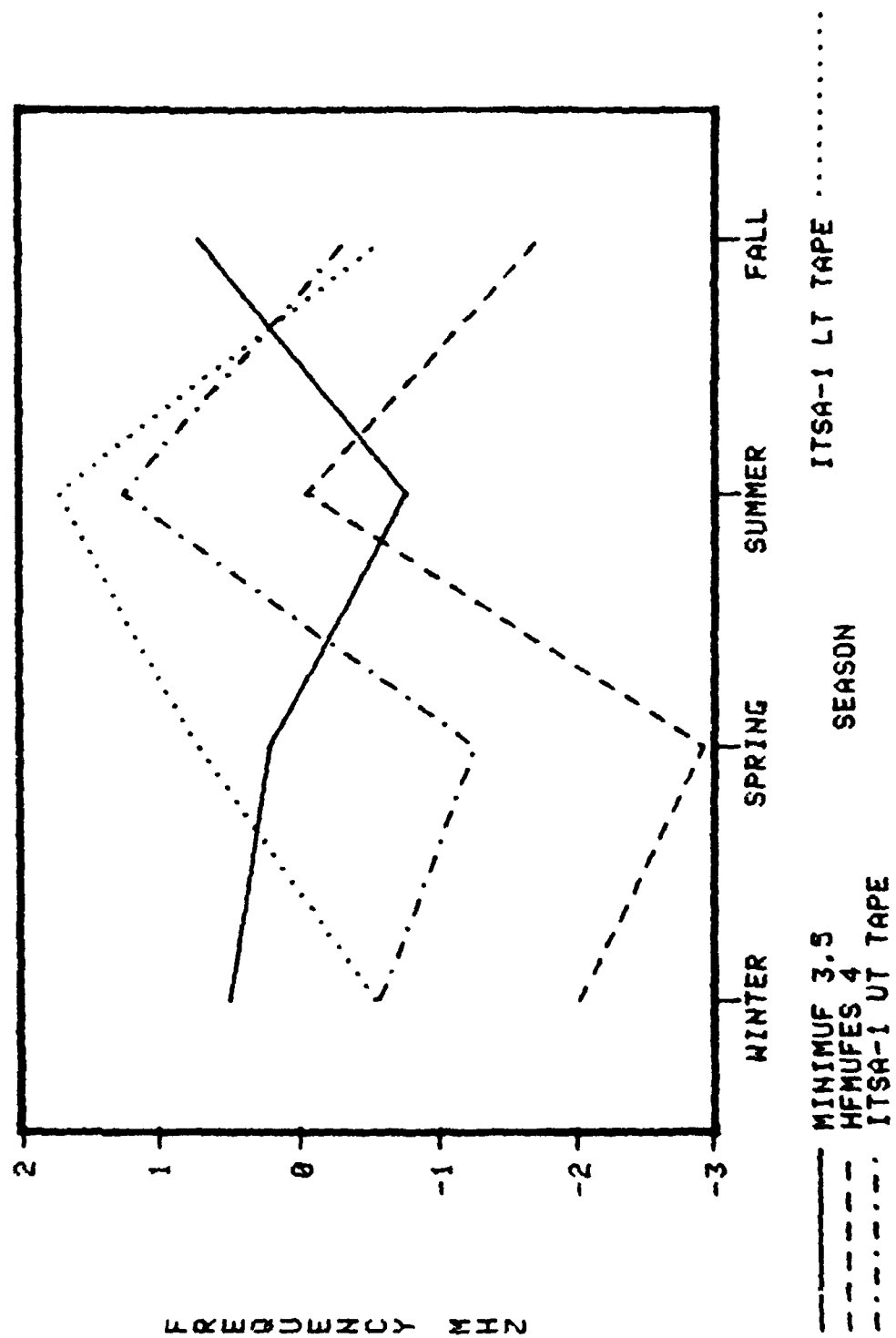
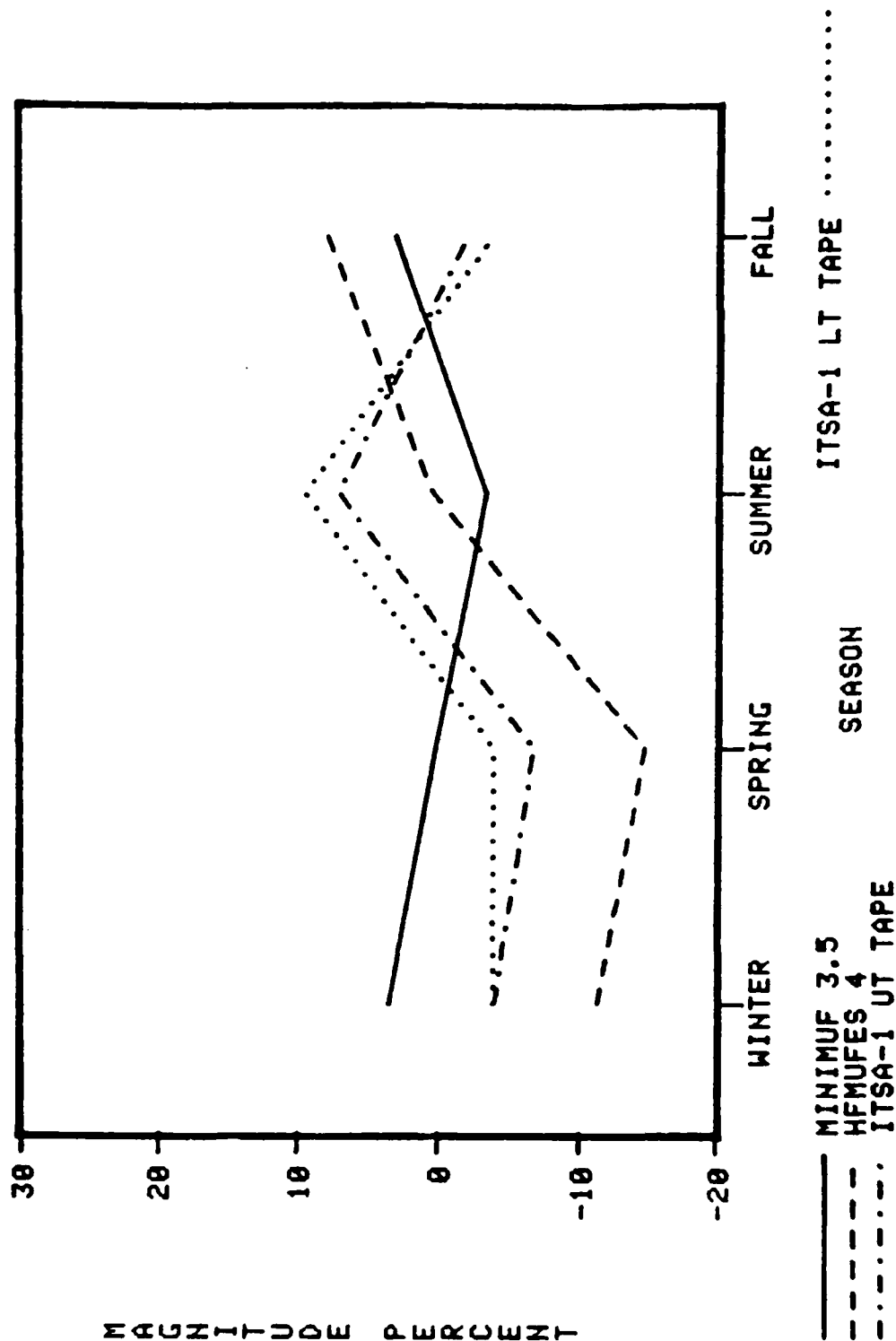Figure 31. Average residual (bias) as a function of season.

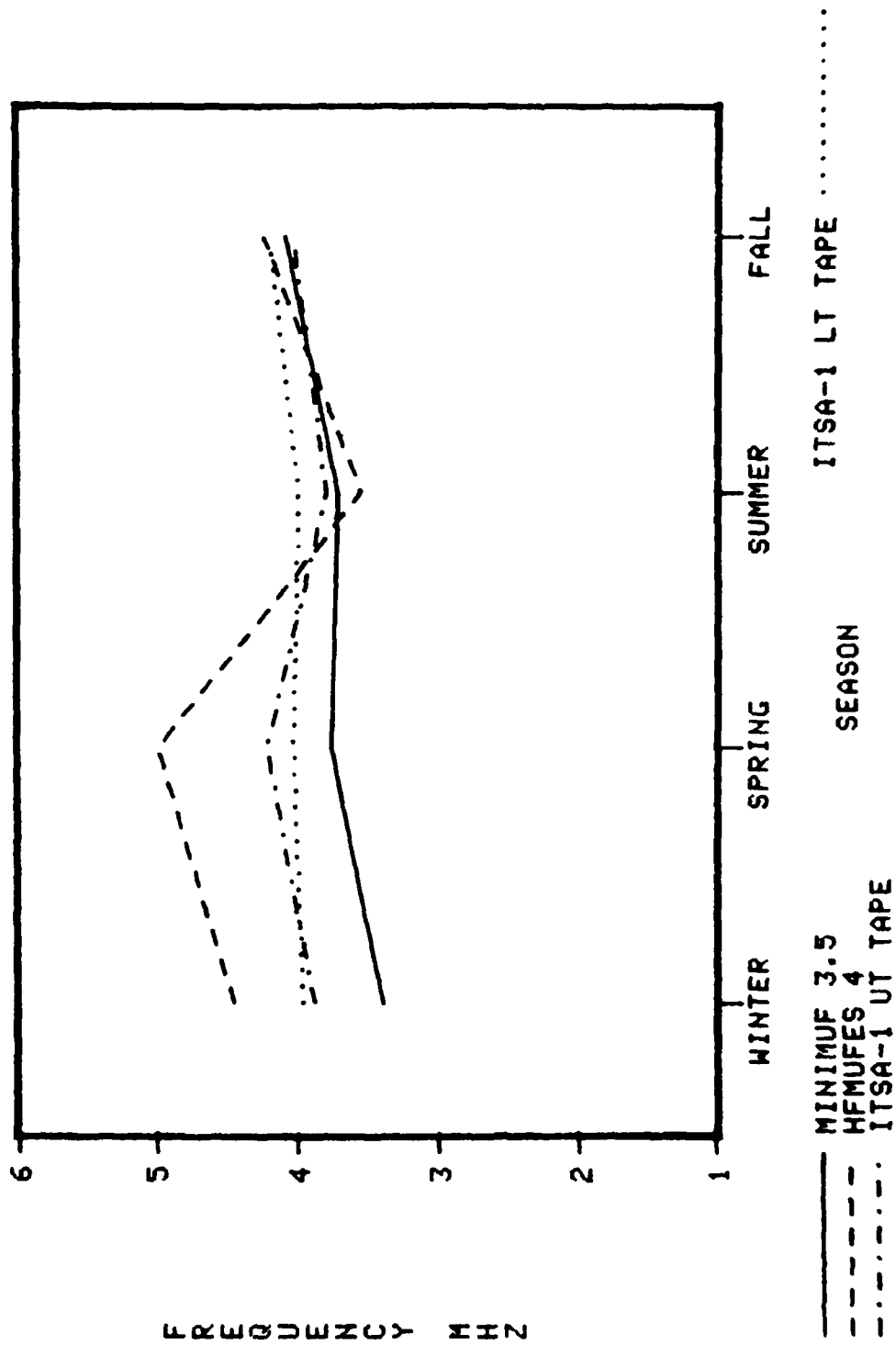Figure 32. Average relative residual (relative bias) as a function of season.
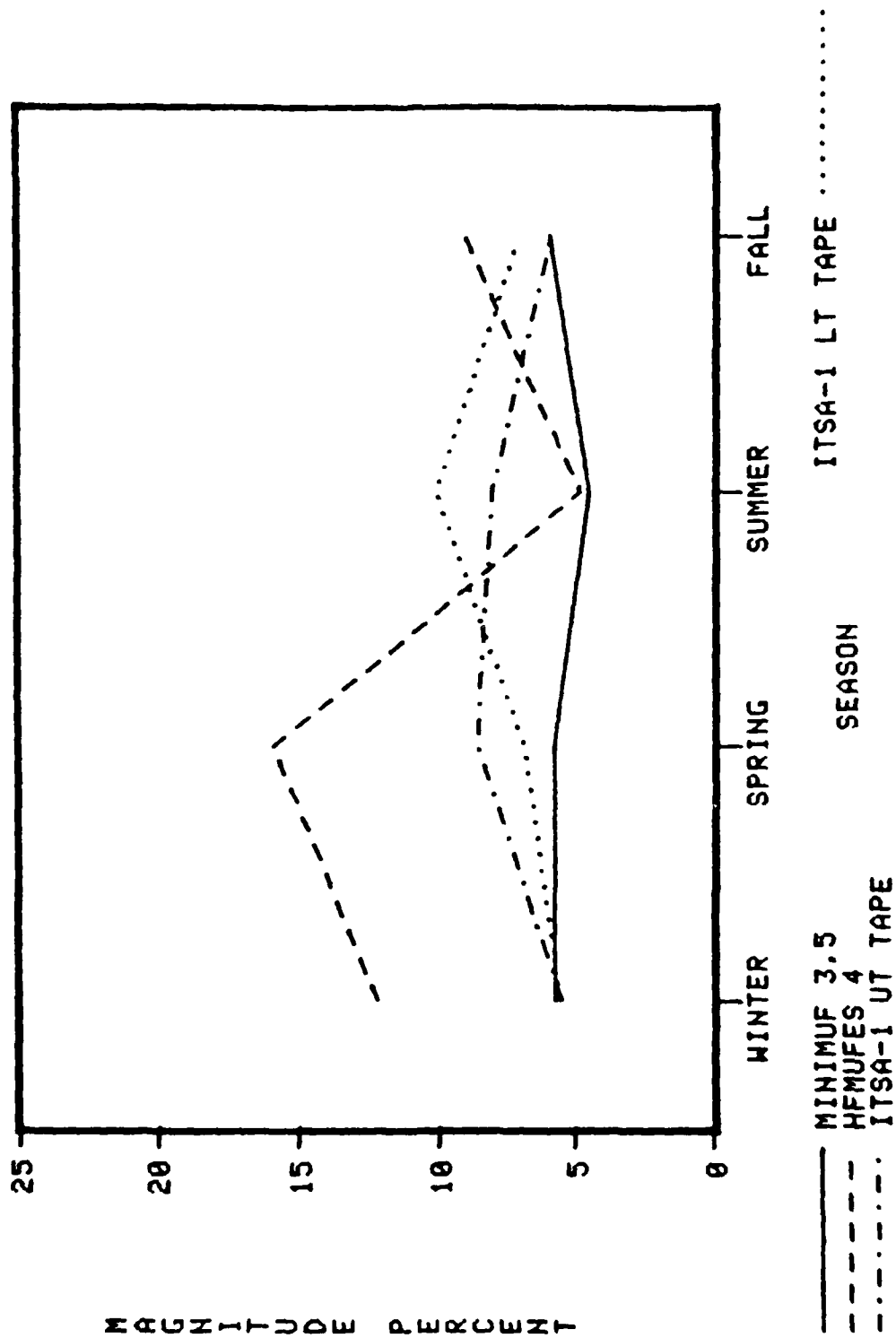
Figure 33. RMS error in MHz as a function of season.

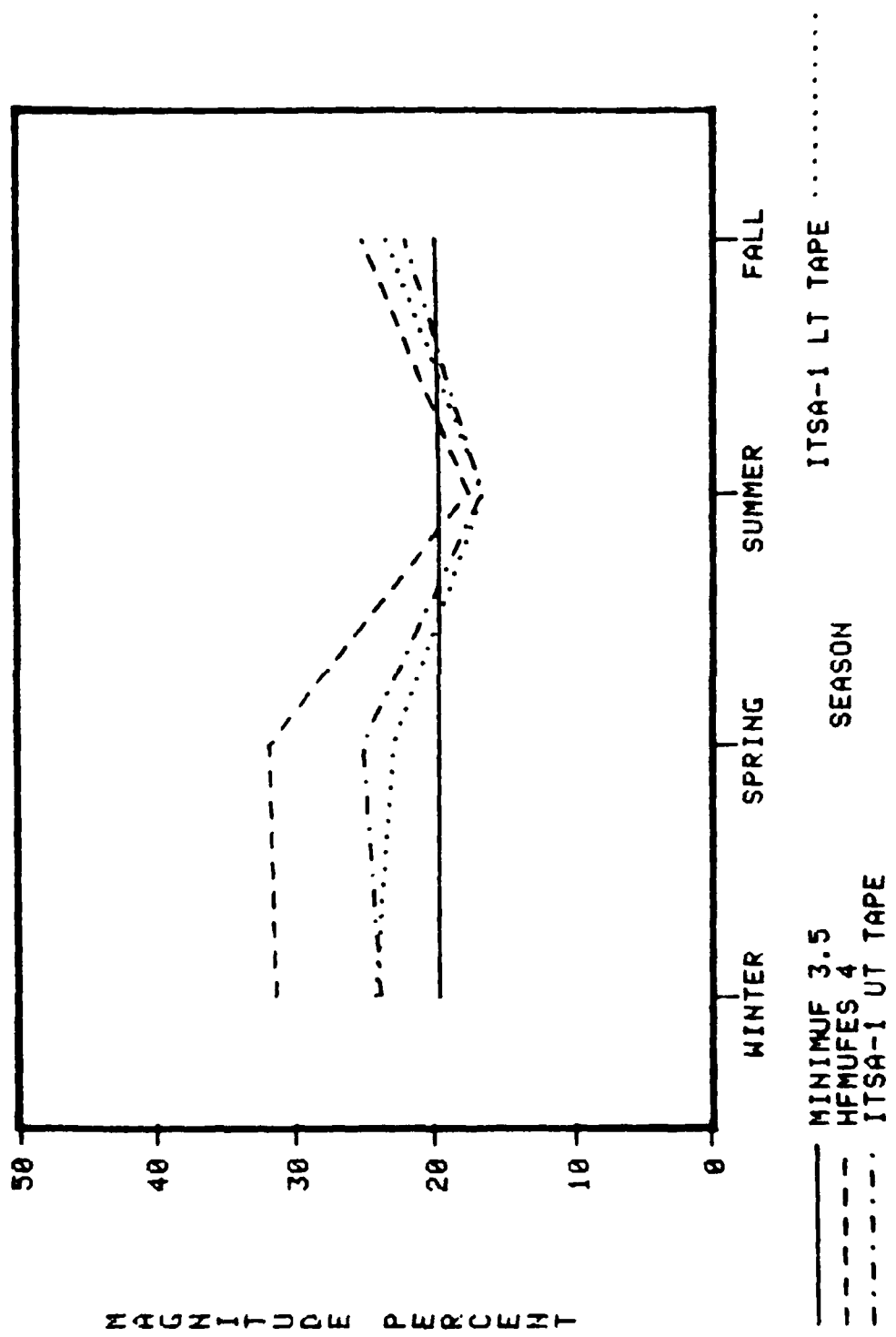Figure 34. Relative rms error as a function of season.

Figure 35. Magnitude of the error (average absolute relative residual) as a function of season.
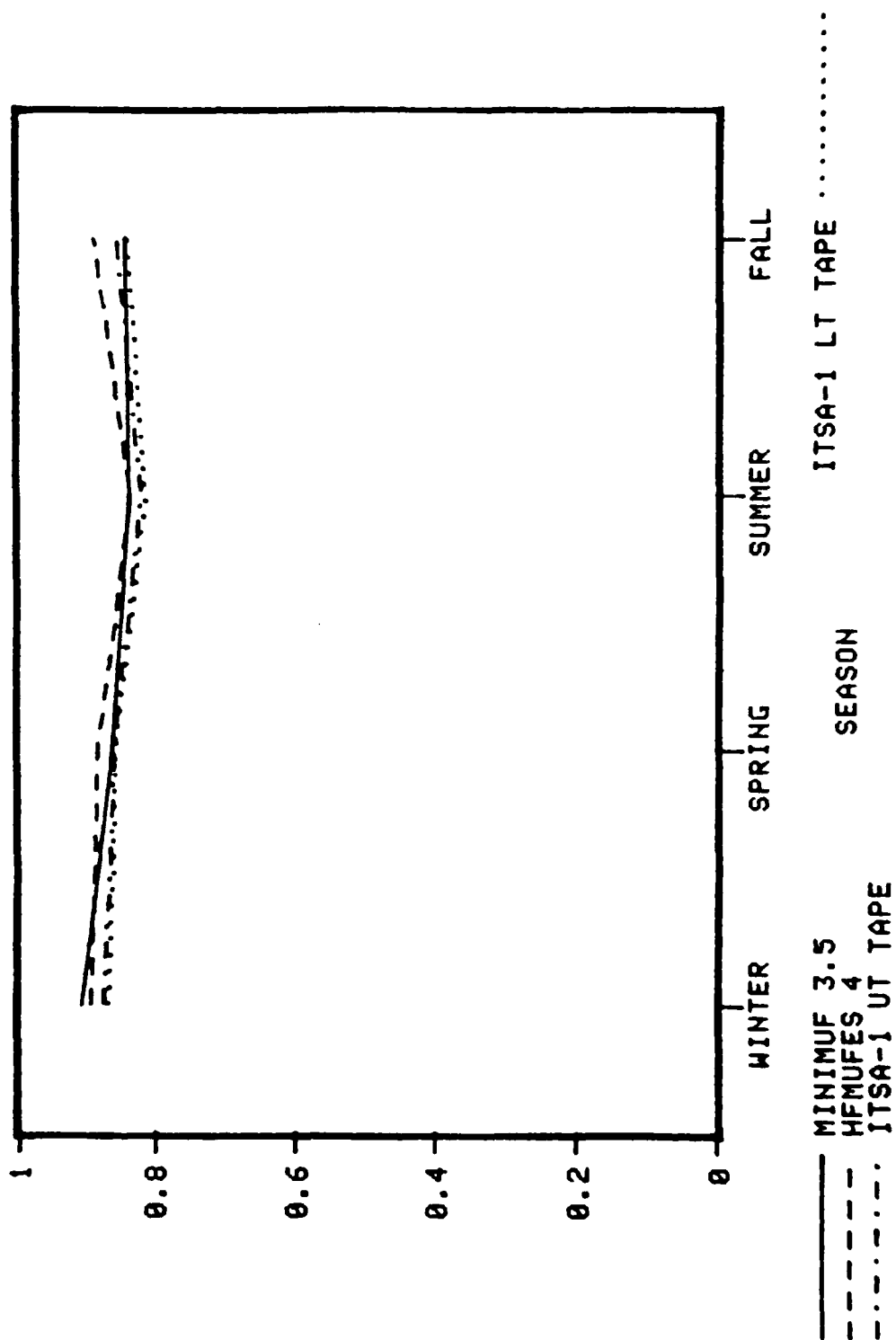
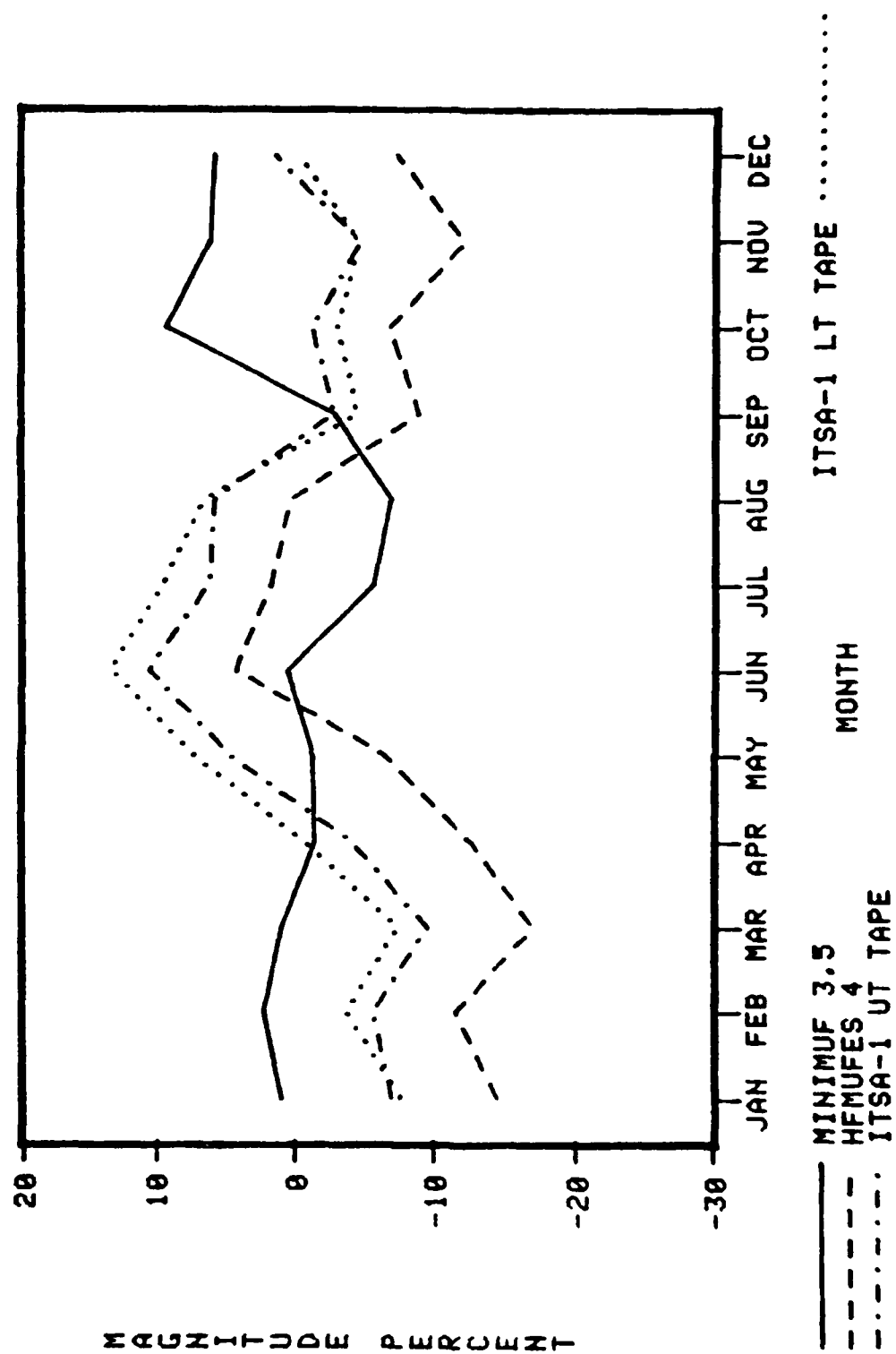Figure 36. Correlation coefficients as a function of season.

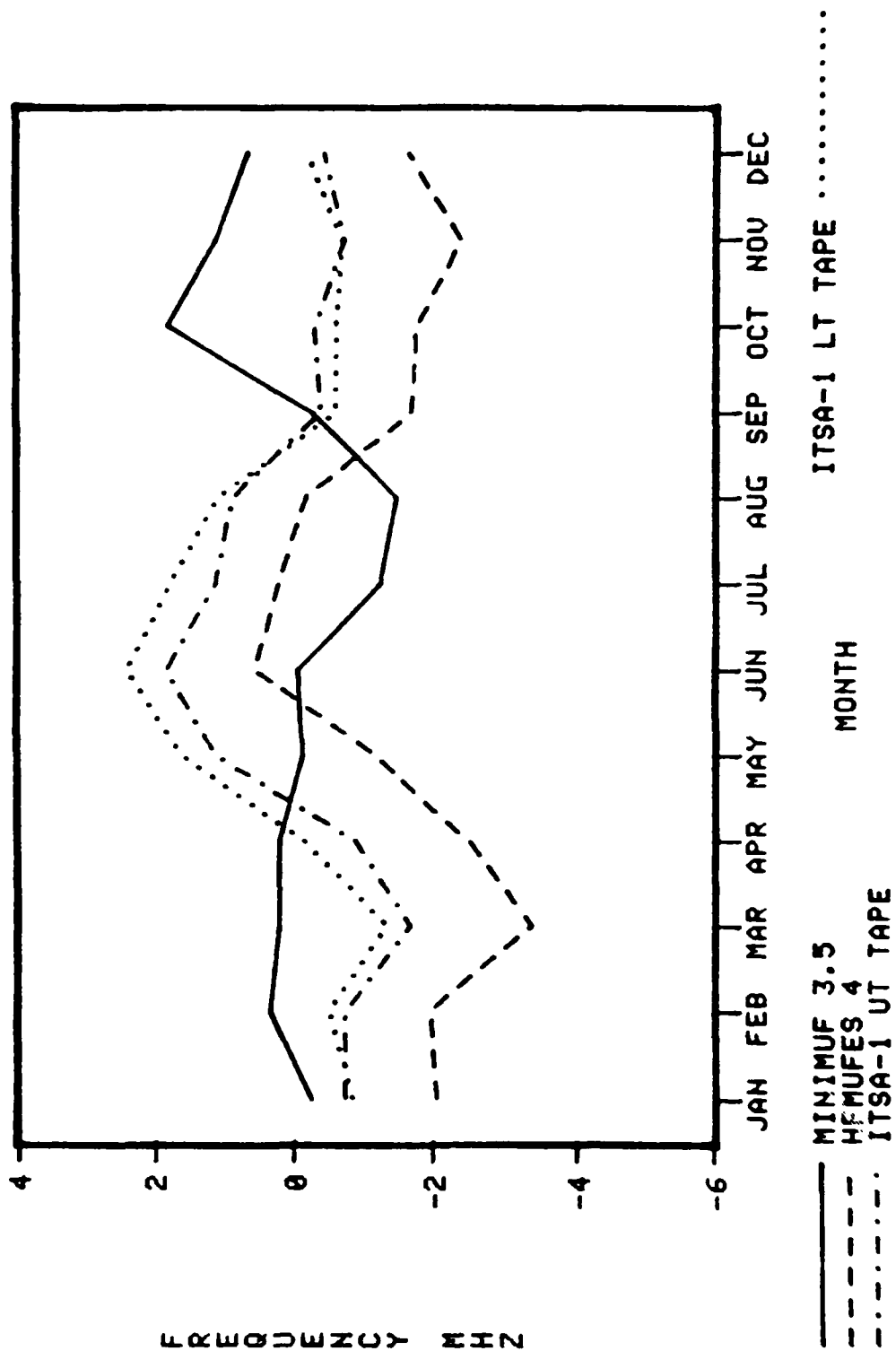Figure 37. Average residual (bias) as a function of month.

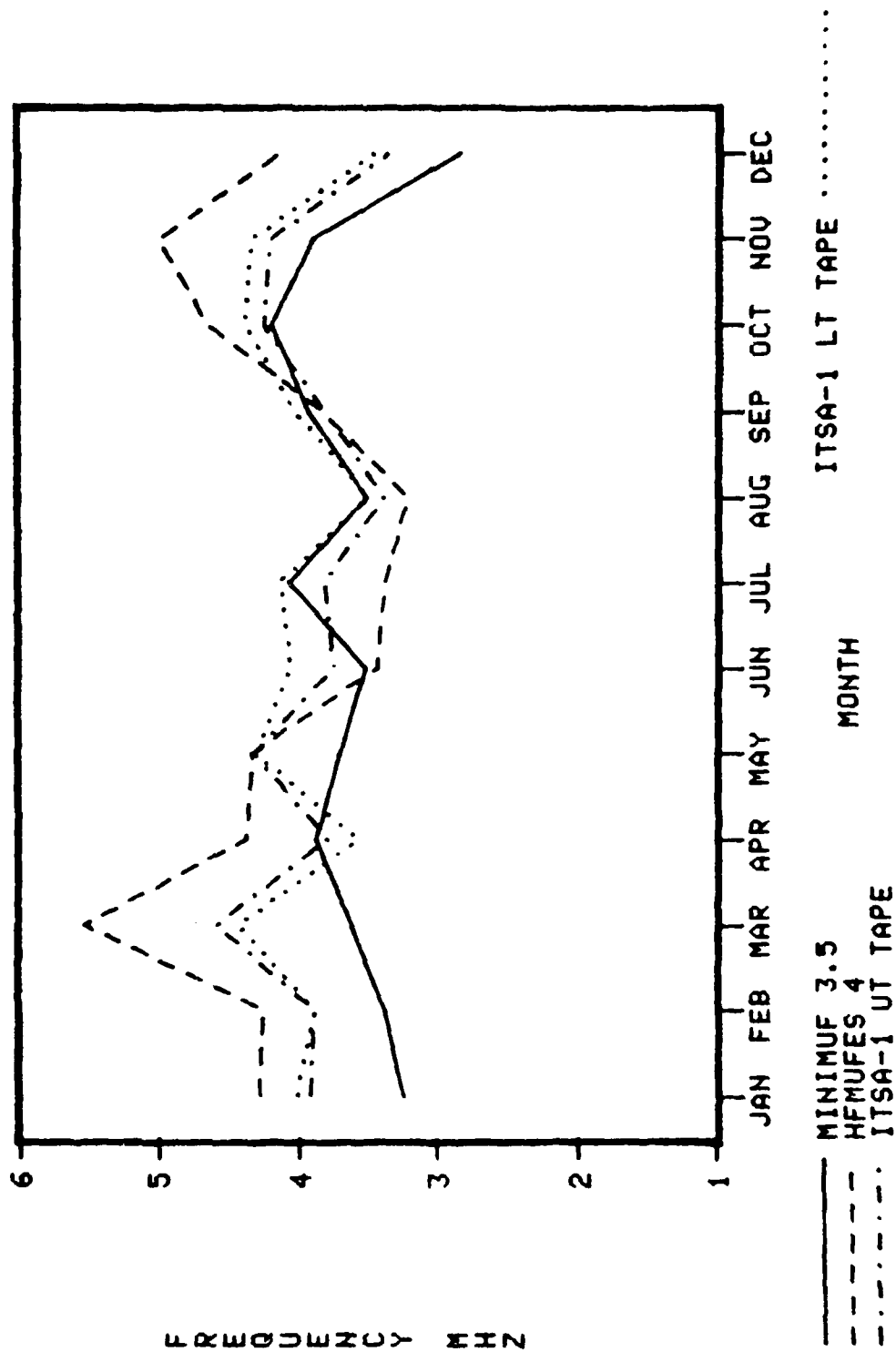Figure 38. Average relative residual (relative bias) as a function of month.

Figure 34. RMS error in MHz as a function of month

MINIMUF 3.5
HFMUFES 4
ITSA-1 UT TAPE
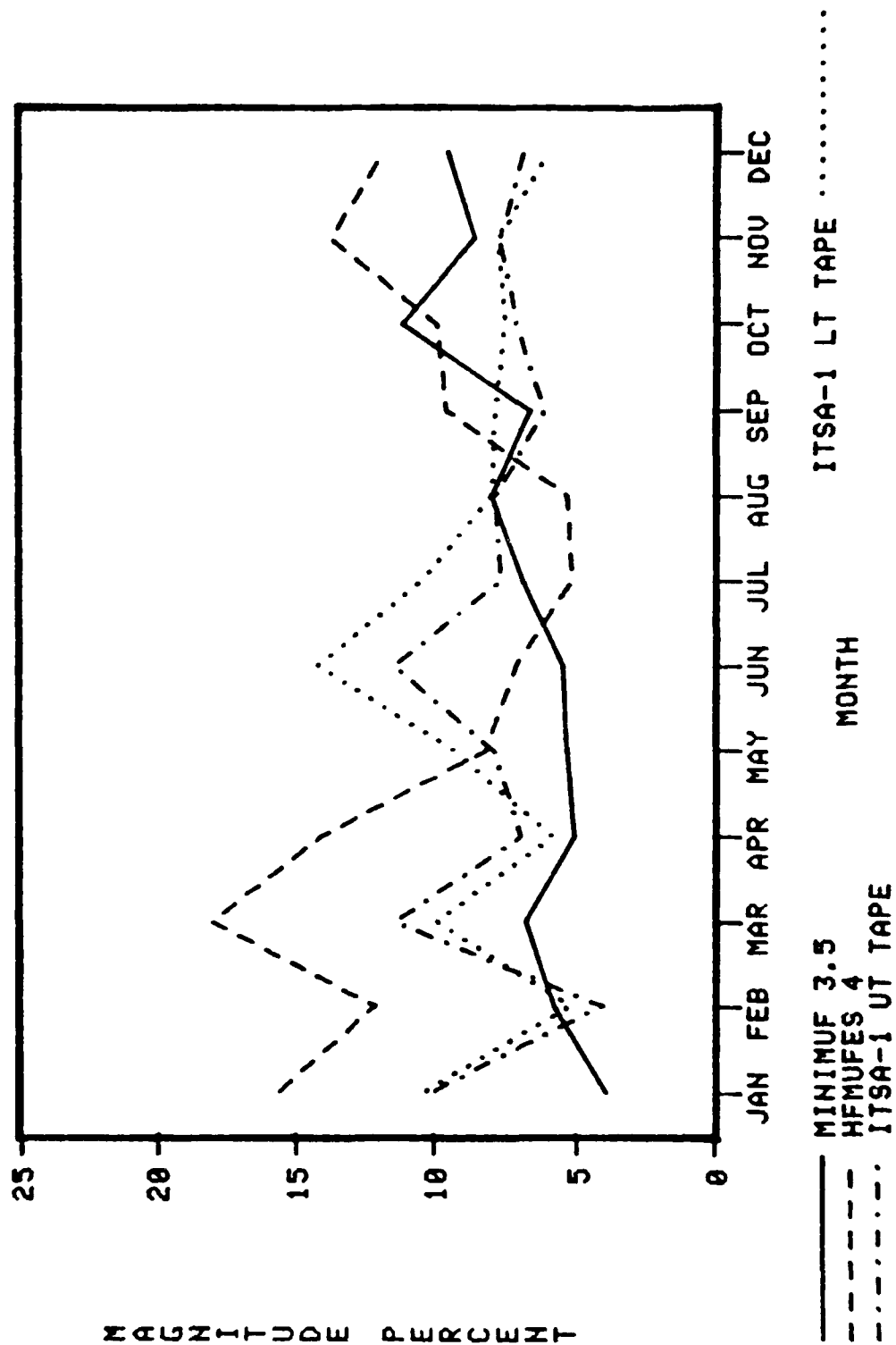ITSA-1 LT TAPE ......

MONTH

FREQUENCY MHz

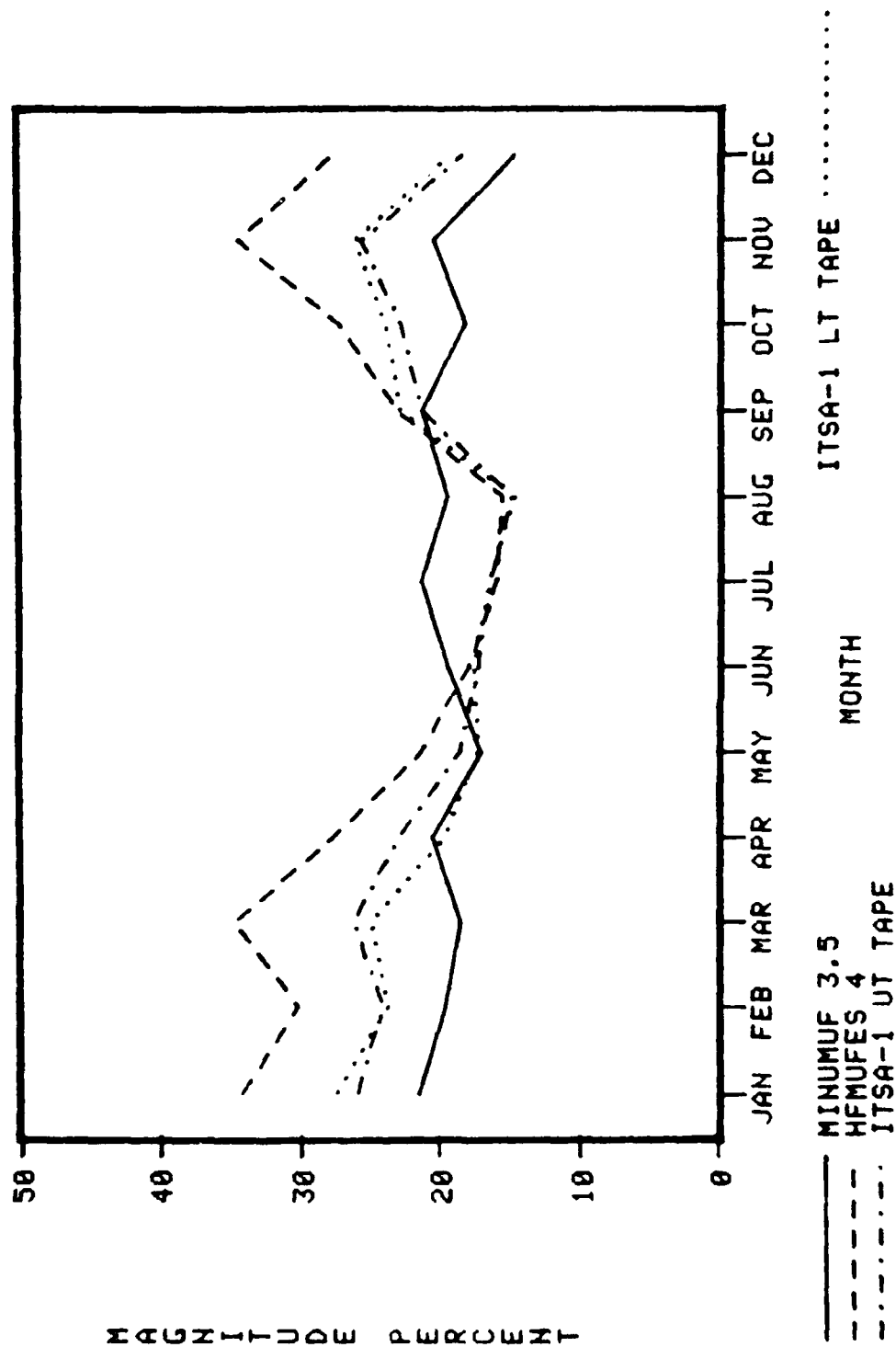Figure 40. Relative rms error as a function of month.

Figure 41. Magnitude of the error (average absolute relative residual) as a function of month.
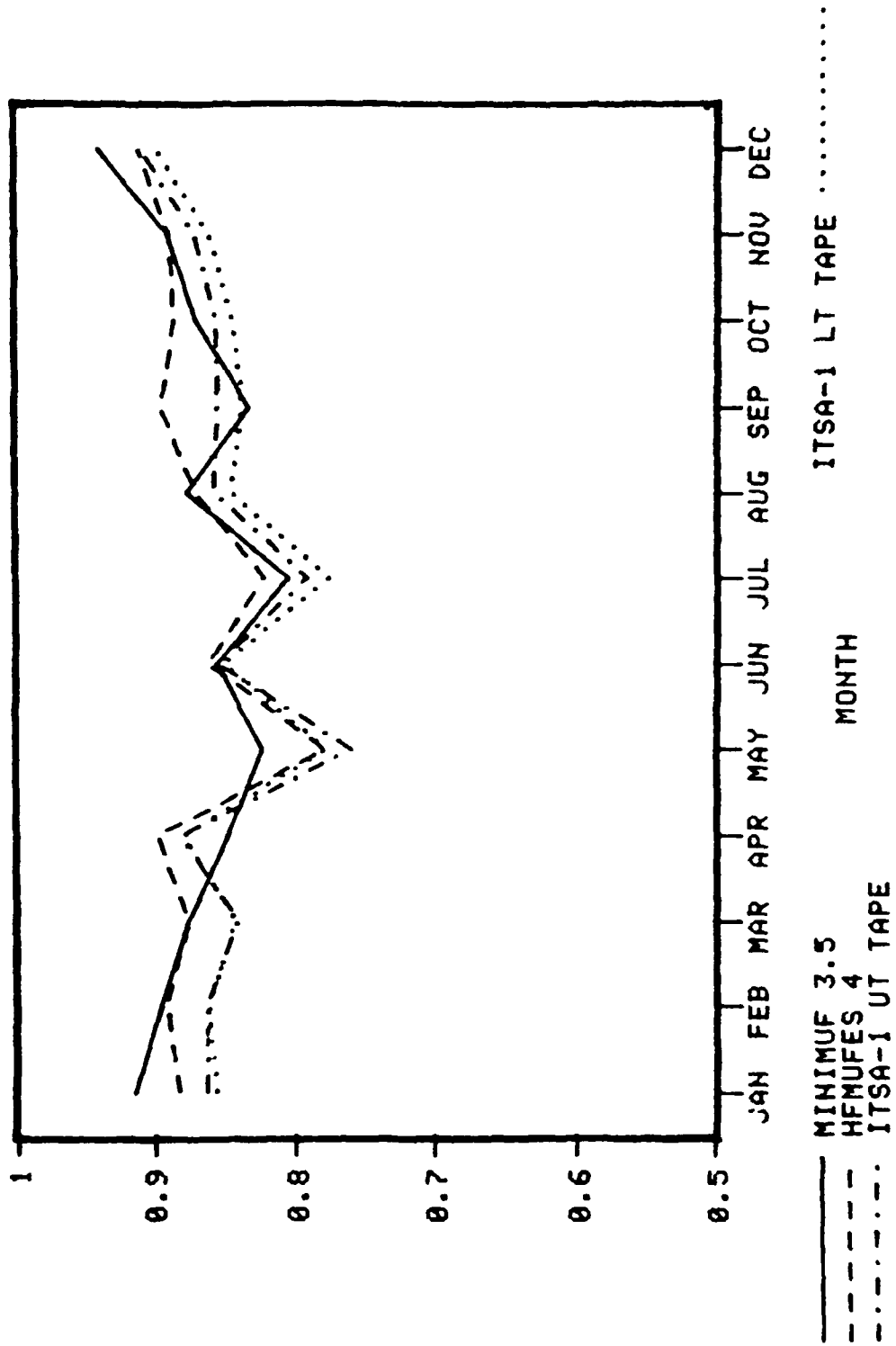
Figure 42. Correlation coefficients as a function of month.

cent during winter and spring, dropping below 20 percent during summer and rising to about 25 percent in the fall.

Figure 30 shows HFMUFES 4 to have the highest correlation coefficient as a function of season. Its highest value is about .9 during the fall, and its lowest value is about 0.85 during the summer. MINIMUF-3.5, itself, never drops below 0.85 either. The monthly dependence of the correlation is somewhat oscillatory, with one or the other program indicated as best.

GEOMAGNETIC LATITUDE

The next tests were made to determine error as a function of geomagnetic latitude. The five categories denote transequatorial (TE) propagation, low latitude (LO) propagation, mid-latitude (M) propagation, high latitude (HI) propagation and transauroral (TA) propagation. These channels show entirely different propagation characteristics and problems. Each path was categorized according to the geomagnetic latitude location of control points. The type determined for each path is given in Table 10. The percentage of the sample in each path type category is given in Table 11.

Path Type	Number of Hours	Percentage of Sample
Transequatorial	176	16.7
Low latitude	64	16.1
Mid-latitude	557	52.9
High latitude	176	12.3
Transauroral	48	4.5

Table 11. Percentage of sample in geomagnetic latitude categories.

Figures 43-48 illustrate the performance of each of the four prediction programs as a function geomagnetic latitude. Figures 43 and 44 show the average residual and average relative residual, respectively. They particularly show that all four programs predict low in the high latitude and transauroral regions. In the transequatorial, low latitude and mid-latitude regions MINIMUF-3.5's bias is nearly zero whereas HFMUFES 4 predicts low in these same regions by as much as 1 MHz. However, HFMUFES 4 has

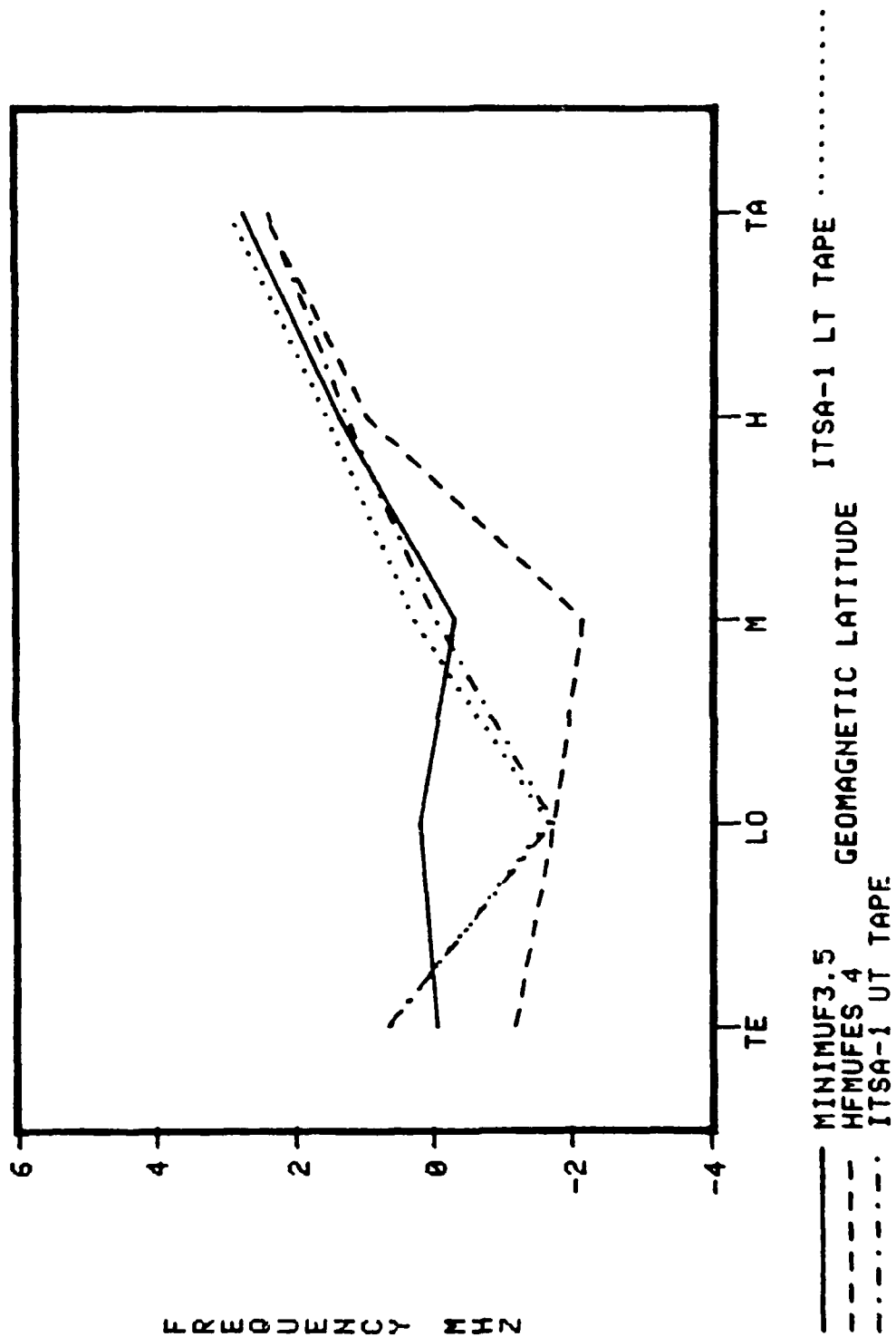Figure 43. Average residual (bias) as a function of geomagnetic latitude location of control points.
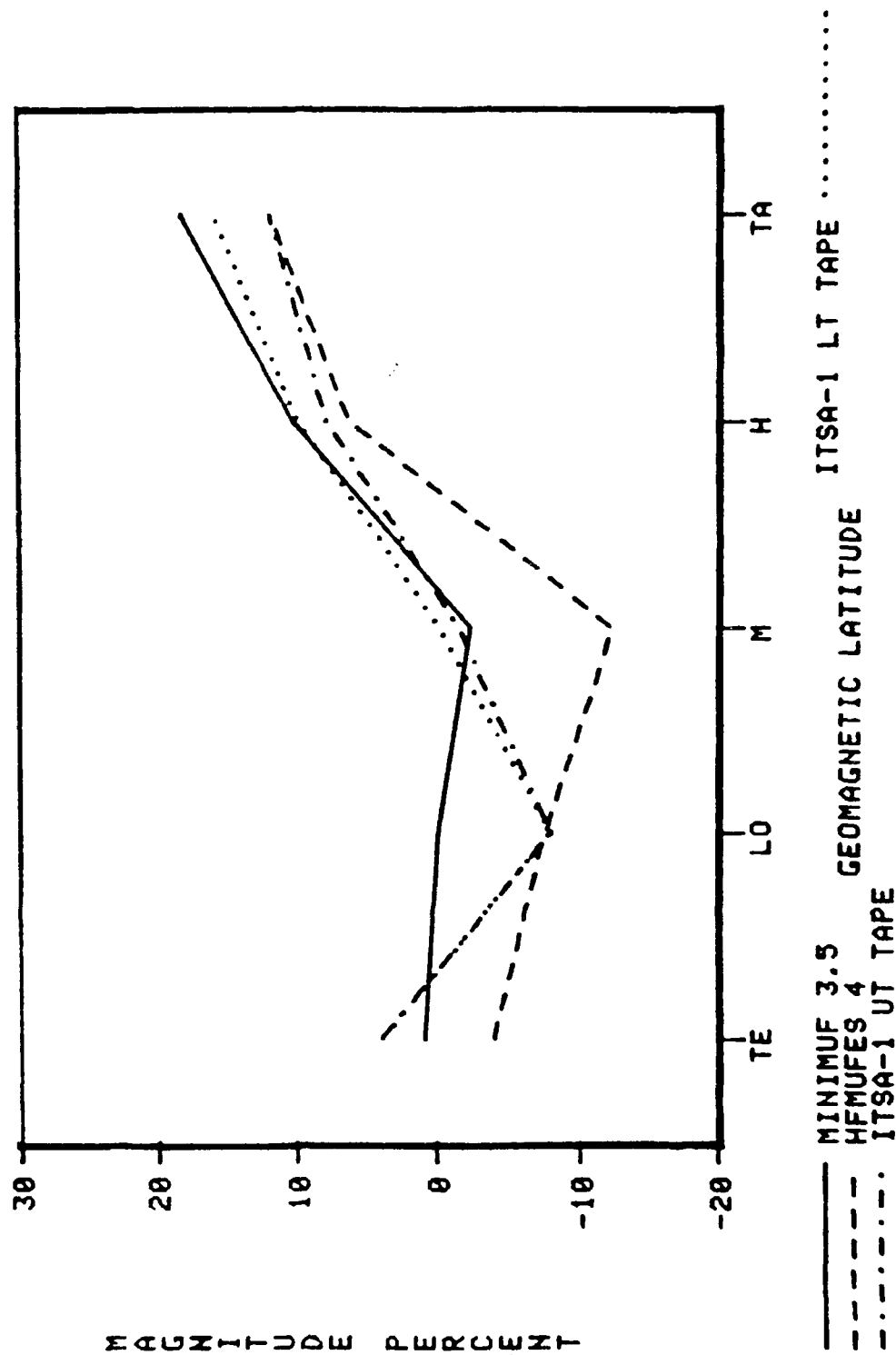
Figure 44. Average relative residual (relative bias) as a function of geomagnetic location of control points
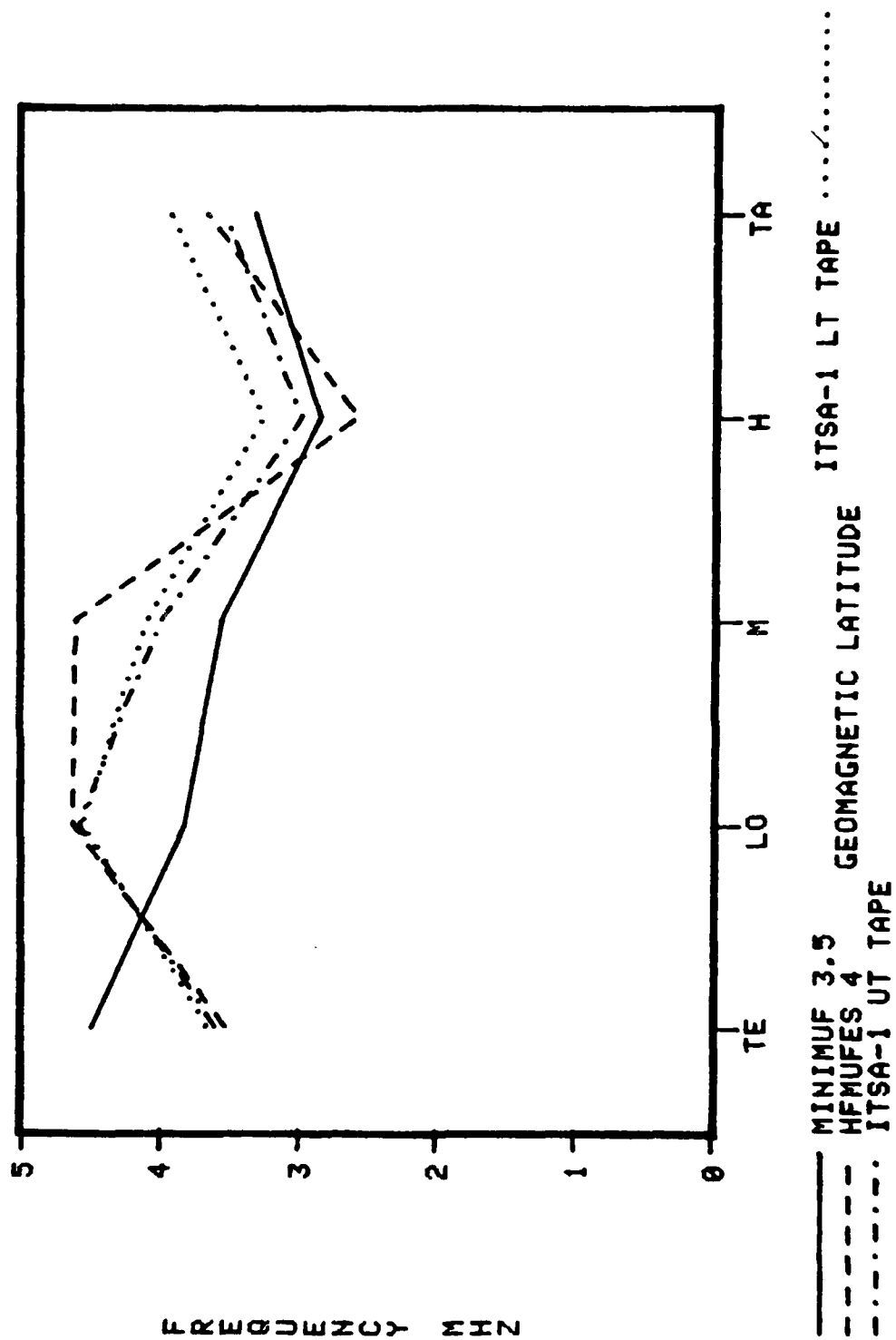
Figure 45. Rms error in MHz as a function of geomagnetic latitude location of control points.

Figure 46. Relative rms error as a function of geomagnetic latitude location of control points.

Figure 47. Magnitude of the error (average absolute relative residual) as a function of geomagnetic latitude location of control points.
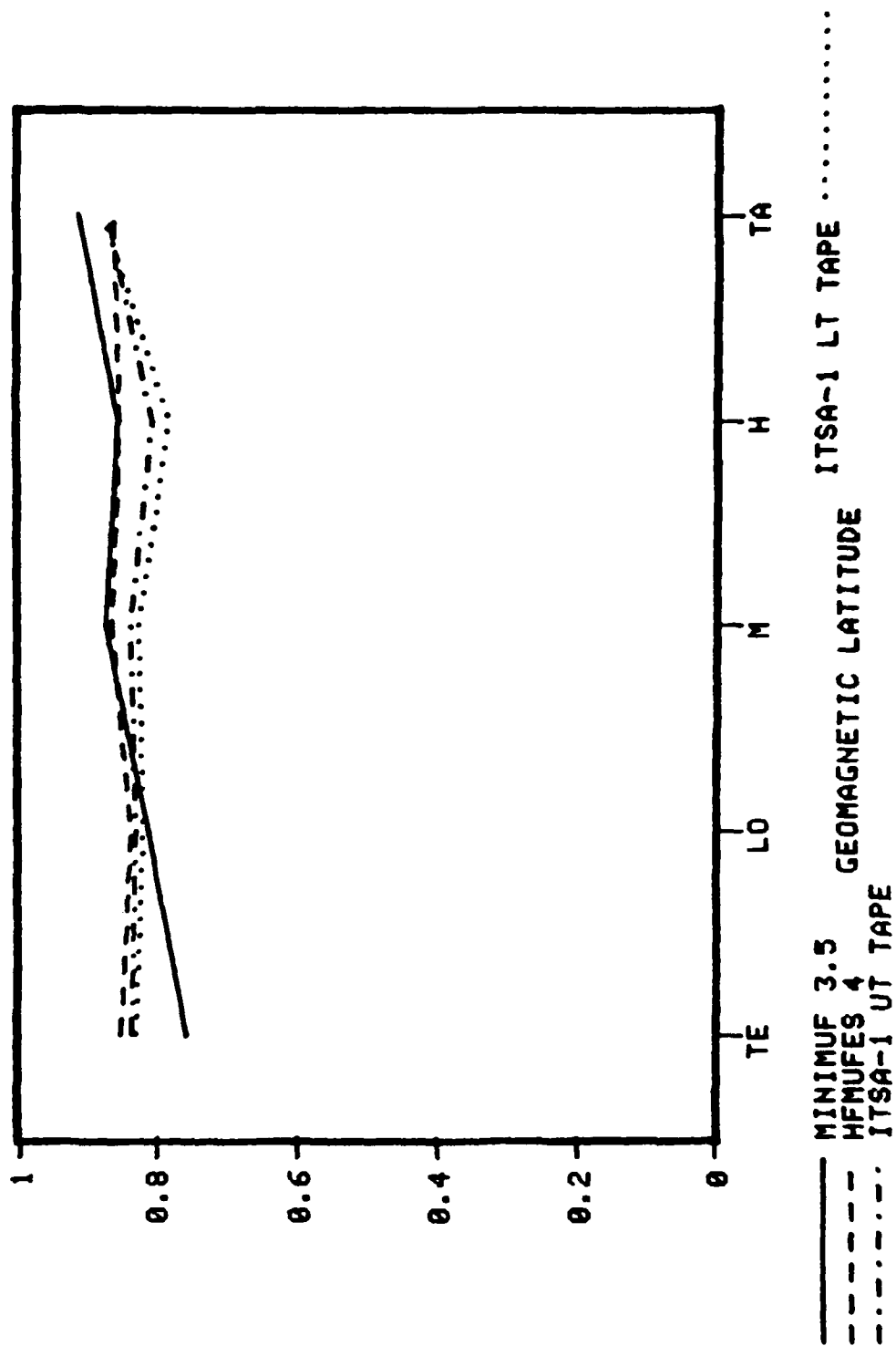
Figure 48. Correlation coefficients as a function of geomagnetic latitude location of control points.

MINIMUF-3.5 are not much different. However, at low latitude the ITSA-1 programs have as much difficulty as does HFMUFES 4.

Figure 46 shows that the relative rms error increases for all four programs as the geomagnetic latitude of the control points increase. What is not expected is the peak for HFMUFES 4 occurring at mid-latitude. In this latitude region one would expect it to perform at its best.

Figure 47 shows that the average magnitude of the error for both HFMUFES 4 and MINIMUF-3.5 peak at mid-latitude with HFMUFES 4 has a value over 30 percent. MINIMUF-3.5 generally has values less than 20 percent at all geomagnetic regions.

Again Figure 48 shows the superior correlation between predicted MUF values by HFMUFES 4 and the observed values except for the transauroral region where MINIMUF-3.5 has the highest values.

SOLAR SUNSPOT NUMBER (SSN)

A major consideration in MUF prediction is the ability of a model to deal with different phases of the solar sunspot cycle. Ideally, it should produce consistent results for SSN values between one and 150. The data were subdivided into four sunspot number categories (actually five, but the fifth contained no data points). Table 12 gives the percentage of the sample in each category.

Sunspot Number (Cycle Phase)	Sample, Path hours	% of Sample
10-30 (minimum)	1728	37.0
31-60 (rise and decline)	240	5.1
61-90 (near maximum)	551	11.8
91-120 (maximum)	2101	45.0
121-150 (high maximum)	0	0.0

Table 12. Percentage of sample in each SSN category.

Figures 49-54 summarize the prediction performance as a function of SSN. Figures 49-53 show the same poor performance of HFMUFES due to its tendency to
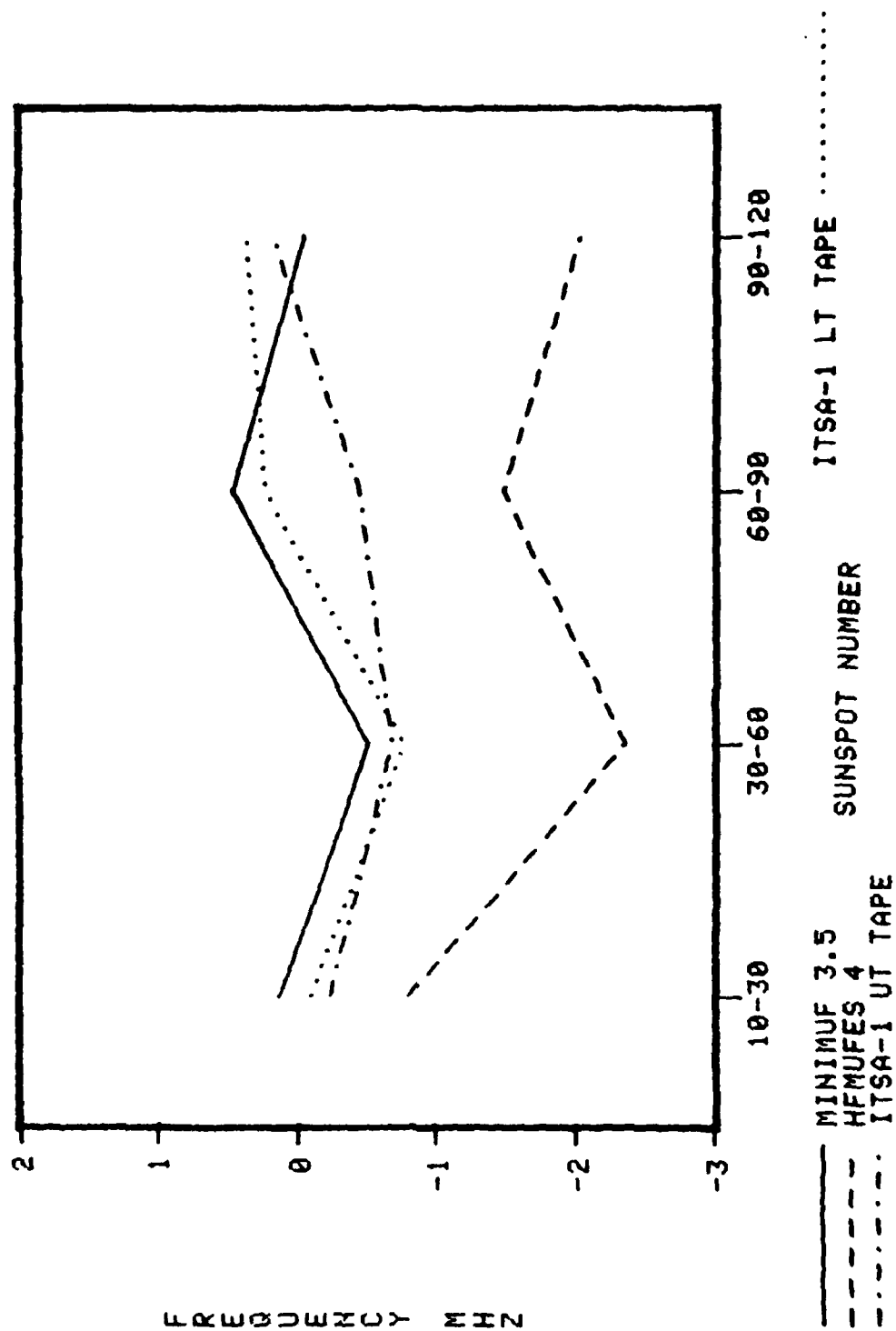
Figure 49. Average residual (bias) as a function of sunspot number.

MINIMUF 3.5   SUNSPOT NUMBER   ITSA-1 LT TAPE ··········
HFMUFES 4
ITSA-1 UT TAPE
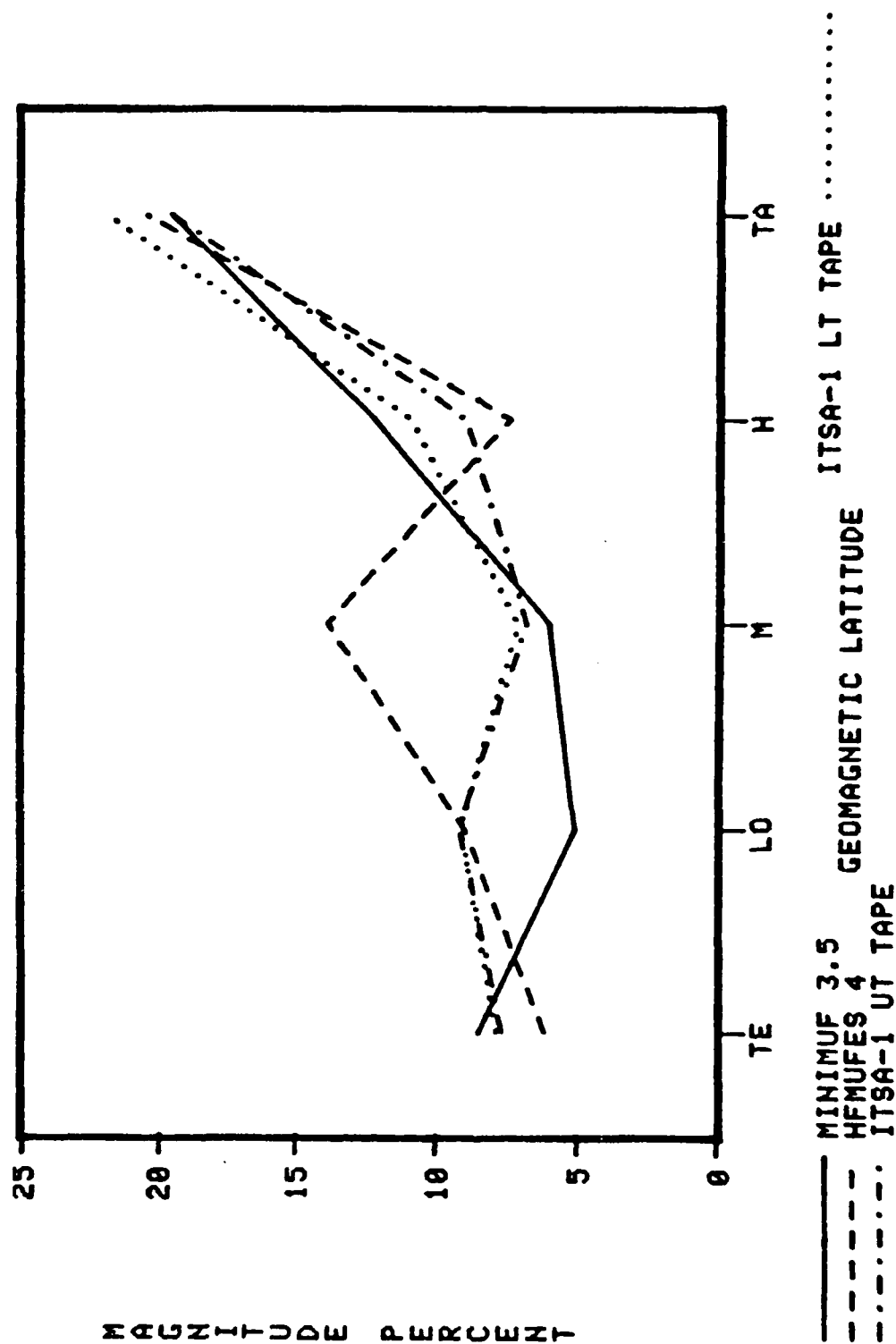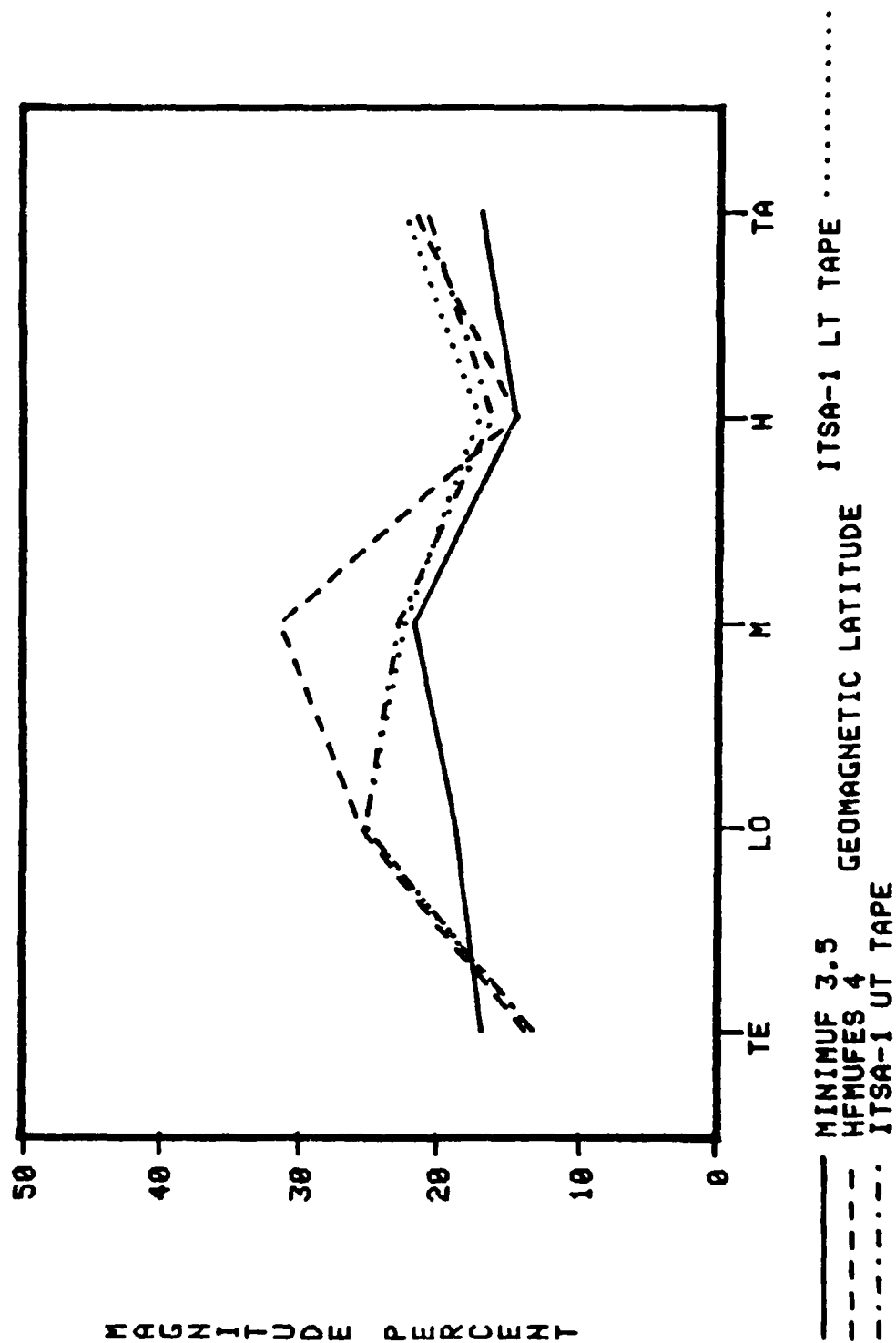
Figure 50. Average relative residual (relative bias) as a function of sunspot number.

Figure 51. Rms error in MHz as a function of sunspot number.

Figure 52. Relative rms error as a function of sunspot number.

Figure 63. Magnitude of the error (average absolute relative residual) as a function of sunspot number.
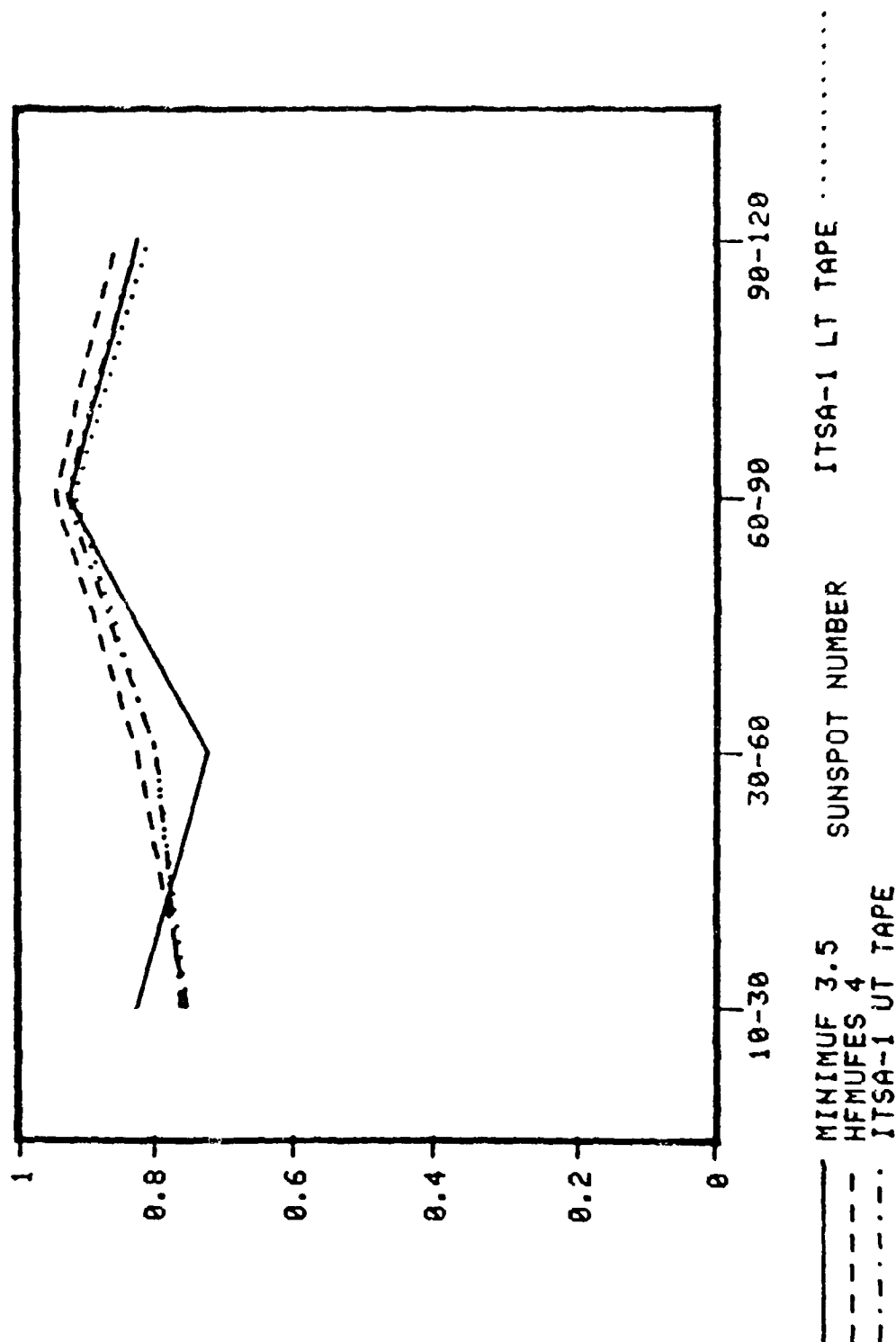
Figure 54. Correlation coefficients as a function of sunspot number.

predict high. The remaining results show the somewhat superior performance of MINIMUF-3.5. Figures 49 and 50 show a spread in bias between a SSN of 60 to 90. Figure 51 shows that the rms error increases with increasing SSN, but Figure 52 shows that the relative rms error decreases with high SSN. This probably is due to increasing MOFs at high SSN, and hence, decreasing relative residuals at high SSNs. The relative rms error seems to peak at SSN between 60 and 90, being at most 8 percent for MINIMUF-3.5. Figure 54 shows again the superior correlation between HFMUFES 4 predicted data and observed MOF data.

DIURNAL TRENDS

One of the most important variations in path MOF is its diurnal variation. This section describes the accuracy of the programs as a function of time of day. To do this, the entire data set was converted to local path time (i.e., the local time at the path midpoint). Figures 55-60 show the results of the comparison of the four programs as a function of midpath local time.

Figures 55 and 56 show the average residual and the average relative residual, respectively. HFMUFES 4 predicts high at all hours having its largest bias of 2.7 MHz (11 percent) at 1600 LT. The bias of the three large scale programs show a strong correlation as a function of local time. The bias of MINIMUF-3.5 has a strong diurnal variation. Starting at 0100 LT the average residual is 1.3 below the observed value. The bias decreases to near zero at 0700 LT, but increases again to 1 MHz low at 1800 LT. The bias steadily decreases then as local time increases to a value of 1.75 MHz high at 2100 LT. It then increases with local time 0.9 MHz low at 2400 LT.

Figures 57 and 58 show the rms error and relative rms, respectively. The most notable feature in these figures is the rms error in the MINIMUF-3.5 prediction from 0600 to 1000 hours local time and from 1700 to 2100 hours local time. Also Figure 58 shows an additional peak in the relative rms error at 0100 LT. The rms error of the other three programs builds up to a peak between 1500 and 1600 LT. However, the daytime relative rms error for HFMUFES 4 is much higher than for the two ITSA-1 programs.

Figure 59 shows average magnitude of the error. During the heart of the daytime, MINIMUF-3.5 has the lowest value (14-17 percent). However, during the transition hours MINIMUF-3.5 values increase tremendously to 25 percent during the morning transition period and 27 percent during the evening

‖‖ 1.0

‖‖ 1.1

‖‖ 1.25   ‖‖ 1.4   ‖‖ 1.6

2.8   ‖‖ 2.5
3.2   ‖‖ 2.2
      ‖‖ 2.0
      ‖‖ 1.8
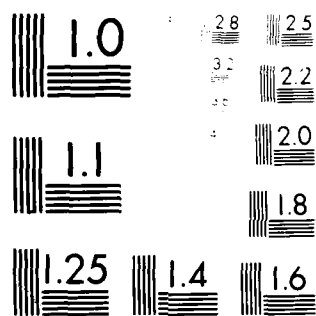
MICROCOPY RESOLUTION TEST CHART
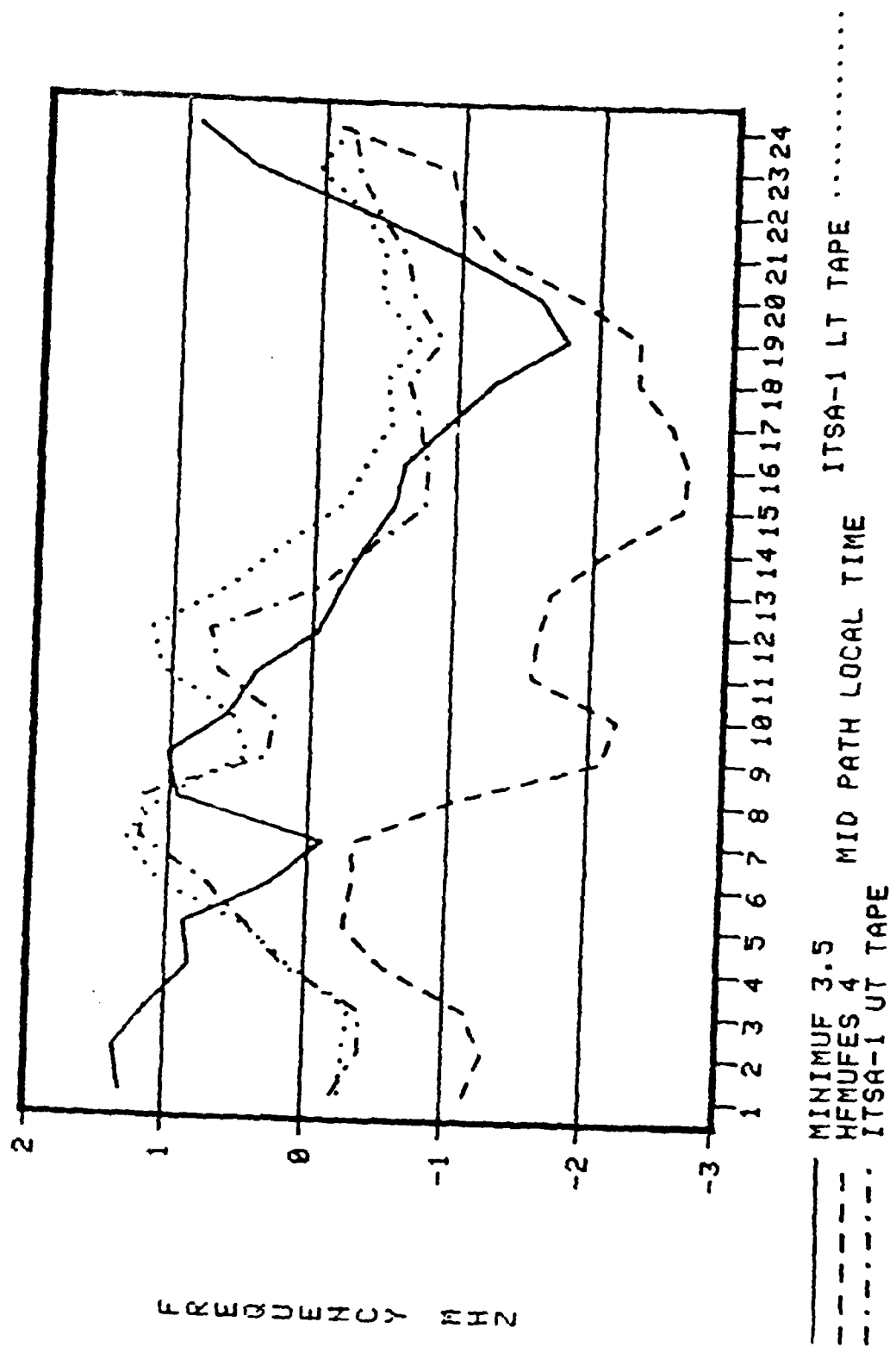
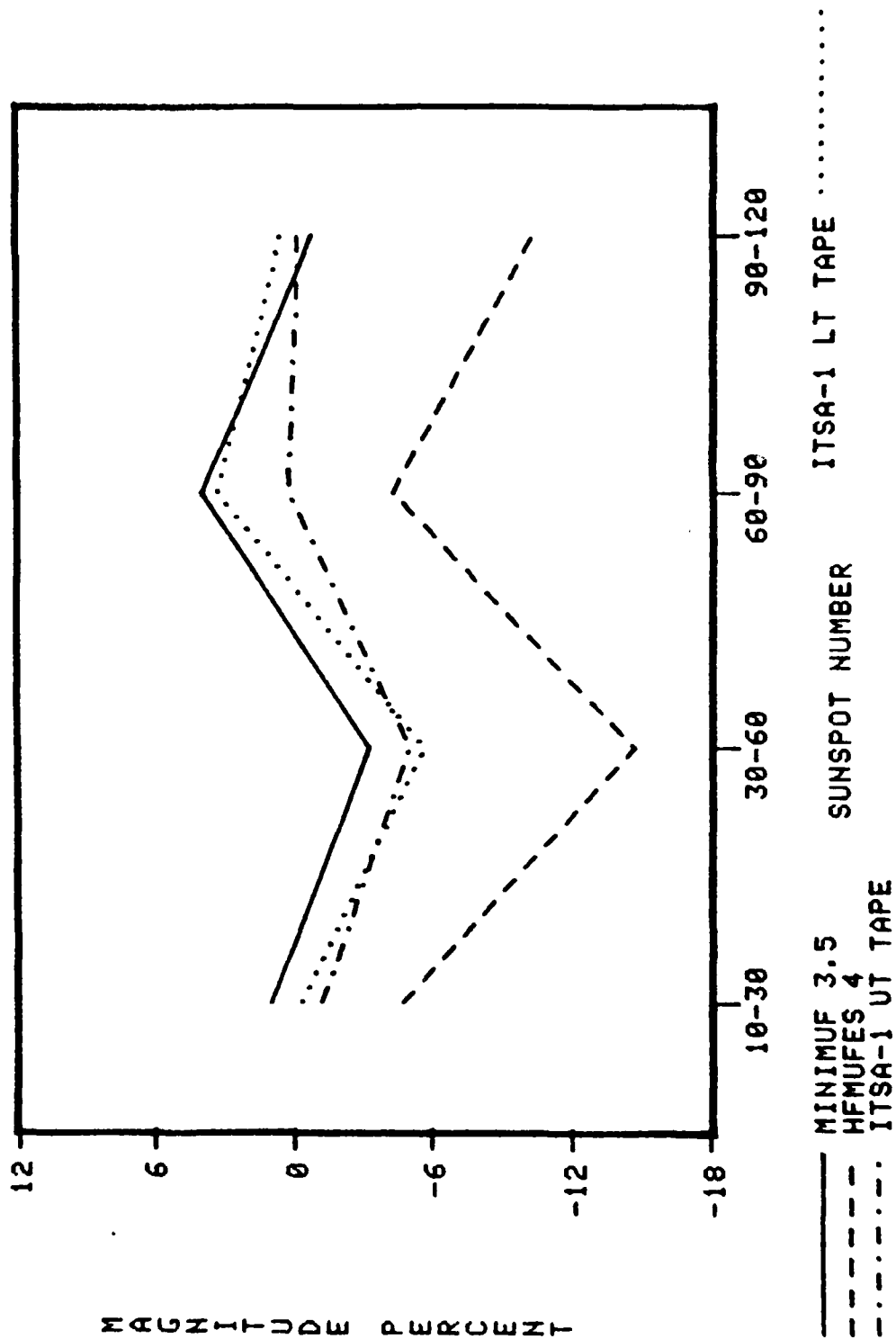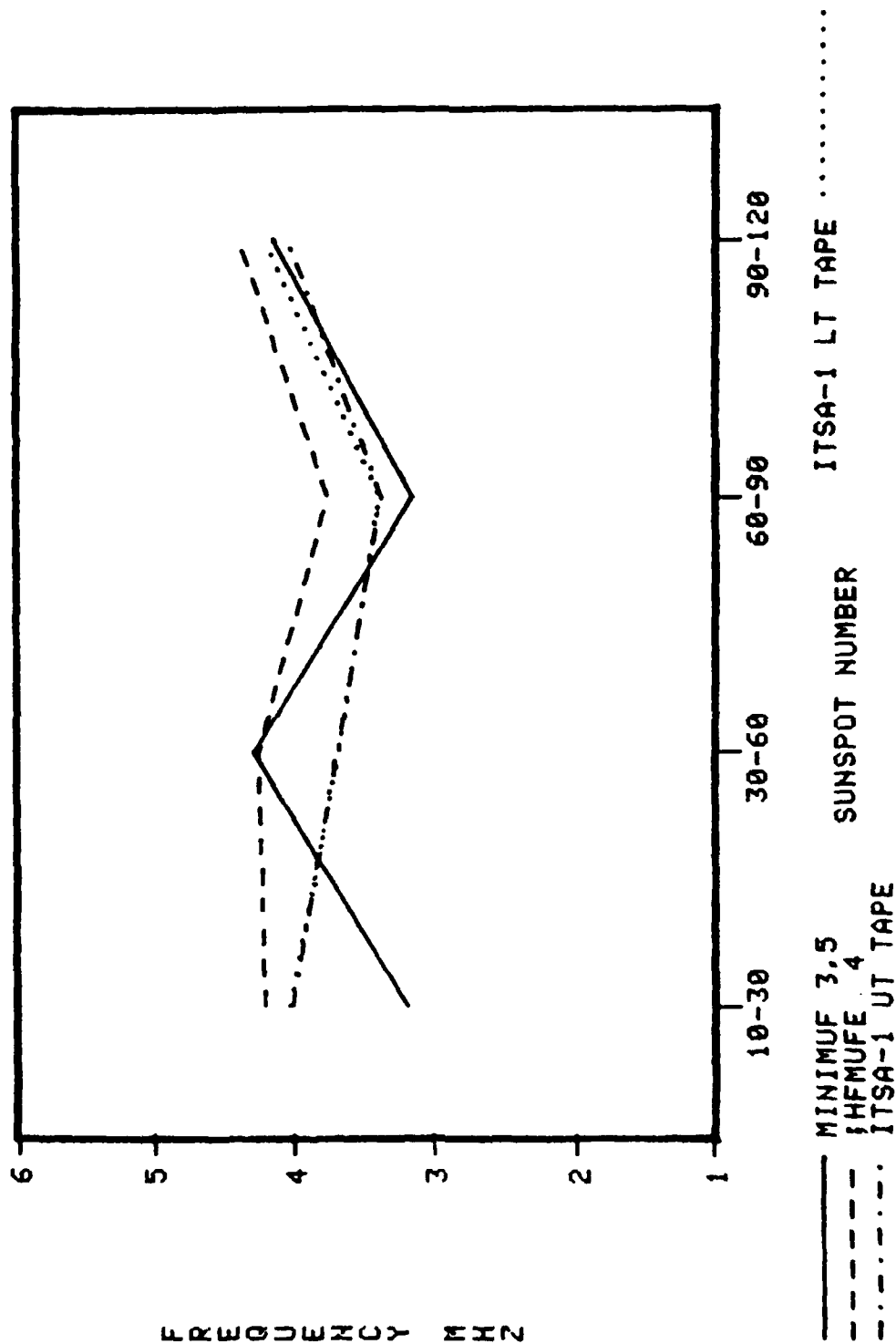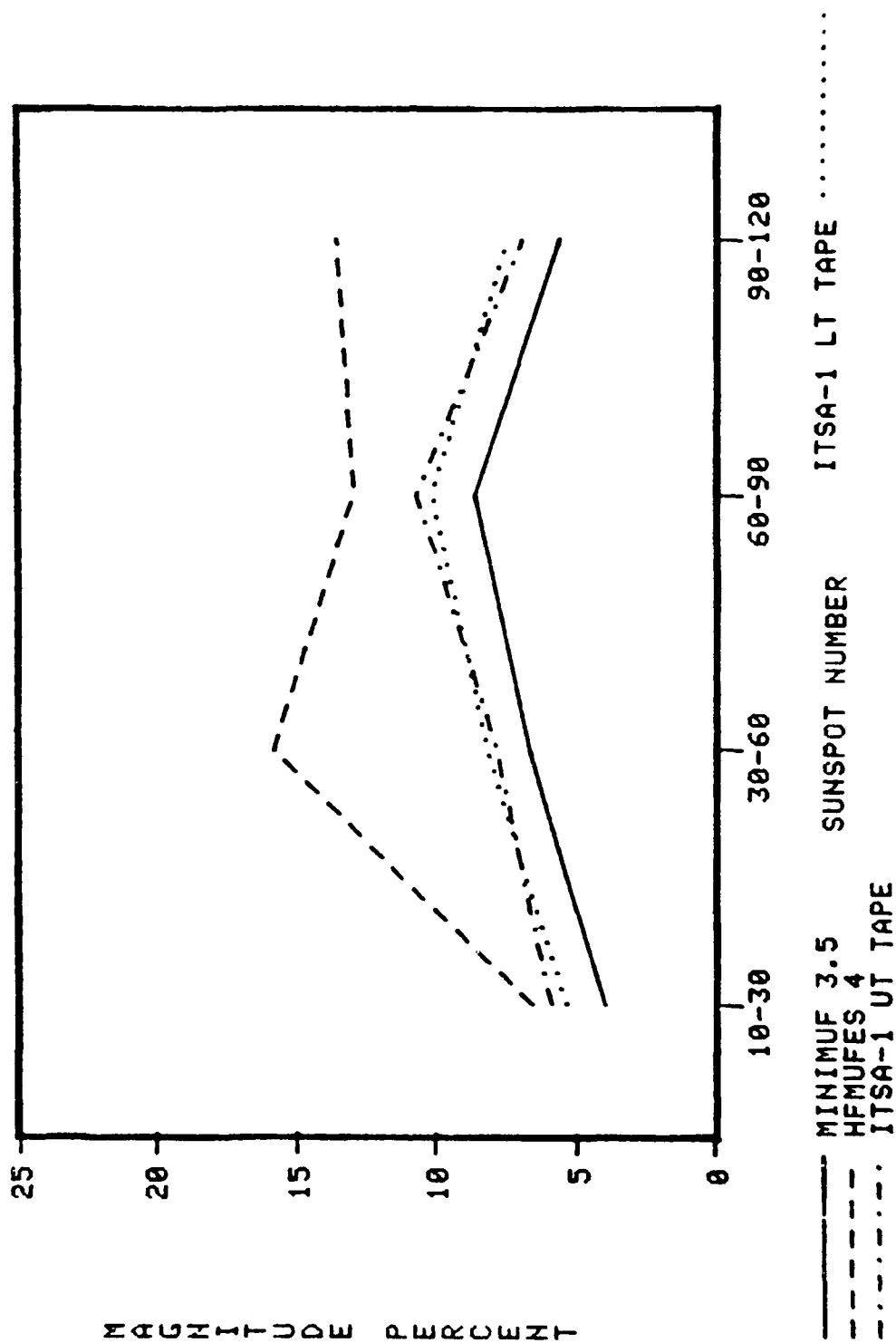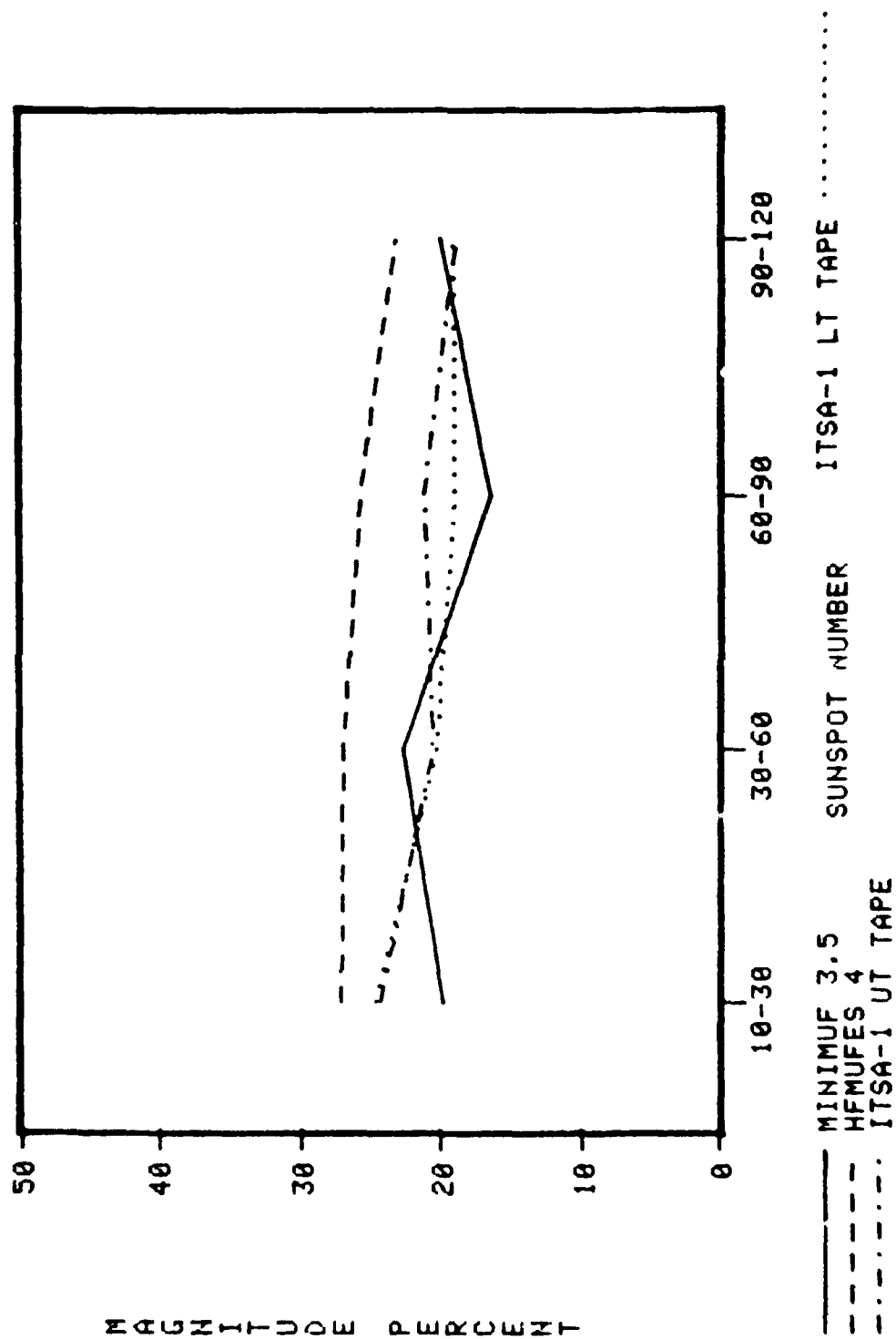Figure 55. Average residual (bias) as a function of local time.
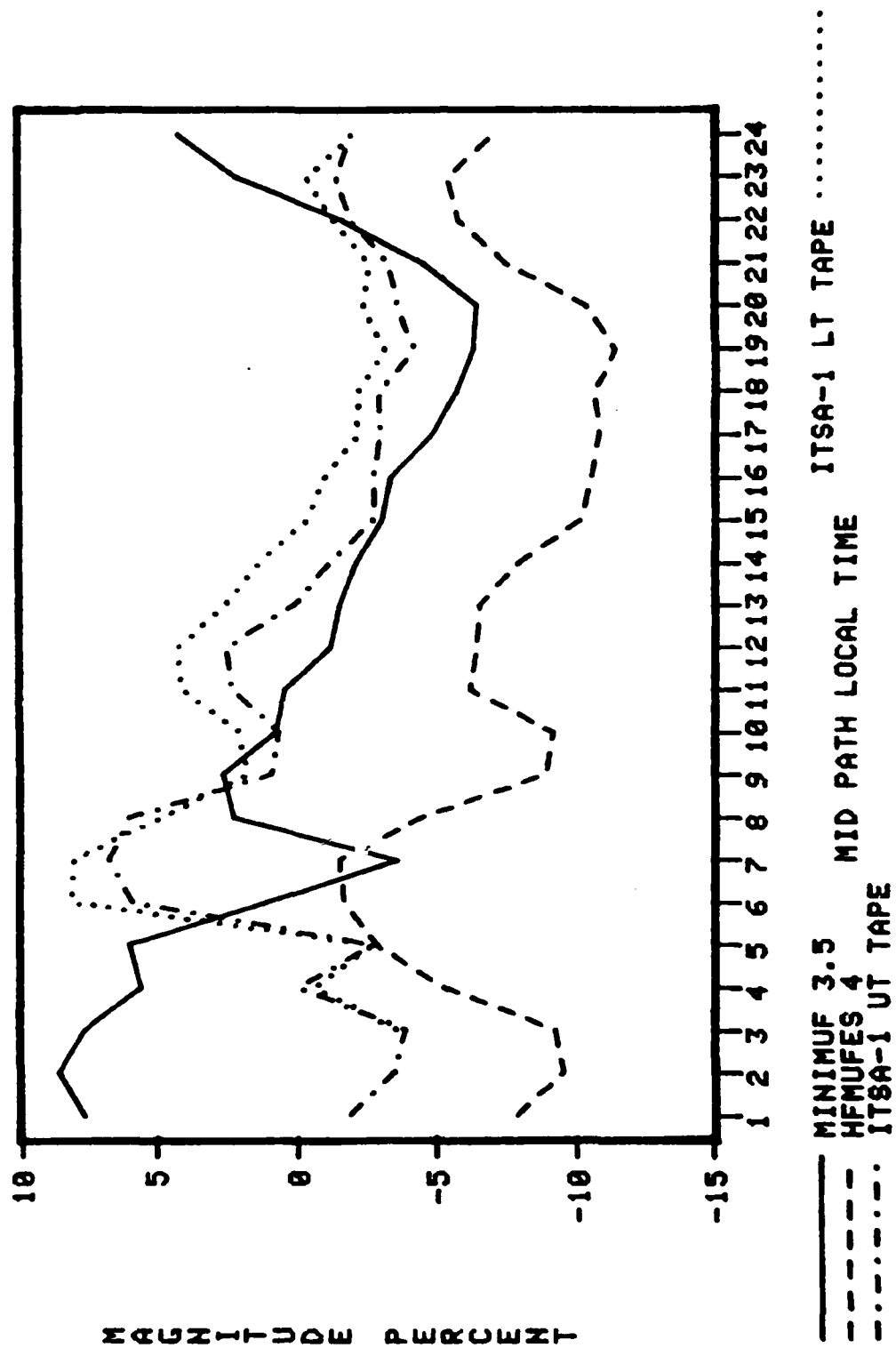
Figure 56. Relative residual (relative bias) as a function of local time.
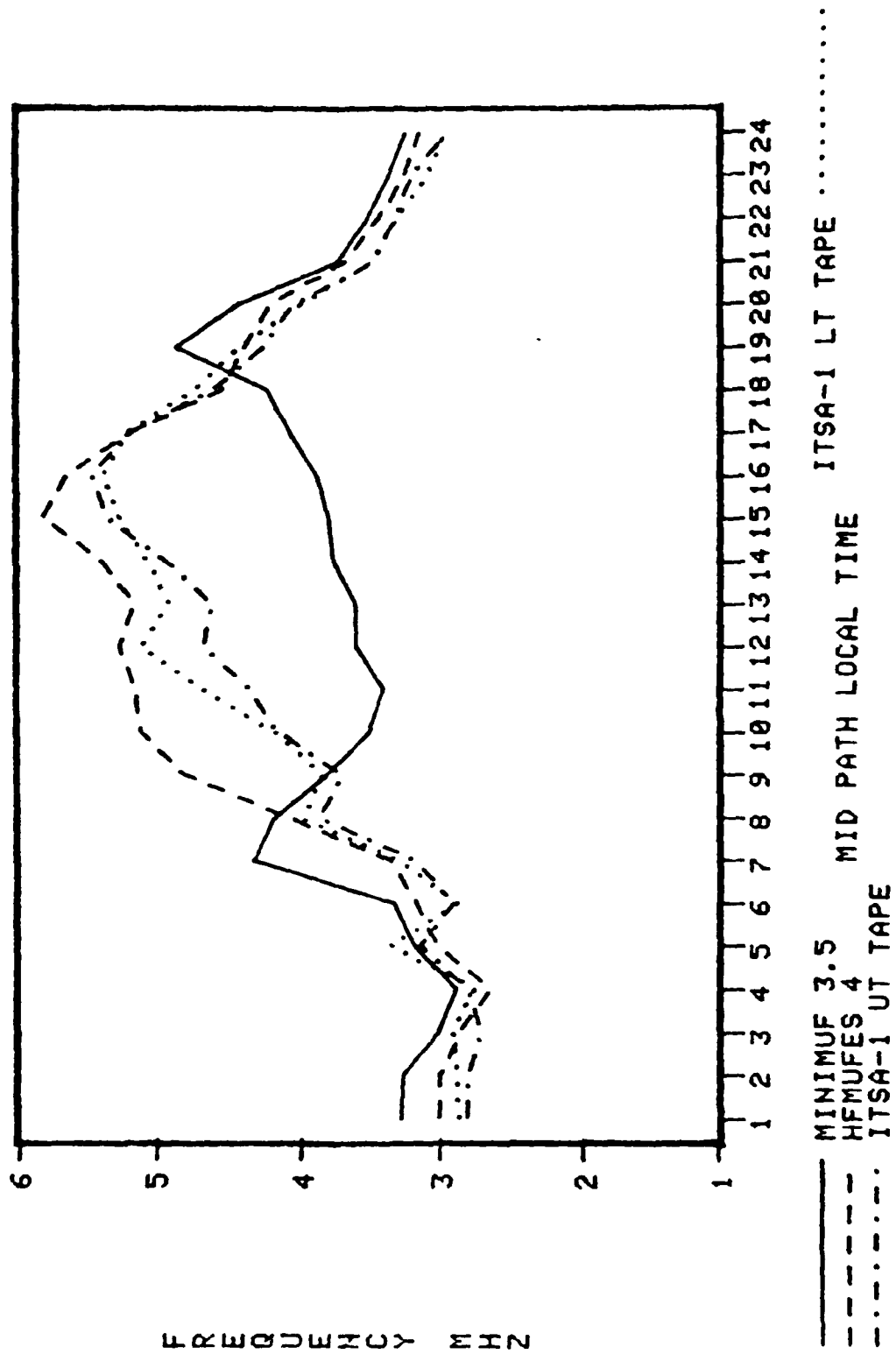
Figure 57. Rms error in MHz as a function of local time.

MINIMUF 3.5
HFMUFES 4   MID PATH LOCAL TIME
ITSA-1 UT TAPE

ITSA-1 LT TAPE

FREQUENCY MHz

87

Figure 58. Relative rms error as a function of local time.

Figure 59. Magnitude of the error (average absolute relative residual) as a function of local time.

89
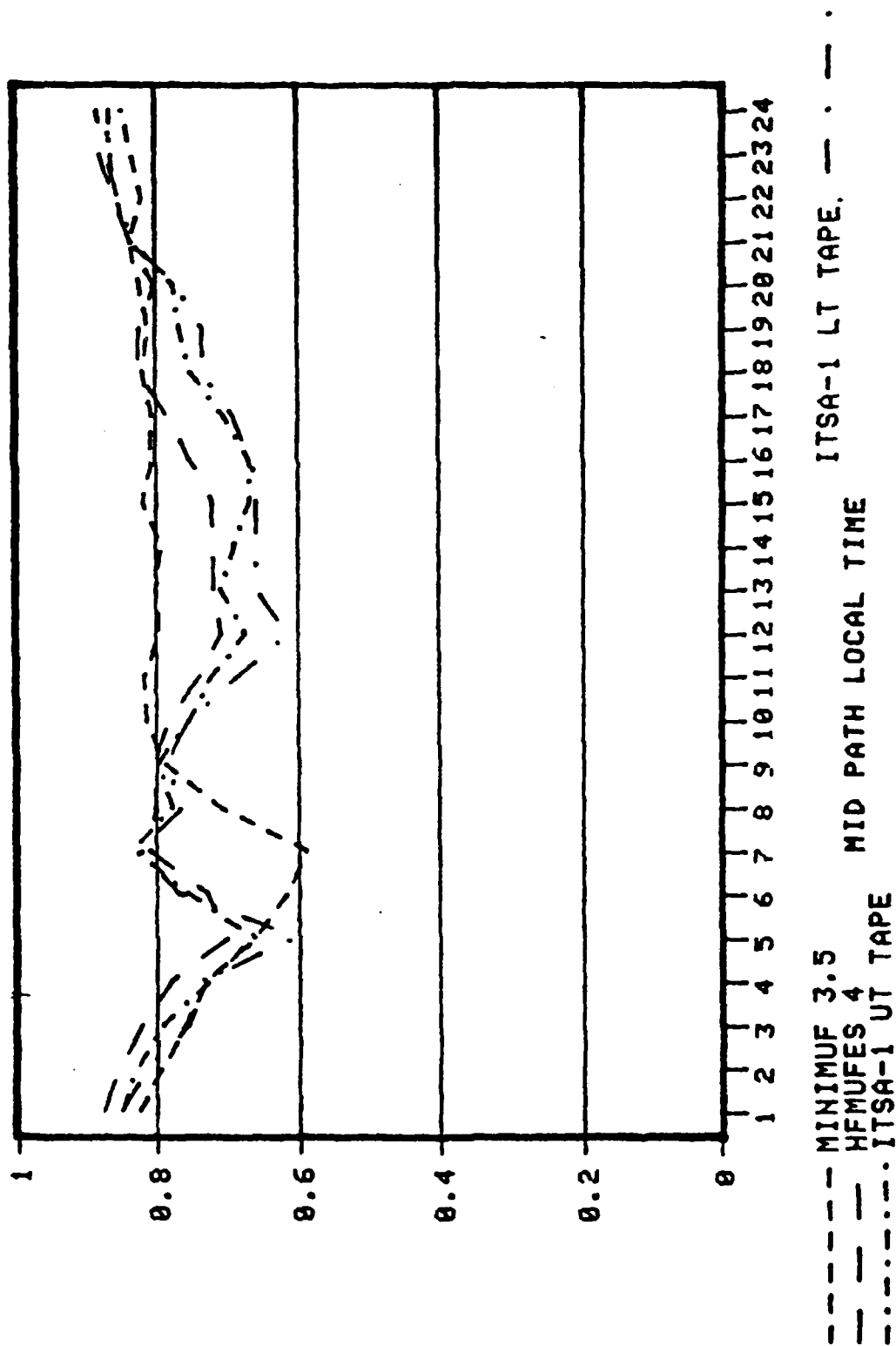
Figure 60. Correlation coefficients as a function of local time.

transition period. The magnitude of the error for HFMU... 4 is again the highest of the four.

Figure 60 shows the correlation coefficient between the predicted and observed values. The correlation is generally high with HFMUFES having the highest values.

GEOGRAPHICAL REGIONS

The last variation to be considered was the effect of different geographical regions on performance of the programs. The subdivision chosen was paths that were either entirely over land (continental), entirely over ocean (ocean) or partly over land and partly over ocean (other). This division was chosen partly because of the sparsity of data in ocean areas to develop the numerical maps of ionospheric coefficients and because oblique sounder data over the ocean areas were used to calibrate MINIMUF-3.5. Table 13 indicates the percentage of the sample in each geographic area. Note the dominance of data from paths over the ocean and the small portion of data entirely over land. Figures 61-66 illustrate the performance as a function of geographic region.

Geographic Region	Path Hours	Percentage of Sample
Continental	624	13.4
Ocean	2738	58.7
Other	1306	28.0

Table 13. Percentage of sample in geographic regions.

Figures 61 and 62 show the average residual and average relative residual, respectively. Note first that HFMUFES 4 performs worst in the ocean areas. In fact, its performance in the other regions is actually better than the other programs. In the ocean areas MINIMUF-3.5 produces the best results.

Figures 63 and 64 show the rms error and relative rms error, respectively. Again HFMUFES 4 has its highest value (nearly 4.7 MHz) over ocean areas. By contrast, over land its rms error drops to 2.5 MHz. As expected MINIMUF-3.5 has its lowest relative rms error over ocean paths.

Figure 65 shows the average magnitude of the error of the four programs. In this figure, as was the case in the previous four figures, HFMUFES 4 is the worst program over ocean paths and the best over land bodies.
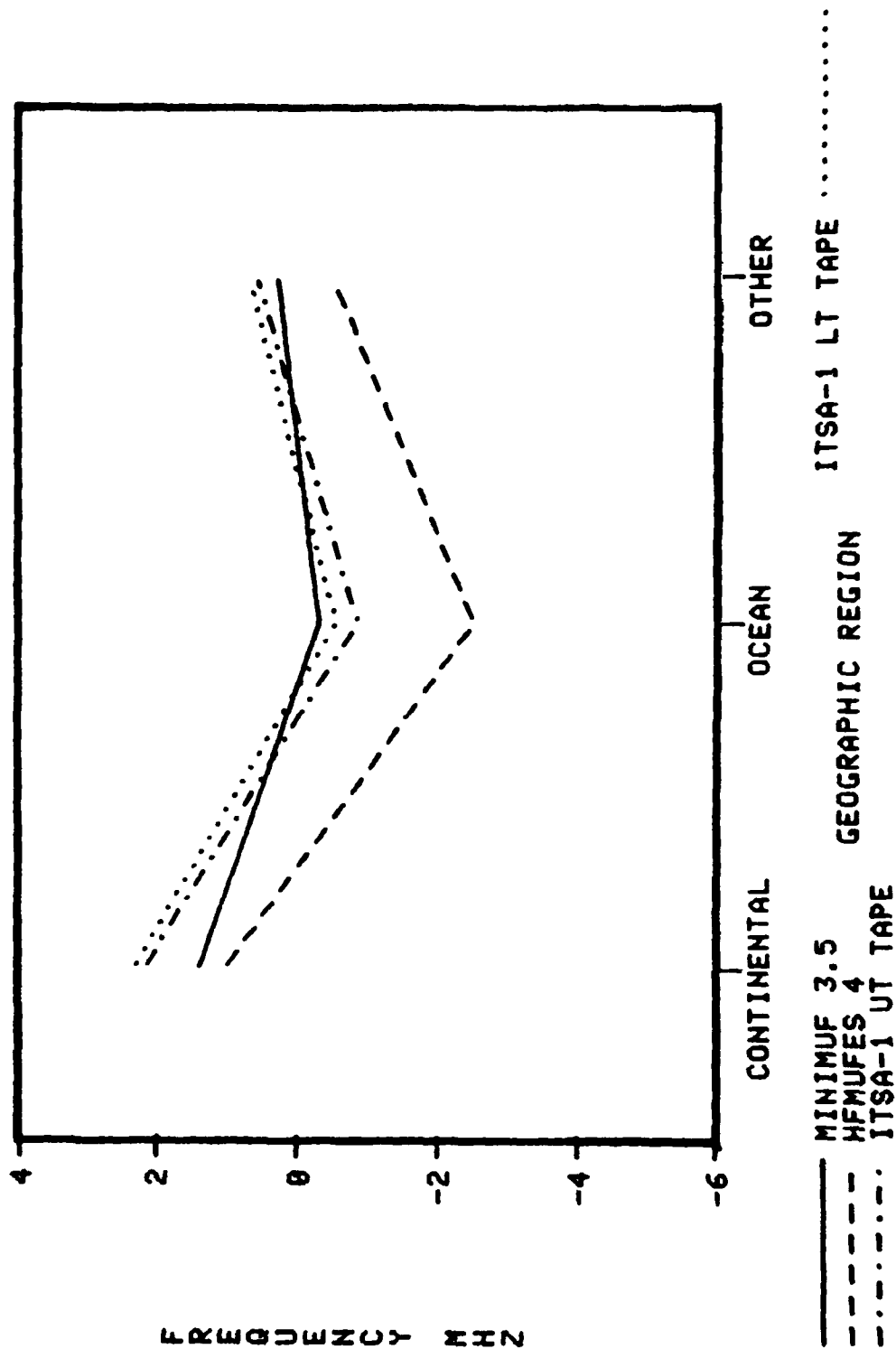
Figure 61. Average residual (bias) as a function of geographic region.

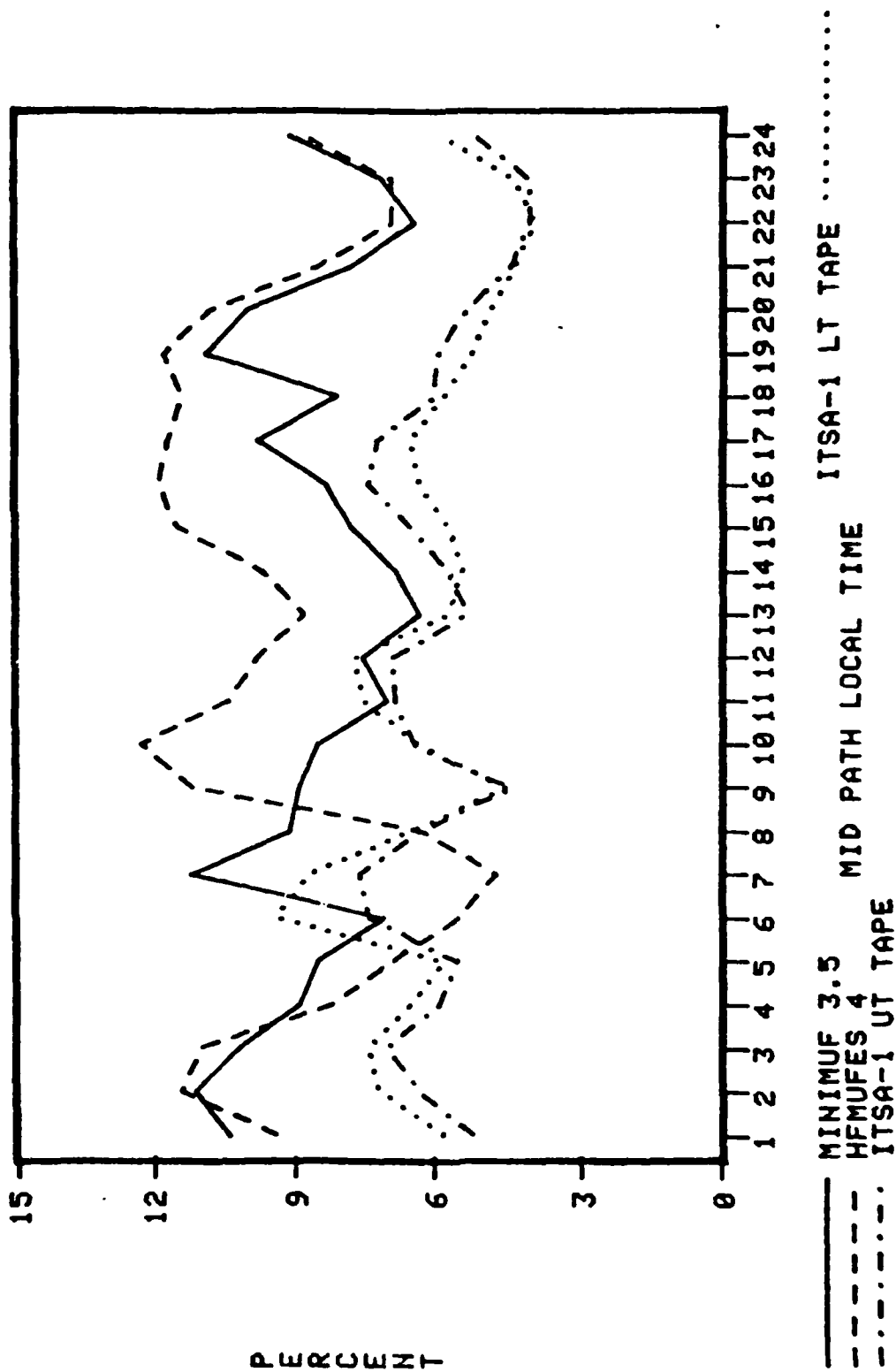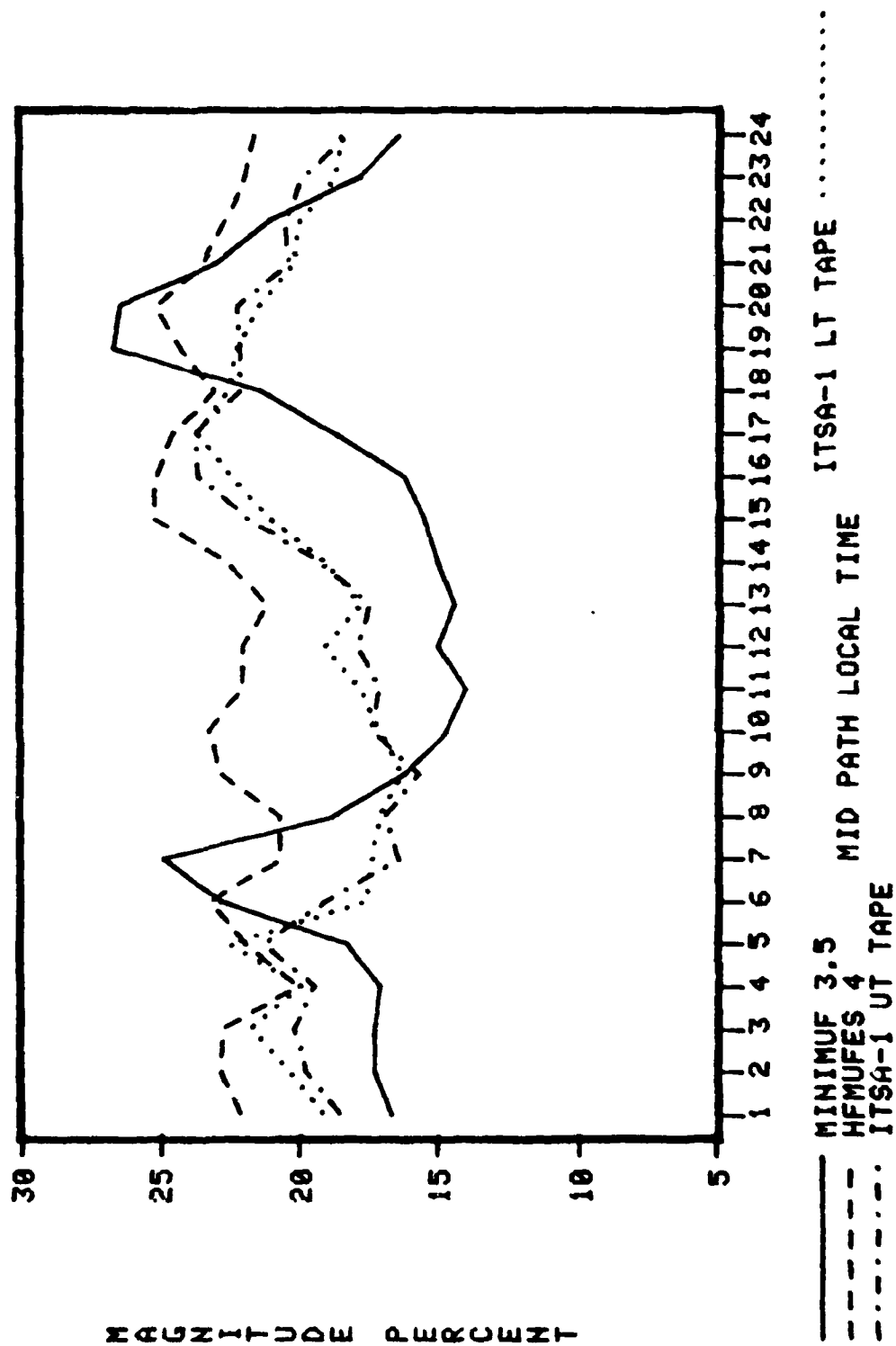Figure 62. Average relative residual (relative bias) as a function of geographic region.
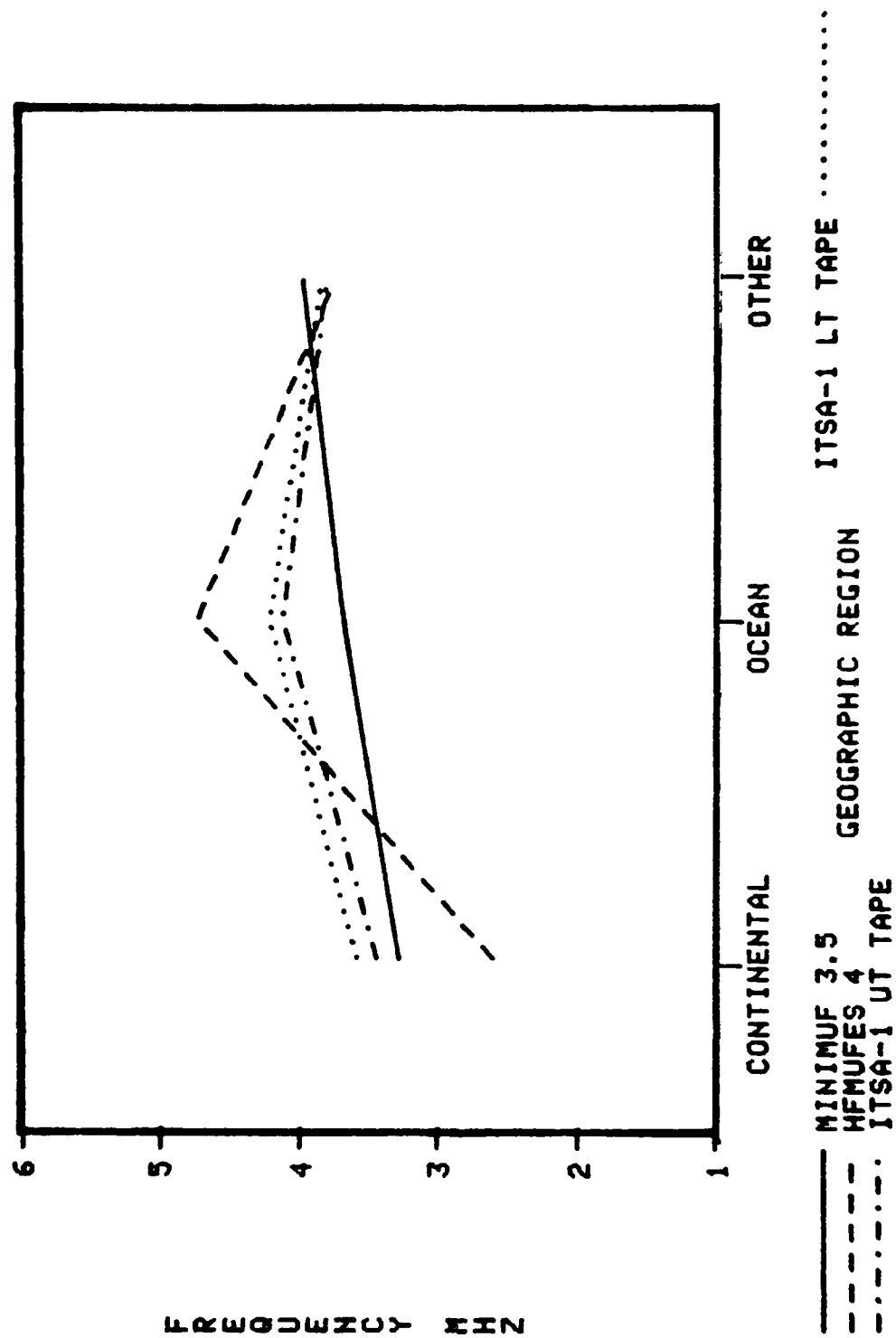
Figure 64. Rms error in MHz as a function of geographic region.
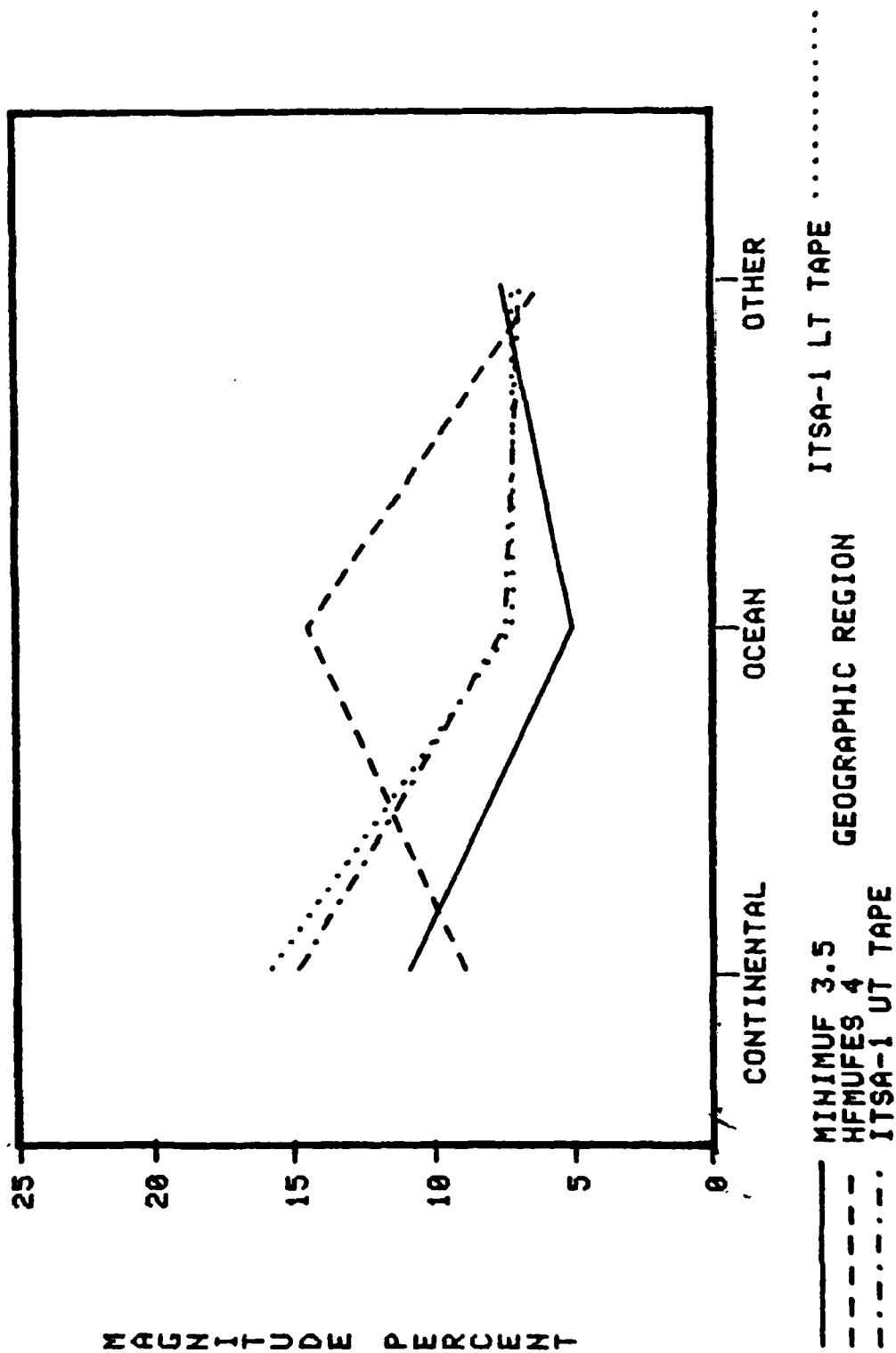
Figure 64. Relative rms error as a function of geographic region.

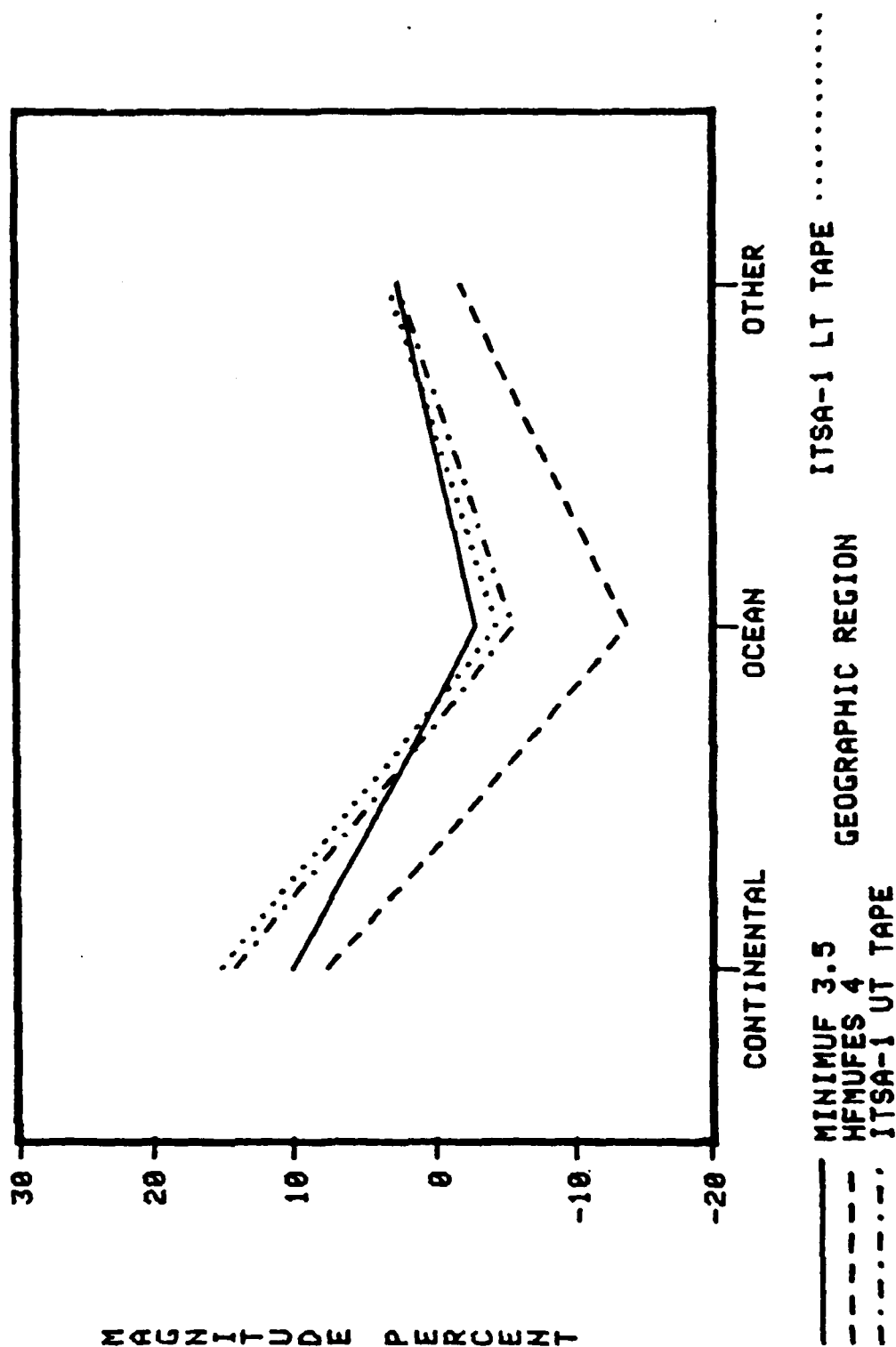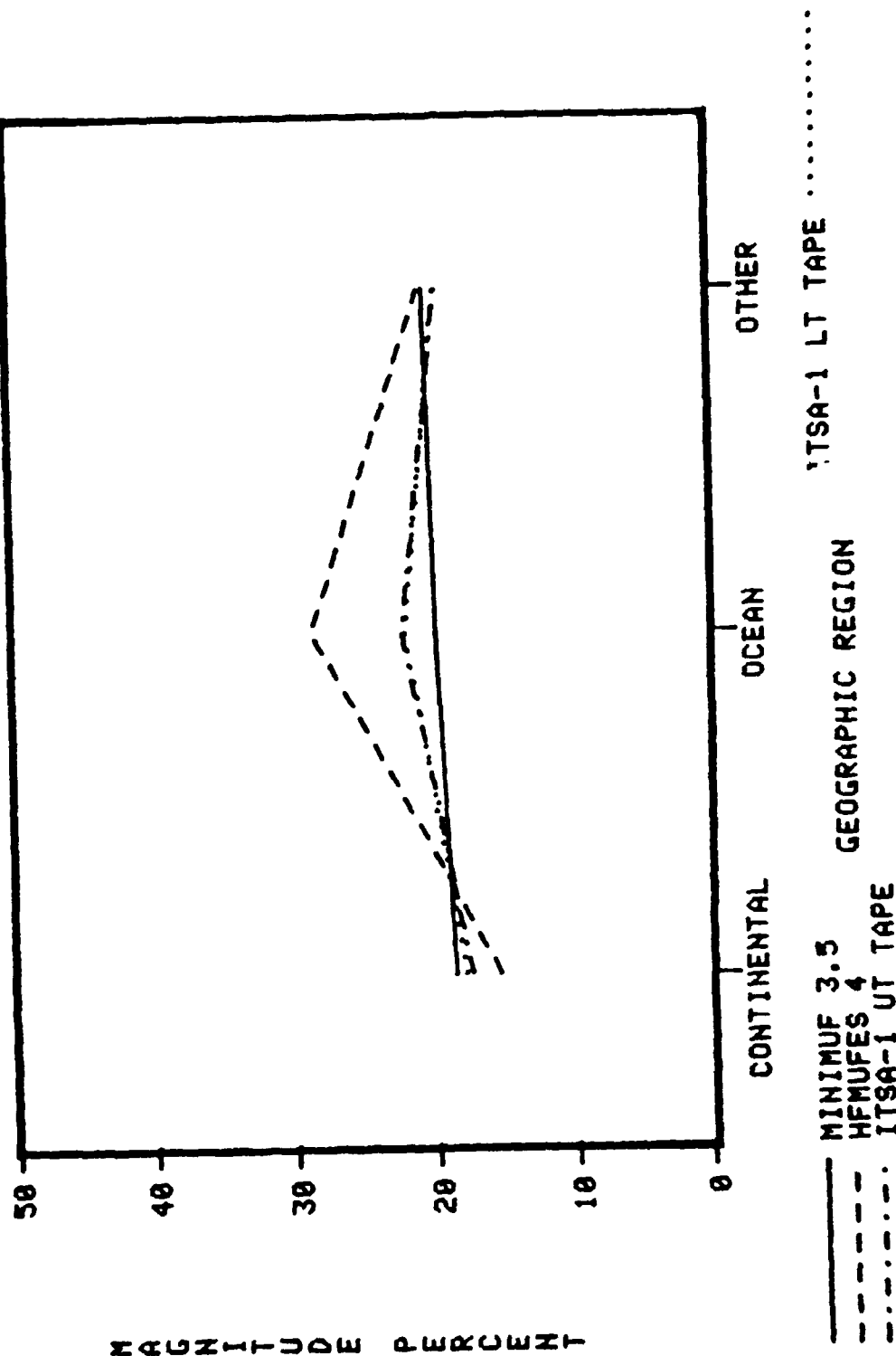Figure 65. Magnitude of error (average absolute relative residual) as a function of geographic region.
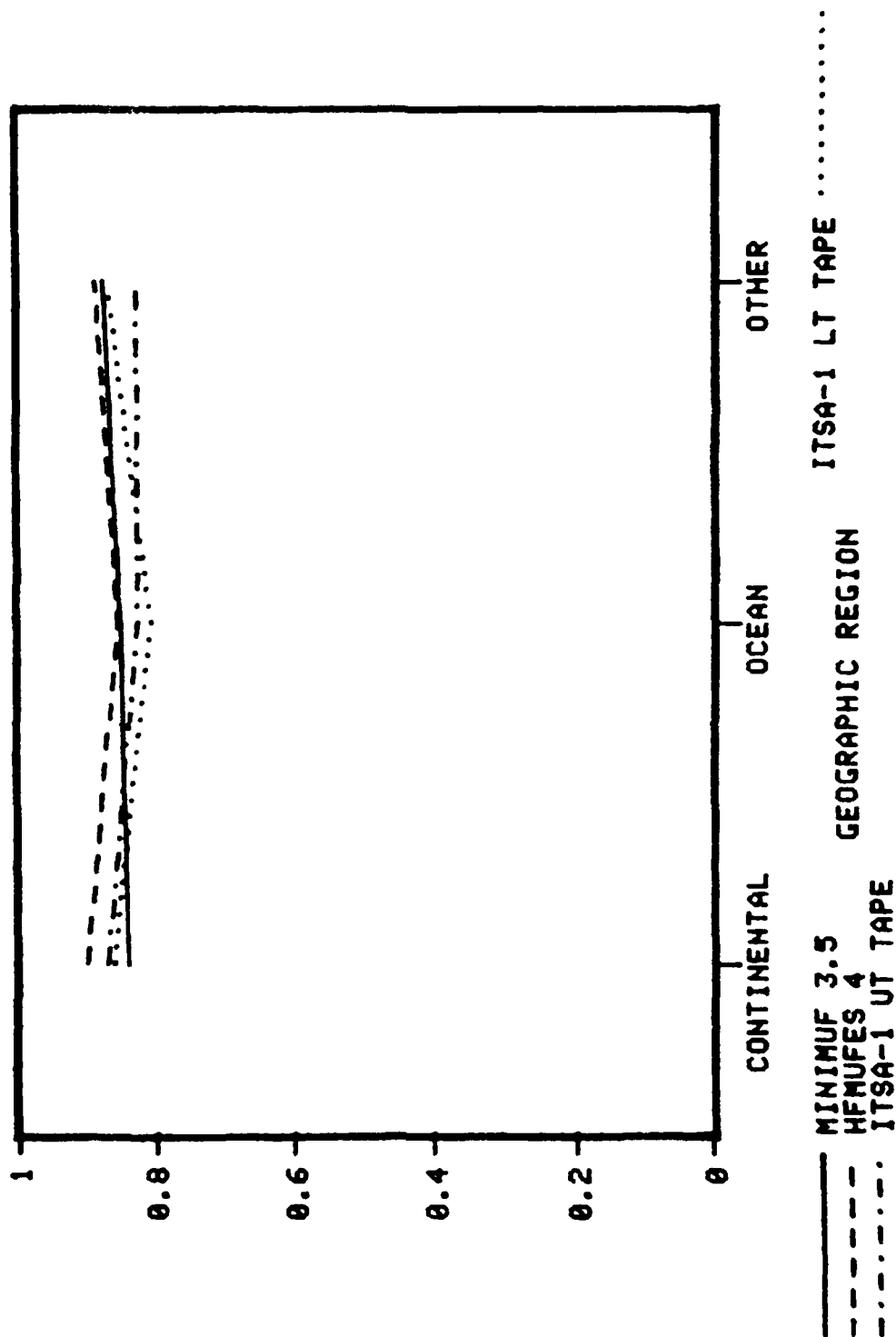
Figure 66. Correlation coefficients as a function geographic region.

Figure 66 shows the correlation coefficient of the four programs as a function of geographical region. All the programs have values greater than 0.8, with HFMUFES 4 being superior.

DISCUSSION OF RESULTS

This report presented the accuracy of predicted MUFs by four prediction programs. This was done by comparing predicted median MUFs to corresponding oblique sounder median MOFs. When compared overall, MINIMUF-3.5 and the two ITSA-1 versions were separated only a few tenths of a percent in bias and rms error and by just one percent in magnitude of the error. However, HFMUFES 4 clearly had the largest bias (7.2 percent high), rms error (8.3 percent) and magnitude of error (26.09 percent). All the programs had difficulty predict-ing high latitude and transauroral paths accurately. For path lengths between 4000 and 5000 km HFMUFES 4 had difficulty predicting accurately. MINIMUF-3.5 had difficulty predicting accurately during the morning and evening transition hours. But perhaps the most surprising result was that HFMUFES 4 was the most accurate over land paths and the least accurate over ocean paths.

EXPLANATION FOR HFMUFES 4'S PERFORMANCE

The performance of HFMUFES 4 was disappointing except over land. As it is is the most recent of the ITS-78 line of HF prediction programs, one would expect its results to be most accurate overall. There are two possible explanations for the inaccuracy in HFMUFES 4 MUF prediction. These are: (1) bias in the numerical map of f_oF2 coefficients and (2) method of determining the k' sec ϕ factor in the MUF calculation.

Bias in f_oF2 Coefficients

One of the major differences in the three large scale programs is the numerical map of f_oF2 coefficients. In earlier versions of the ITSA-1 program, f_oF2 is a function of local time.[19] Later versions of the program calculated f_oF2 as a function of universal time and so-called modified magnetic dip.[20] In HFMUFES 4 the numerical coefficients of the F2 layer critical frequency were revised to include solar cycle and seasonal variations of f_oF2.[24]

The numerical mapping procedures involved two principal analyses of the vertical ionosonde data. First, a so-called "screen analysis" was made of available A- and B-data to produce approximate values of the ionospheric characteristic (called C-data) at carefully chosen locations ("screen points") in large regions, such as oceans, where no ionosonde stations were available. The C-data were then combined with the original A- and B-data in forming a second (and final) analysis. A-data referred to measurements at stations taken during the actual month in question. B-data referred to values of the characteristics obtained from interpolation or extrapolation in time at a station which did not report data for the specific month in question, but was active for a period of time before or after. B-data were used to fill gaps where A-data were not available.

In the oblique incidence sounder data used to compare the programs, 58.7 percent of the sample was for paths entirely over the ocean. Hence, any bias in the numerical maps due to the use of C-data, which is also primarily from ocean areas, would be reflected in the bias in the MUF predictions and the bias in f_oF2 would be accentuated by k' sec ϕ factor in the MUF calculation. In the case of HFMUFES 4, the numerical map is more complex than in ITSA-1. Hence, its bias may be larger than the other two programs over the ocean.

As the C-data only approximates what may have been recorded by vertical ionosondes over ocean areas, the only clue to the bias in the numerical map representing f_oF2 in HFMUFES 4 is that published for the A- and B-data.[24] Table 14 gives both the average deviation (bias) and average relative deviation of the predicted f_oF2 from the observed f_oF2 for each month of 1964 and 1967, periods of low and moderately high solar activity. The number of stations with available observed data varied from month to month between 70 and 100. Bias on the negative side (predictions too large) appears in 1964 and the latter part of 1967 and a large positive bias occurs in the first part of 1967.

Year	Month	R	Average deviation (MHz)	Average relative deviation (%)
1964	1	20	-0.36	-9.82
	2	18	-0.30	-7.66
	3	15	0.03	0.19
	4	13	0.05	-1.76
	5	11	-0.16	-4.49
	6	10	-0.08	-3.34
	7	10	-0.20	-5.63
	8	10	0.01	-0.50
	9	10	0.07	1.89
	10	10	0.02	0.44
	11	10	-0.03	-1.52
	12	11	0.11	0.77
1967	1	75	0.19	0.76
	2	79	0.43	4.50
	3	82	0.83	10.03
	4	85	0.55	6.39
	5	87	0.20	1.29
	6	91	-0.06	-2.04
	7	94	0.05	-0.22
	8	95	0.14	1.02
	9	95	-0.05	-2.30
	10	95	0.08	0.63
	11	97	-0.32	-7.47
	12	101	-0.15	-4.50

Table 14.   Median deviations from numerical map predictions of f_oF2 in HFMUFES 4 (analysis in running average sunspot number R).

Some examples of bias in the predicted values of f_oF2 in HFMUFES 4 for stations not used in forming the numerical map are given in Table 15. Tbilisi, Khabarovsk and Cape Zevgari are at mid-latitude; and Port Moresby, Cocos Island and Ouagadougou are at low latitude. First the table shows the bias to be generally negative (predicted values too high). Then the bias at low latitude is higher, being as large as -26.7 percent.

Year	Month	Tbilisi	Khabarovsk	Cape Zevgari	Port Moresby	Cocos Island	Ouagadougou
1964	1	-10.0	-1.4		-7.2	-14.0	
	3	2.7	3.4		-7.2	-21.0	
	5	-3.2	-2.4		-12.8	-13.0	
	7	-6.4	-6.1		-15.3	-13.0	
	9	2.3	10.7		-14.7	-7.8	
	11	1.5	4.9		-6.4	-7.0	
1967	1	-1.9		-9.6	3.7	-0.1	-4.6
	3	9.0		2.2	9.1	7.6	0.6
	5	1.2		2.7	0.7	-10.1	0.1
	7	-2.8		2.6	-9.5	-26.7	-4.0
	9	0.5			-6.5	-9.1	-5.0
	11	-15.9			-5.2	-4.7	

Tbilisi (41.7N, 44.8E), Khabarusk (48.5N, 135.1E), Cape Zevgari (34.6N, 32.9E), Port Moresby (9.4S, 147.1E), Cocos Island (12.2S, 96.8E), Ouagdougou (12.9N, 2.0W)

Table 15. Median relative deviations in percent from numerical map predictions of $f_o F2$ in HFMUFES 4 for several stations.

VERTICAL-TO-OBLIQUE TRANSFORMATION

Since the basic data available on a world-wide basis are obtained from vertical ionosondes, a transmission must be effected in the application to an oblique path. The determination of oblique propagation characteristics from vertical data is relatively simple in the case of a plane stratified iono- sphere and in the absence of the earth's magnetic field. Considerable modifi- cation is brought about by the inclusion of ionosphere curvature, electronic collisions and the magnetic field, and the general theory is complicated.

The relationship between the frequency f_{ob} of the curve incident obliquely on a flat layer and the equivalent vertical frequency f_v is

$$f_{ob} = f_v \sec \phi \qquad (8)$$

where ϕ is the angle between the vertical and the oblique ray at the bottom of the layer. Equation (8) is known as the secant law. It shows that a given ionospheric layer can reflect higher frequencies as the obliquity of the ray paths increase. For a flat ionosphere the MUF is given by

$$MUF = f_c \sec \phi \qquad (9)$$

where f_c is the critical frequency.

For a curved ionosphere the above relationships must be corrected to

$$f_{ob} = f_v \, k \, \sec \phi \qquad (10)$$

where $k \sec \phi$ is often referred to as secant ϕ (corrected). The MUF is given by

$$MUF = f_c \, k \, \sec \phi. \qquad (11)$$

In the large scale prediction programs, it is assumed that the two layers (E and F2) can be represented by parabolic layers. For the parabolic layer assumption, $k \sec \phi$ is a function of h_m, height of maximum electron density of the layer; of y_m, the semi-thickness of layer; of the critical frequency, f_c and of the range D. The variation with distance of the $k \sec \phi$ factor for a parabolic layer of $y_m/h_o = 0.4$ is reproduced in Figure 67.[39] The curves are parametric in height of maximum electron density h_m ($= h_o + y_m$). For a height of 200 km, $k \sec \phi$ reaches 4.0, corresponding to the tangential ray, at a ground range of slightly over 4000 km. Whereas, for a h_m of 400 km, $k \sec \phi$ reaches a maximum value of just under 3.0 with a ground range in excess of 6000 km. The variation of ground range with distance for various small angles of elevation (0°, 1°, 3° and 5°) are also shown. For these angles the increase in $k \sec \phi$ as a function of range is small.

When the critical frequency f_c is multiplied by $k \sec \phi$ in Equation (11), additional bias in the predicted MUF is introduced. This increase in bias becomes greater with increasing range D and will be higher for layers with low height of maximum electron density h_m. For path lengths in the range 4000 to 5000 km, the bias in the critical f_c will be multiplied by numbers varying from 2.6 to 4.0. The effect on the error in predicted MUF due to the $k \sec \phi$ factor is non-linear; whereas, the effect due to bias in critical frequency is linear.
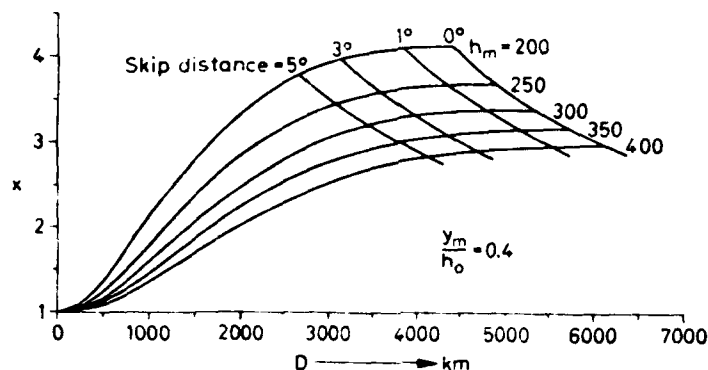
Figure 67. k sec ϕ factor versus distance for different heights of the maximum of the layer .

If the parameters h_o (bottom of the layer) and y_m are known, together with the critical frequency f_c, it is possible to determine k sec ϕ and, hence, MUF by iteration of the formula provided by Appleton and Beynon.[40-41] The procedures for this iteration are different in HFMUFES 4 and in ITSA-1. In addition, different numerical maps for $f_o F2$, the parameters h_o and y_m are determined differently in the three programs.

APPLICATION OF LINEAR REGRESSION

Regression analysis can be used to establish the relationship between variables. Regression analysis was used to determine whether a linear relationship exists between the predicted and observed MUFs. A linear relationship would establish that the error in the predicted MUF (see Equation (11)) was due mainly to the bias in the critical frequency. A non-linear relationship would indicate that the error in the predicted MUF was mainly due to the k sec ϕ factor in the MUF calculation.

Regression analysis of the predicted MUFs on the observed MOFs was first calculated as a function of range. Figure 68 gives the standard error of the
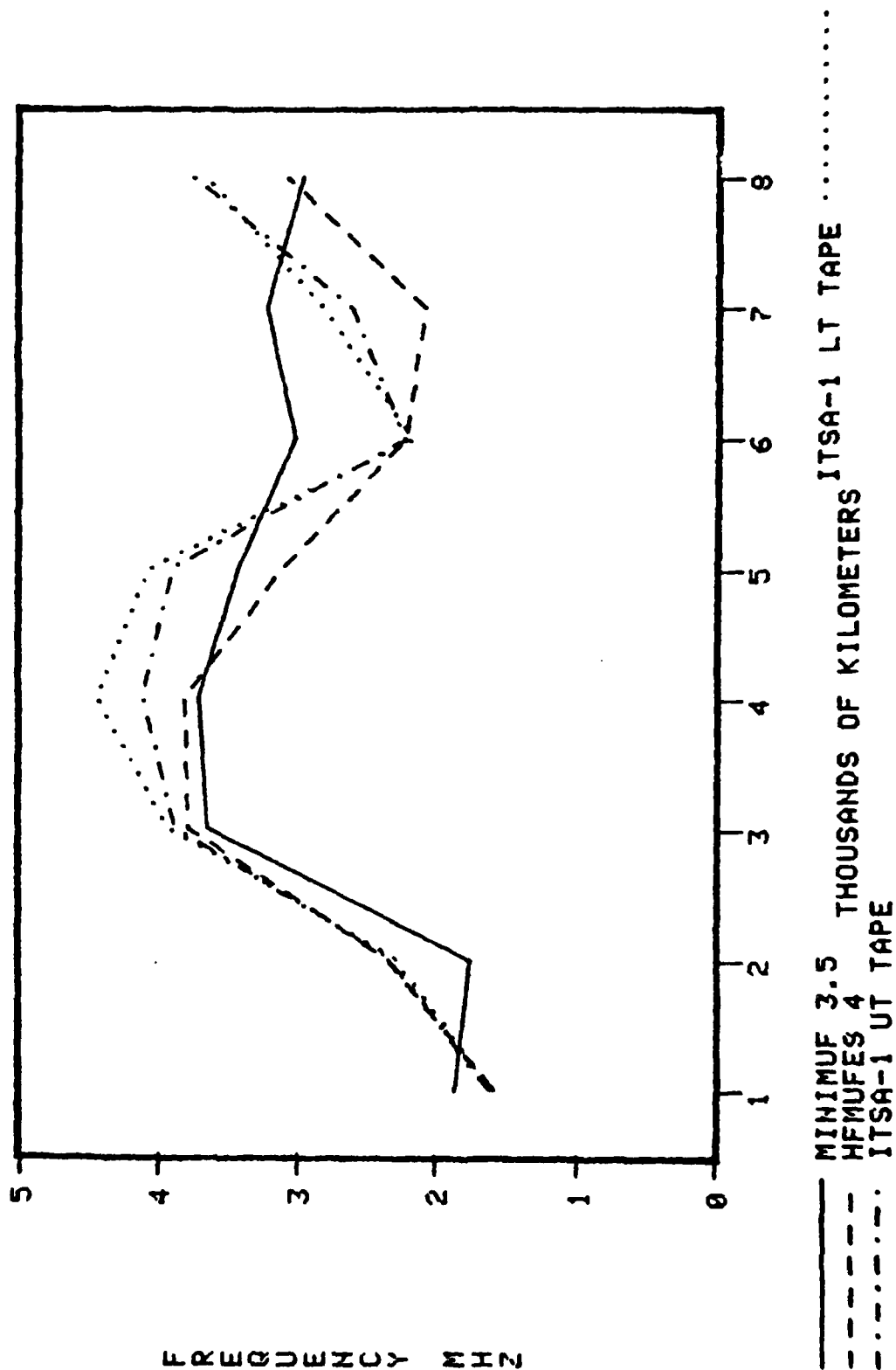
Figure 68. Standard error of estimate as a function of distance.

MINIMUF 3.5

HFMUFES 4   THOUSANDS OF KILOMETERS   ITSA-1 LT TAPE ....

ITSA-1 UT TAPE

FREQUENCY MHz

estimate as a function of distance for each of the four programs. The corresponding figure without regression is Figure 21. There is a considerable lowering of rms error in all four programs. The largest change occurs for the three large scale programs in the 1000 to 5000 km range. The largest change occurs for HFMUFES 4. Under linear regression it performs better than the two ITSA-1 programs and is the best program beyond 4000 km.

After having removed the linear errors in predicting MUF (the bias in the critical frequency), Figure 68 shows the remaining non-linear errors. Note first the remarkable similarity between all three large scale programs in the first 3000 km. Figure 68 also shows a remarkable similarity to Figure 67, the figure showing the k sec ϕ factor as a function of range. There is the same large rise in the first 3000 km and the same leveling off in the next 1000 km. Then there is a decrease in error due to a change in mode and a reduction in the corresponding k sec ϕ factor. After 6000 km there is a new increase in error due to an increasing k sec ϕ factor for the second hop mode. However, MINIMUF-3.5 does not have a corresponding decrease in error at 6000 km as the other three programs. This might indicate an error in its calculation of its k sec ϕ factor (M factor as it is called in its terminology). Figure 69 shows the standard rms error for HFMUFES 4 with and without regression, showing clearly a linear relationship between the predicted MUF and observed MOFs.

Figure 70 shows the standard error of the estimate of linear regression as a function of geomagnetic latitude of control points. The corresponding figure without regression is Figure 45. Here again, note the reduction in rms error for all four prediction programs. In particular, note that HFMUFES 4 now performs better than the other two large size programs. Figure 71 shows the improvement of HFMUFES 4 under linear regression. At mid-latitude there is nearly a 1 MHz improvement in rms error. Figure 72 shows the improvement in rms error for MINIMUF-3.5 with linear regression. The improvement occurs mainly for transequatorial, high latitude and transauroral paths.

The results of linear regression as a function of mid-path local time was examined next. The corresponding figure without regression is Figure 57. There is some improvement shown in Figure 73 in the performance of the large computer programs with the largest occurring during the daytime. HFMUFES 4 was shown to have the best performance under regression of the three large programs. Figure 74 shows the improvement under linear regression for HFMUFES
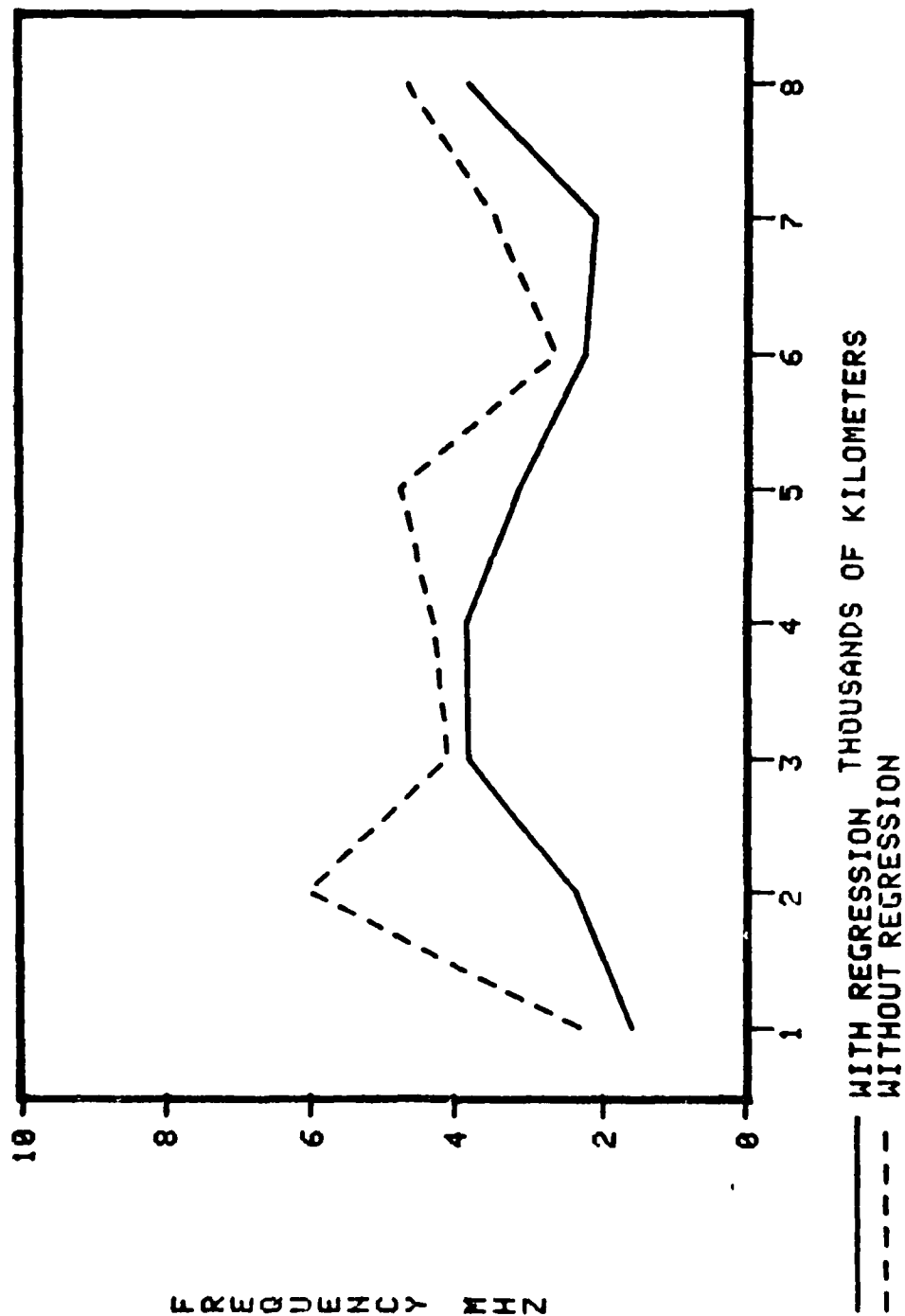
Figure 69. Standard rms error of estimate for HFMUFES 4 as a function of distance.

WITH REGRESSION   THOUSANDS OF KILOMETERS
WITHOUT REGRESSION

Figure 70. Standard error of the estimate as a function of geomagnetic latitude location of control points.

MINIMUF 3.5   GEOMAGNETIC LATITUDE   ITSA-1 LT TAPE ·········
HFMUFES 4
ITSA-1 UT TAPE

Figure 71. Standard rms error of the estimate for HFMUFES 4 as a function of geomagnetic latitude location of control points

Figure 72. Standard rms error of estimate for MINIMUF-3.5 as a function of geomagnetic latitude location of control points.
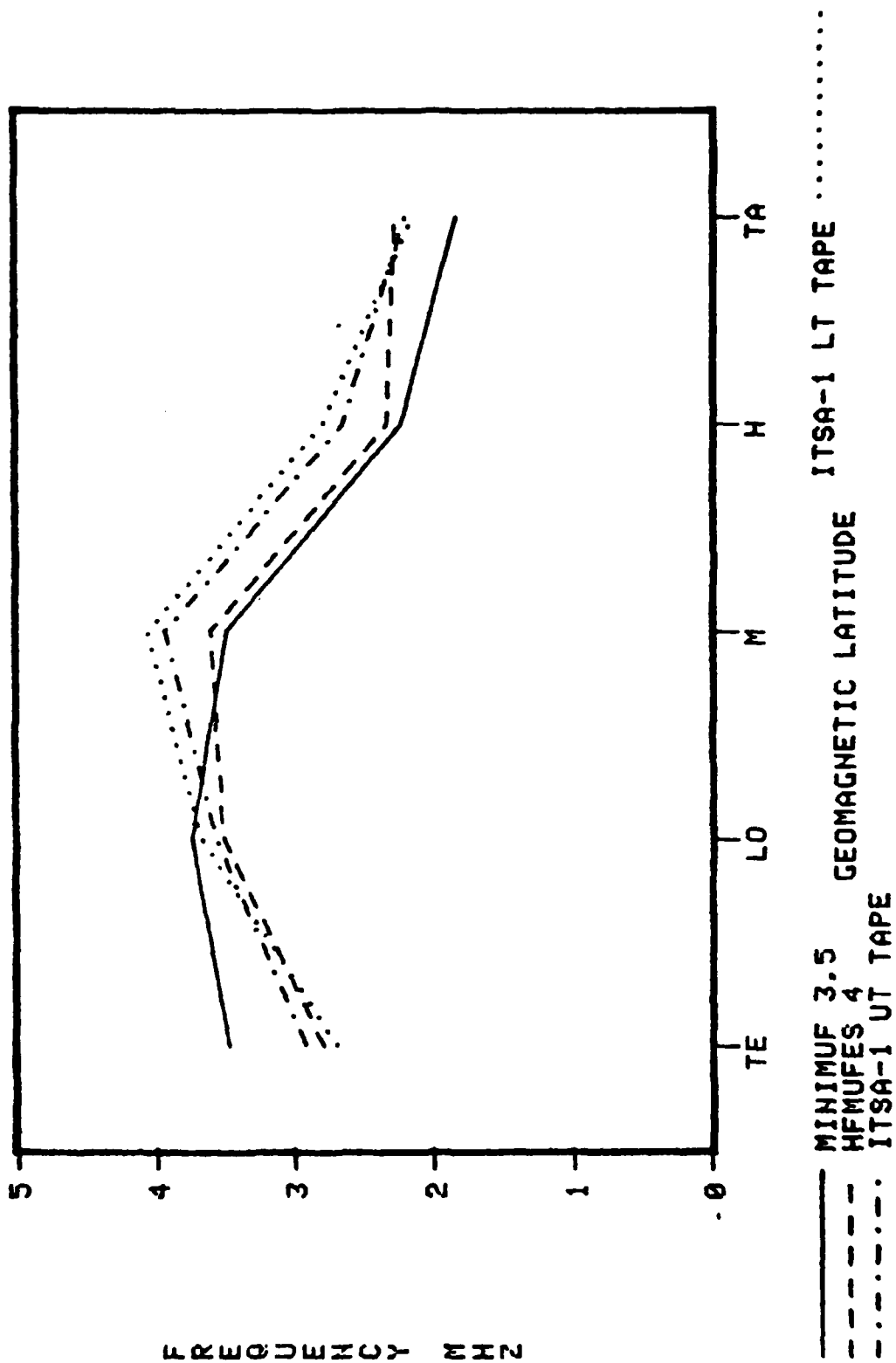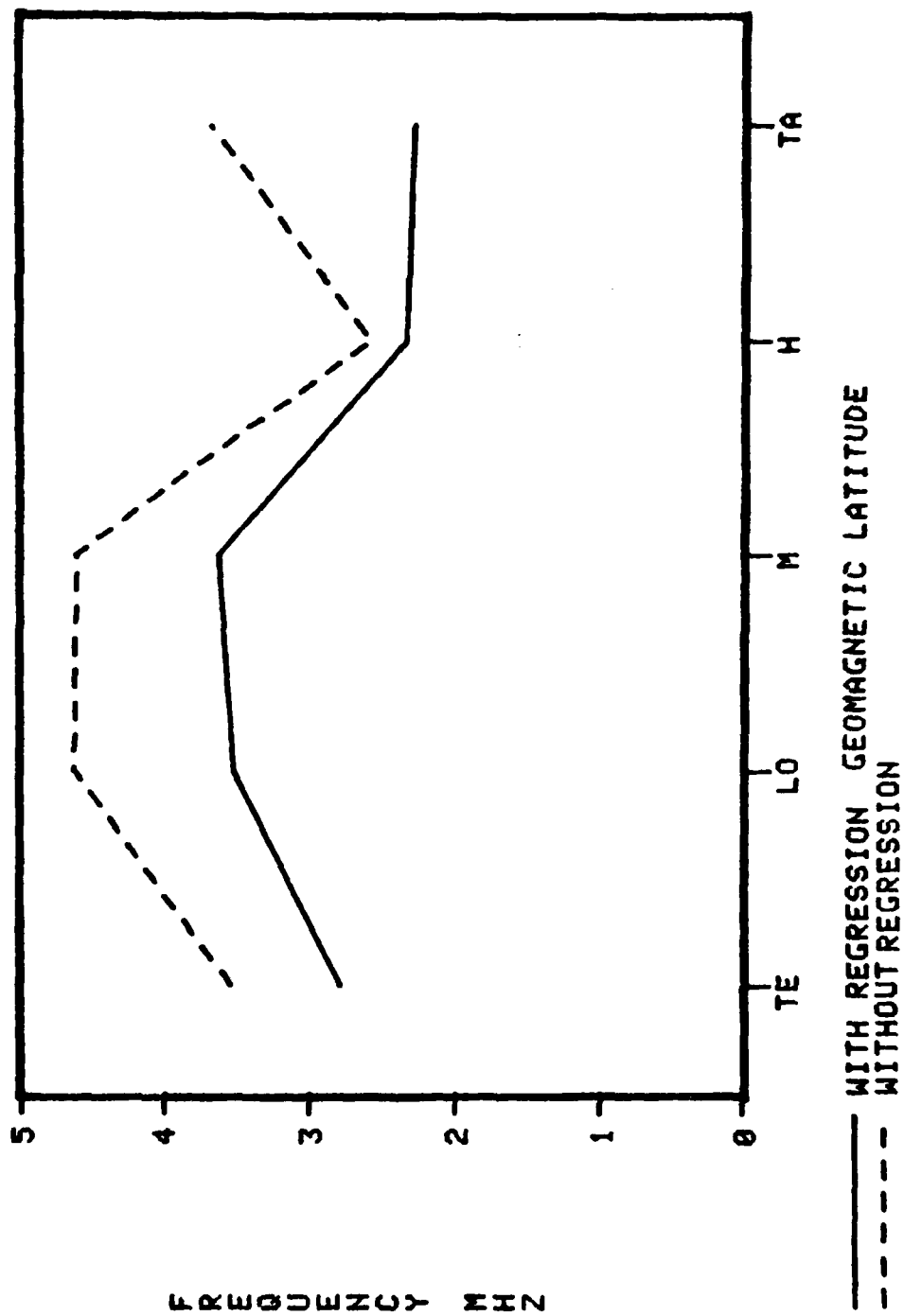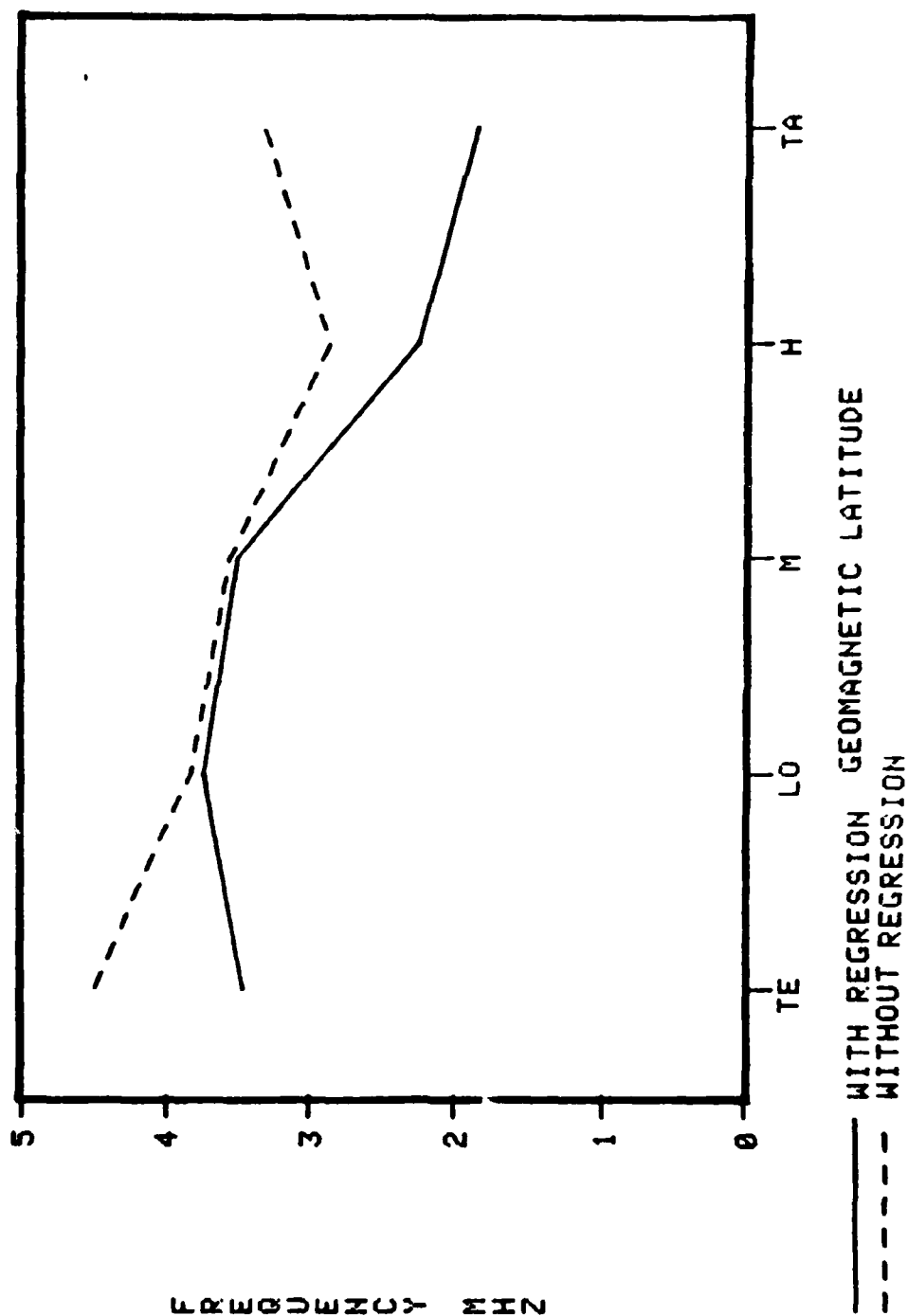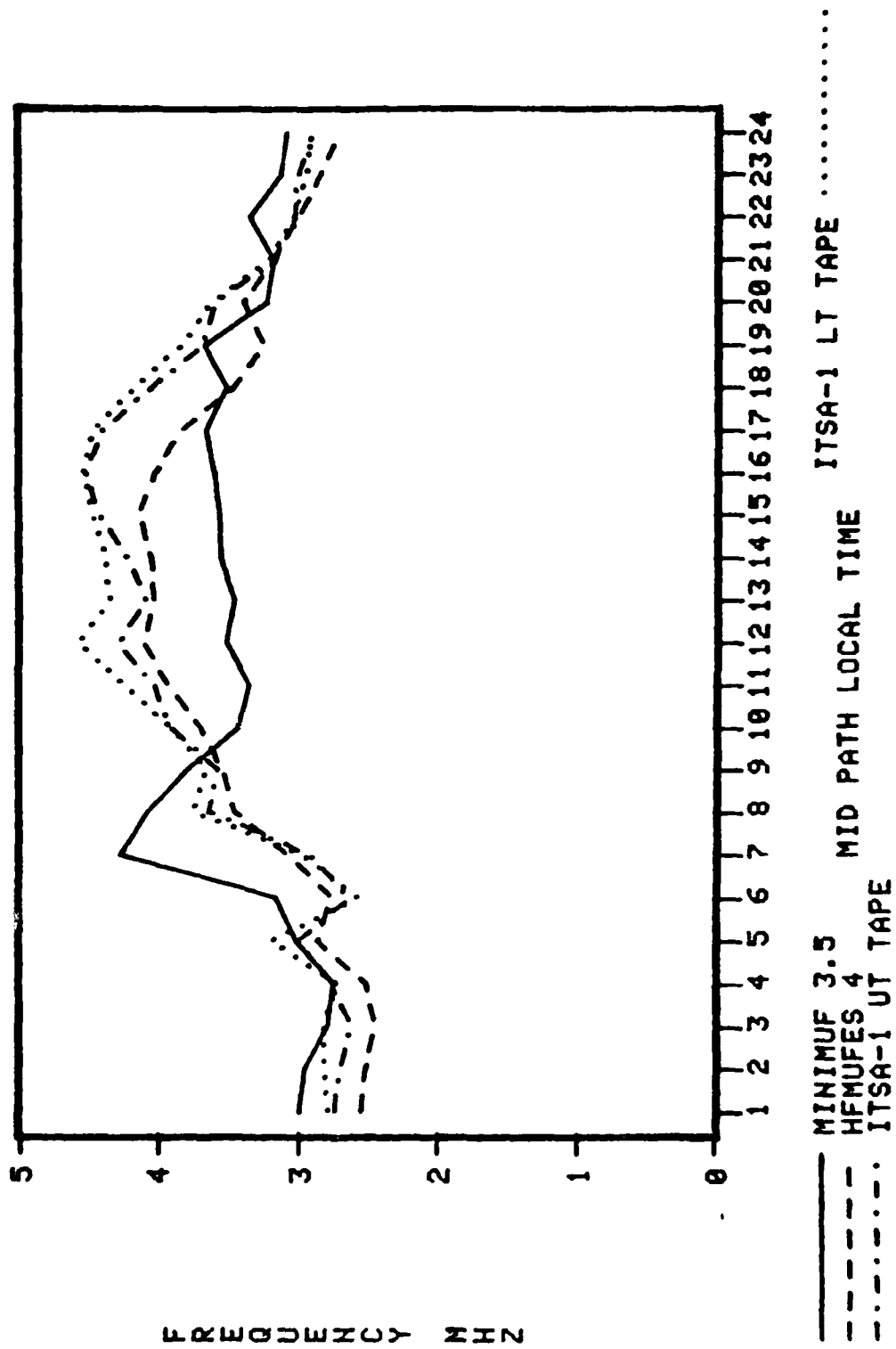
109

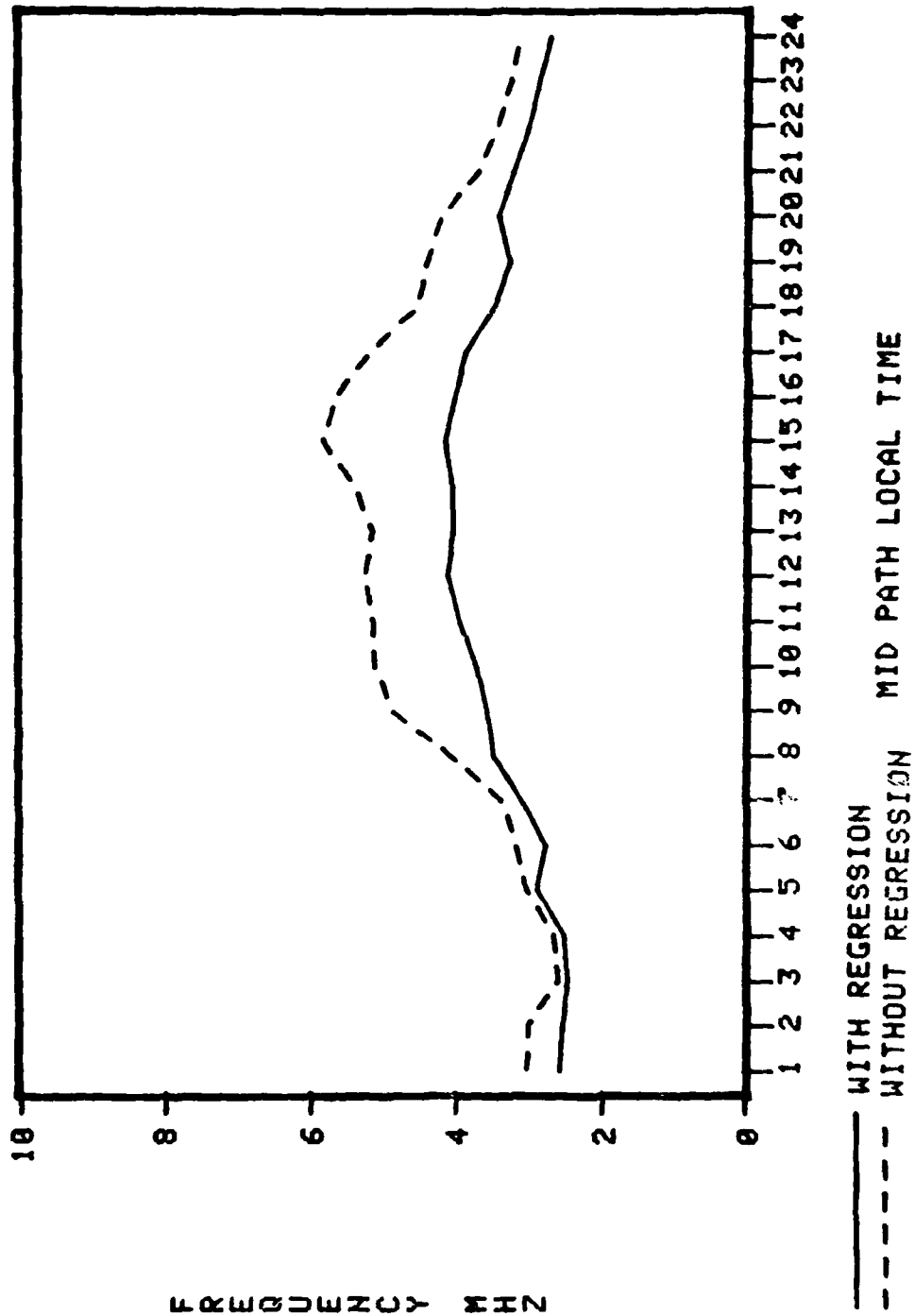Figure 73. Standard error of estimate as a function of local time.

Figure 74. Standard error of estimate for HFMUFES 4 as a function of local time.

4. During the daytime, the improvement is more than 1 MHz. Figure 75 shows the results of linear regression applied to MINIMUF-3.5. Note that an improvement is made in its performance during the evening transition hours, but that during the morning transition hours there is no improvement. This non-linear error indicates that the $k \sec \phi$ factor part of the MINIMUF-3.5 MUF calculation needs further improvement.

Finally, linear regression was applied as a function of geographic region. The results are shown in Figure 76. The corresponding results without regression are displayed in Figure 63. For MINIMUF-3.5 the biggest improvement is for continental paths and paths that are a combination of land and ocean. As MINIMUF-3.5 was optimized for ocean paths, little improvement is seen there. The other three programs show an improvement in all regions with the improvement for HFMUFES 4 being the greatest. Figure 77 compares the results of HFMUFES rms error as a function of geographic region with and without regression. Particularly, it shows a vast improvement over ocean areas (more than 1 MHz improvement). This indicates that the error in HFMUFES is primarily due to the bias in the critical frequency over ocean area.
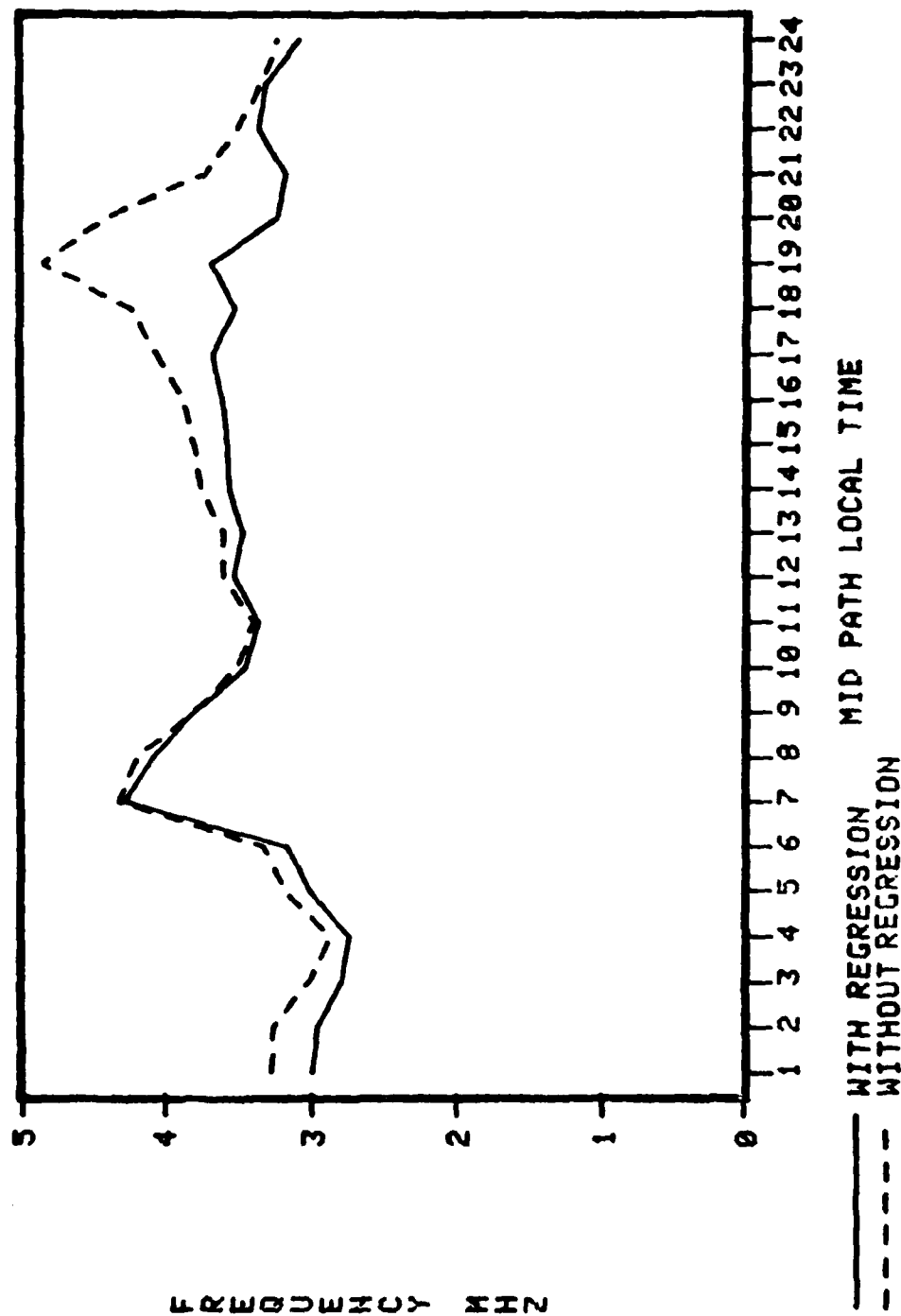
Figure 75. Standard rms error of estimate for MINIMUF-3.5 as a function of local time.
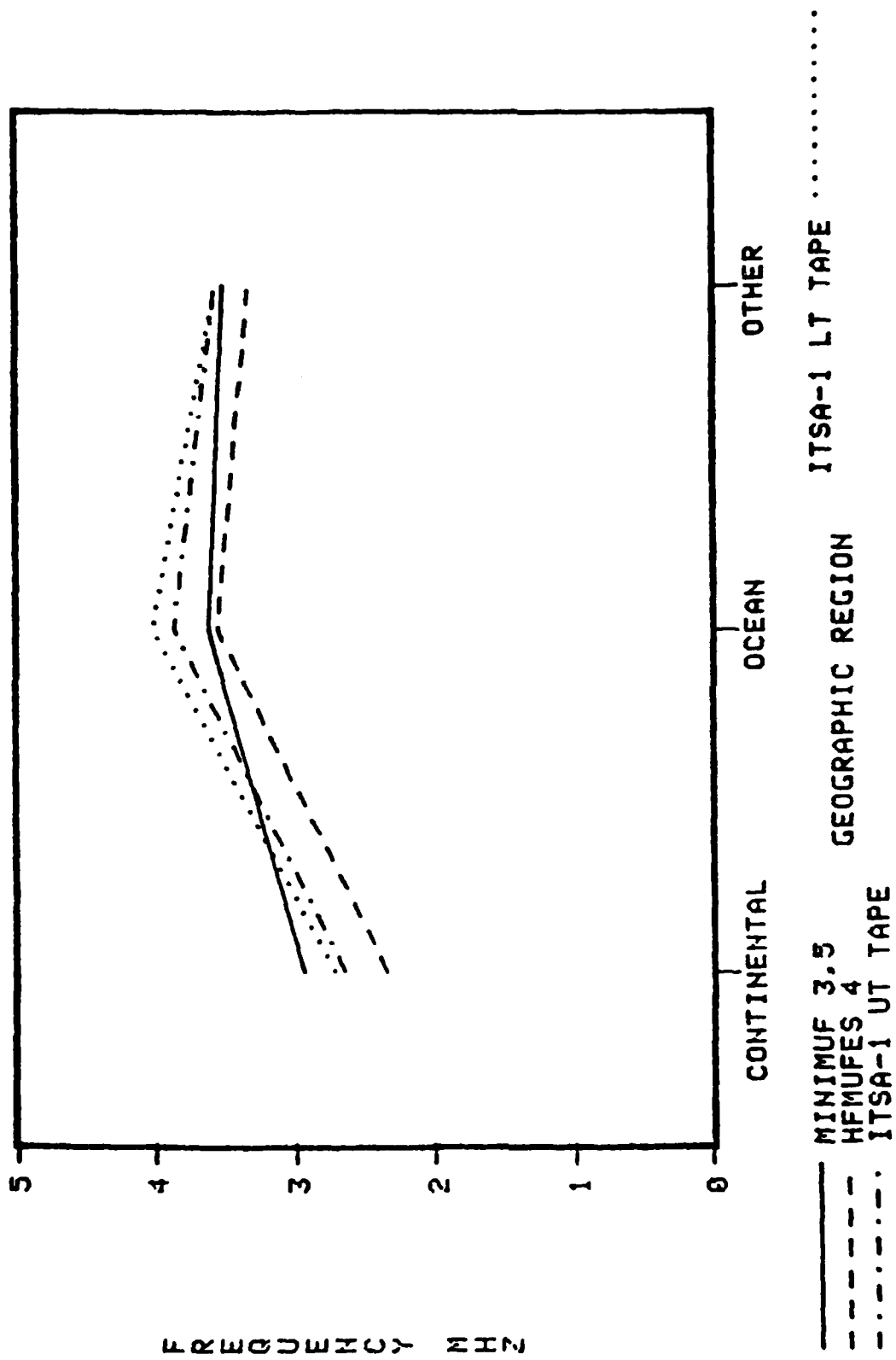
113

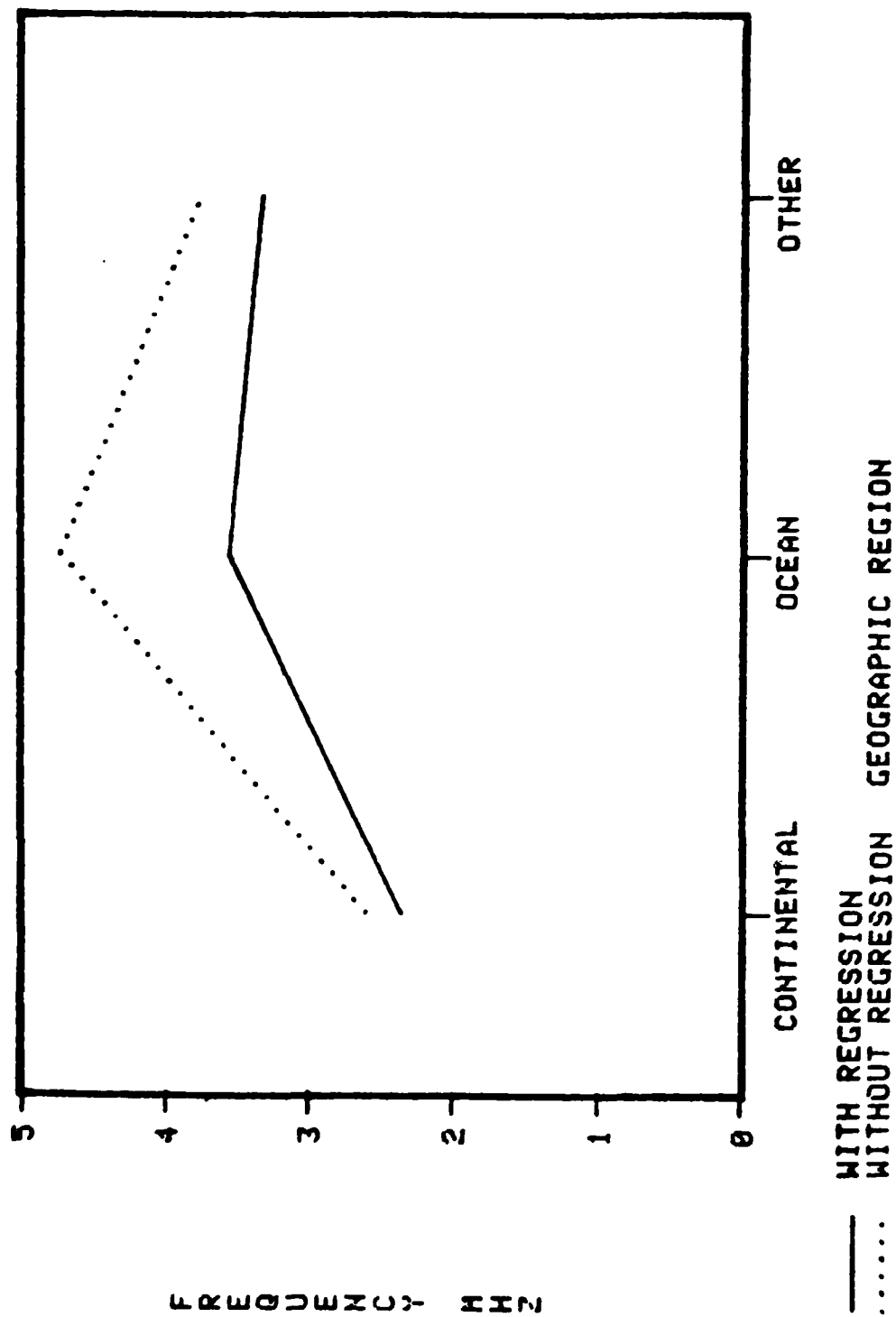Figure 76. Standard error of estimate as a function of geographic region.

Figure 77. Standard rms error of estimate for HFMUFES 4 as a function of geographic region.

WITH REGRESSION
WITHOUT REGRESSION

CONCLUSIONS

For the particular oblique path studies and conditions assumed, the following conclusions about the accuracy of HF MUF prediction can be stated:

1. MINIMUF-3.5 appears most accurate overall

2. The version of ITSA-1 with ionospheric characteristics mapped in universal time is slightly more accurate than ITSA-1 with ionospheric characteristics mapped in local time

3. MINIMUF-3.5 had difficulty predicting accurately during the sunrise and sunset transition hours and for path lengths 5000 to 7000 km

4. Except for land paths, the performance of HFMUFES 4 was disappointing

5. HFMUFES 4 had difficulty predicting MUFs accurately for paths over ocean areas and for paths with lengths between 4000 and 5000 km

6. All of the programs had difficulty predicting MUFs accurately at high latitudes

The inaccuracy of HFMUFES 4 is due in part to the existing bias in the numerical map of f_oF2 over ocean areas. Except for a few ionosonde stations on islands like Hawaii, there were no real ocean area vertical ionosonde data used to generate the numerical map. Instead, ocean area data were generated by interpolating between existing land stations.

When the critical frequency f_c is multiplied by the so-called "k sec ϕ factor," additional error in the predicted MUF is introduced. This increase in error rises with increasing range and is higher for layers with low height of maximum electron density.

The use of linear regression analysis demonstrated that the source of error in HFMUFES 4 predicted MUFs (and to some extent ITSA-1 predicted MUF) was due to the bias in the input critical frequency data, not inaccuracies in the k sec ϕ factor. This occurs because the bias in critical frequency affects the MUF linearly; whereas, the k sec ϕ factor affects the MUF non-linearly. In the case of HFMUFES 4, the bias in critical frequency is accentuated by the k sec ϕ factor.

In the case of MINIMUF-3.5, linear regression showed that the errors in predicted MUFs during the sunrise transition period and for path lengths 5000

116

to 7000 km were non-linear effects. These errors then can be attributed to k
sec ϕ factor (M factor) in its calculation of MUF. However, linear regression
did remove the sunset transition error. This indicates that there is some
bias in its critical frequency calculation -- perhaps in its location of
control points.

RECOMMENDATIONS

As a result of this study, the following recommendations are made:

1. The use of MINIMUF-3.5 where the only desired output is MUF and FOT

2. The use of the universal time ionospheric data tape in NTP 6 Supp. 1
predictions

3. The development of an improved M factor equation for use in MINIMUF-
3.5

4. Augmentation of the MOF data base to represent better the Atlantic
Ocean, northern latitudes and transequatorial paths

5. The use of this augmented data base to more accurately assess the
errors in predicted MUF

6. The assessment of minimum take-off angle on accuracy of predicted MUF

7. The use of multiple-linear regression to remove the bias in predicted
MUF due to the bias in predicted f_oF2

REFERENCES

1. National Bureau of Standards Circular 462, Ionospheric Radio Propagation, 25 June 1948.

2. Sailors, DB, "HF Propagation Predictions: Program Proliferation the Real World," paper presented at URSI Annual Meeting, Boulder, Colorado, 14-17 October 1974.

3. Naval Ocean Systems Center Technical Report 186, MINIMUF-3: A Simplified HF MUF Prediction Algorithm, by RB Rose, JN Martin, and PH Levine, 1 February 1978.

4. Commander, Naval Telecommunications Commander, Naval Telecommunications Publication 6 Supp-1, Recommended Frequency Bands and Frequency Guide, 1980.

5. Environmental Sciences Services Administration Technical Report TER 1-IISA-1, Predicting Statistical Performance Indexes for High Frequency Telecommunications Systems, by DL Lucas and GW Haydon, August 1966.

6. Office of Telecommunications Report 76-102, Predicting the Performance of High-Frequency Skywave Telecomunication Systems (the use of the HFMUFES 4 Program), by GW Haydon, M Leftin, and R Rosich, September 1976.

7. Stanford Research Institute, Technical Report 1, Contract DA 36-039 SC-66 381, IBM 704 Program to Determine the Maximum Usable Frequency (MUF) and the Lowest Useful High Frequency (LUF) for HF Radio Propagation, by EA Clarke, March 1959.

8. Stanford Research Institute Final Technical Report 2, Contract DA 36-039 SC-85 052, The HF Propagation Prediction Programs for the IBM 7090 Computer, by EM Young and EA Clarke, May 1962.

9. Navy Electronics Laboratory Report 1358, A High Frequency Propagation Prediction Program for the CDC 1604 Computer, by DB Sailors, 28 February 1966.

10. National Bureau of Standards Technical Note 2, World Maps of F2 Critical Frequencies and Maximum Usable Frequency Factors, by DH Zacharisen, April 1959.

11. National Bureau of Standards Technical Note 2-2, Supplementary World Maps of F2 Critical Frequencies and Maximum Usable Frequency Factors, by DH Zacharisen, October 1960.

12. International Radio Consultative Committee 10th Plenary Assembly, Geneva 1963, Report 322; World Distribution and Characteristics of Atmospheric Radio Noise, 1964.

13. National Bureau of Standards Report 6789, MUF-FOT Predictions by Electronic Computers, by DL Lucas and GW Haydon, 14 August 1961.

14. National Bureau of Standards Report 7619, Predicting the Performance of Band 7 Communication Systems Using Electronic Computers, by DL Lucas and GW Haydon, 15 October 1962.

15. Collins Radio Company Research Report 288, The Collins HF Propagation Prediction Program, by G. Bergemann and R. Decker, 1 September 1963.

16. Koide, FT, "A Computer Method of HF Ionospheric Propagation Prediction and Analysis", IEEE Trans. on Antennas and Propagation, Vol. AP-11, pp 540-558, September 1963.

17. AVCO Corporation Technical Report RAD-TR-63-37, Contract AF 30 (602)-2809, Natural Communications Study Phase 1 Feasibility Study on a Reliable Polar High-Frequency Communications System, by GE Hill et al., 24 June 1964.

18. Environmental Sciences Services Administration Technical Report ITSA-1, Predicting Statistical Performance Indexes for High Frequency Ionospheric Telecommunication Systems, by DL Lucas and GW Haydon, 29 August 1966.

19. Jones, WB and RM Gallet, "Methods for Applying Numerical Maps of Ionospheric Characteristics," J. Res. NBS, Vol. 66D, pp 649-662, November-December 1962.

20. National Bureau of Standards Technical Note 337, Advances in Ionospheric Maping by Numerical Methods, by WB Jones, RP Graham, and M Leftin, 12 May 1966. (Also Environmental Science Services Administration Technical Report ERL 1-7-ITS 75, May 1969.)

21. Bell Aerosystems Co. Report A70009-230, TR RADC-TR-67-396, HF and LF Propagation Models for Interference Prediction, by LR Spogen, Jr., JL Lloyd, and EP Moore, August 1967.

22. Environmental Sciences Services Administration Technical Report ERL 110-ITS 78, Predicting Long-Term Operational Parameters of High Frequency Sky-Wave Telecommunication Systems, by AF Barhausen, JW Finney, LL Proctor, and LD Schultz, May 1969.

23. Office of Telecommunications ITS Research Report 3, Global Representation of Annual and Solar Cycle Variation of foF2 Monthly Median 1954-1958, by WB Jones and DL Obitts, October 1970.

24. Office of Telecommunications ITS Research Report 2, World Maps of Atmospheric Radio Noise in Universal Time, by DH Zacharisen and WB Jones, October 1970.

25. Office of Telecommunications Report 76-88, Numerical Representation of Monthly Median Critical Frequencies of the Regular E Region (foE), by M. Leftin, May 1976.

26. Office of Telecommunications Report 76-102, Predicting the Performance of High Frequency Sky-wave Telecommunication Systems (The Use of the HFMUFES 4 Program), by GW Haydon, M. Leftin, and R. Rosich, September 1976.

27. Naval Ocean Systems Center Technical Document 201, <u>MINIMUF-3.5</u>, by RB Rose and JN Martin, 26 October 1978.

28. Naval Ocean Systems Center Technical Note 758, <u>Further Verification of the MINIMUF-3.5 HF MUF Prediction Algorithm for: (1) Frequencies above 32 MHZ; (2) Path Lengths of Less than 250 NMI</u>, by RB Rose, 20 September 1979.

29. Stanford Research Institute Contract No. 3853(00), Technical Summary Report 4, <u>Long Range Propagation Experiment,</u> by A. Selby, February 1964.

30. National Bureau of Standards Report 7217, <u>Boulder-Barrow Sweep Frequency Oblique Pulse Experiment</u>, LH Tveten, 8 January 1962.

31. Chief of Naval Operation (OEG) letter (OEG)154-70 to Director, OEG, Subject: "Data for Comparison of Ionospheric Sounder Measurements with Predicted Optimum Frequencies for Communication Circuits," 12 March 1970.

32. Booz-Allen Applied Research, Inc., Contract No. 93296 Project Serial No. SS-267, Task 7645, <u>An Examination of the Data Presently Available for the Development of a Short Term Warning Capability</u>, 23 February 1966.

33. Stanford Research Institute Technical Summary Report 9, Contract No. 3853(00)ARPS Order 196-62, <u>Long Range Propagation Experiment: A Comparison of Eastern and Western Hemisphere Propagation</u>, by EJ Baumann, TI Dayharsh, and WA Hall, November 1965.

34. General Electric Co. Contract AF 30 (602)-3946, Int. Report 6, RADC-TR-67-618, <u>Expanded Little IDA, Experimental Results,</u> by DT Olmsted, JA Reeve, and G. Shepelavey, December 1967.

35. Stanford Research Institute Final Report, Contract No. 3853(00), ARPA Order 196-62, <u>Long Range Propagation Experiment,</u> by AH Selby, December 1965

36. United States Army Electronic Command Technical Report 4144, <u>Field Test of a Near Real-Time Ionospheric Forecasting Scheme (200 km),</u> by GE Krause, RJ D'Accardi, and EL Roswell, III, August 1973.

37. United States Army Electronic Command Technical Report 4145, <u>Field Test of a Near Real-Time Ionospheric Forecasting Scheme (500 km),</u> by GE Krause, RJ D'Accardi, and EL Roswell, III, August 1973.

38. Harnett, DL, <u>Introduction to Statistical Methods</u>, Addison-Wesley Publishing Co., 1st Edition, pp 284-333, 1970.

39. National Bureau of Standards Monograph 80, Ionospheric Radio Propagation, by K. Davies, p. 172, April 1, 1965.

40. Appleton, EV and WJG Beynon, "The Application of Ionospheric Data to Radio Communications, Part I", <u>Proc. Phys. Soc. London,</u> Vol. 52, pp 518-533, July 1940.

41. Appleton, EV and WJG Beyon, "The Application of Ionospheric Data to Radio Communications, Part II", <u>Proc. Phys. Soc. London,</u> Vol. 59, pp 58-76, January 1947.

ENL

DATE